Jørgen Lausund Grinna

A Performance and Kinetic Study of PEI-Impregnated Mesoporous Silica Spheres for Low-Temperature Carbon Capture.

Master's thesis in Chemical Engineering and Biotechnology
Supervisor: De Chen, IKP

July 2020

NTNU
Norwegian University of
Science and Technology

Jørgen Lausund Grinna

A Performance and Kinetic Study of PEI-Impregnated Mesoporous Silica Spheres for Low-Temperature Carbon Capture.

Master's thesis in Chemical Engineering and Biotechnology
Supervisor: De Chen, IKP
July 2020

Norwegian University of Science and Technology
Faculty of Natural Sciences
Department of Chemical Engineering

NTNU
Norwegian University of
Science and Technology

Preface

This thesis is written as part of the "Low-Temperature Carbon Capture Team" for the Catalyst Group (KinCat) within Department of Chemical Engineering and marks the end of the five-year study program of Chemical Engineering and Biotechnology at Norwegian University of Science and Technology (NTNU).

I want to express my gratitude to all who are involved in the KinCat group, for making an incredible working environment for both employees and students. I would like to extend my sincere thanks to my supervisor Professor De Chen for his resourceful ideas and academic guidelines during this project. Thanks to PhD candidate Dumitrita Spinu for always being available and supportive, and for the valuable help I got.

I would also like to thank the Estelle Marie Vanhaecke, Anne Hoff and Karin Dragsten, for instrument training and technical support. I am also grateful for the encouragement and constant positivity they provided to the students. Thanks to my fellow students who I shared reading hall with during this project for making a great study environment. Finally, I would like to thank my friends and family for their great support throughout my education.

This project was affected by the global pandemic caused by Covid-19. Therefore, I want to express my gratitude to the Department of Chemical Engineering and all who contributed to the reorganization of the routines so I could complete this master thesis in the best possible way under restricted conditions.

Trondheim, July 31, 2020

Jørgen Lausund Grinna

Abstract

Post-combustion carbon capture is one of the most promising technologies to combat ever-increasing greenhouse gas emissions. Adsorption of CO_2 from flue gas using high-efficiency solid sorbents have demonstrated many advantages, and in this work, amine-modified mesoporous silica spheres (MSS) has been investigated. CO_2 adsorption measurements of MSS impregnated with polyethylenimine (PEI) were conducted by thermal gravimetry in order to investigate the effect of (i) physical properties of support, (ii) PEI loading, (iii) silica coating, (iv) CO_2 partial pressure and (v) adsorption/desorption temperatures.

The modification of MSS with PEI was achieved by the wet impregnation method, and a suggestion for silica coating method using silicate as a precursor was proposed. The physical properties of the MSS sorbents were characterised by nitrogen physisorption. MSS showed relatively small surface areas and pore volumes of the support compared to other mesoporous silica support on the market. The largest surface area achieved was 137 m^2/g with a pore volume of 0.51 cm^3/g. However, all sorbents showed fast adsorption kinetics and were able to regenerate in pure N_2. In 5% CO_2 gas, the PEI inside the pores exhibited the highest CO_2 adsorption capacity of 2.21 mmol/g at 75 °C with a 40 wt% PEI loading. The CO_2 adsorption capacity resulted in a relatively low amine efficiency of 0.121 mmol CO_2/ 2 mmol N.

The sorbents showed excellent cyclic adsorption/desorption stability where no sorbent lost more than 2% of its CO_2 adsorption capacity after nine cycles. For temperature swing adsorption/desorption (75 °C/120 °C), the most stable sorbent achieved 95.5% of its CO_2 uptake after 9 cycles. Two silica coating methods were proposed and tested in order to make the sorbets more robust for temperature swing adsorption/desorption. However, the coating methods did not improve the stability of the sorbents.

The kinetic study demonstrated the fastest adsorption rate at higher CO_2 partial pressure due to a higher driving force, and with a temperature at 75 °C due to a lower diffusion limitation. Also, a lower PEI loading resulted in faster adsorption kinetics. Experimental CO_2 adsorption data were analysed by five different adsorption kinetic models. Adequacy of the models was investigated, and the fractional-order kinetic model showed the overall best agreement with the experimental CO_2 adsorption on PEI impregnated MSS. A high correlation coefficient validated the proper agreement, in addition to, a low root mean square error and a low average absolute deviation percentage between the predicted model and experimental CO_2 uptake with different physical properties of support, PEI loadings, adsorption temperatures and CO_2 partial pressures.

Sammendrag

Karbon-fangst av røykgass er en av de mest lovende teknologiene for å bekjempe de alltid økende utslippene av drivhusgasser. Adsorpsjon av CO_2 fra røykgass ved bruk av effektive solide sorbenter har vist mange fordeler, og i denne oppgaven har amin modifiserte mesoporøse silika sfærer (MSS) blitt undersøkt. Målinger av CO_2 adsorpsjon på polyethylenimine (PEI) impregnerte MSS ble utført med termisk gravimetri for å undersøke effekten av (i) de fysiske egenskaper til MSS, (ii) PEI-mengde, (iii) silika beskyttelsesbelegg, (iv) ulike partialtrykk av CO_2 og (v) adsorpsjon/desorpsjons temperaturer.

MSS ble impregnert med PEI ved bruk av våt-impregnerings metoden, og forslag til metoder for silika belegg ved bruk av silikater som reaktanter ble foreslått. Målinger av de fysiske egenskapene til MSS sorbenter ble utført med fysikalsk adsorpsjon av nitrogen, og resultatene viste relativt små overflatearealer og porevolum av MSS prøvene sammenlignet med andre mesoporøse silika materialer som finnes på markedet. Det største oppnådde overflatearealet var på 137 m^2/g med et porevolum på 0,51 cm^3/g. Imidlertid viste alle sorbentene rask adsorpsjonskinetikk, og var i stand til å regenerere i 100% N_2 gas. I 5% CO_2 gass, viste MSS den høyeste CO2-adsorpsjonkapasiten på 2,21 mmol/g ved 75 ℃ med en PEI-mengde på 40 vekt%. CO_2-adsorpsjonkapasiten resulterte i en relativt lav amineffektivitet på 0,121 mmol CO_2/2 mmol N.

Sorbentene viste ekstremt god syklisk adsorpsjon/desorpsjonsstabilitet, der ingen av sorbentene mistet mer enn 2% av sin CO2-adsorpsjonskapasitet etter 9 sykluser. For adsorpsjon og desorpsjon med temperatursvingninger (75 ℃/ 120 ℃), oppnådde den mest stabile sorbenten 95,5% av sin CO_2-adsorpsjonskapasitet etter 9 sykluser. To forslag til metoder for silika belegg ble testet for å gjøre sorbentene mer robuste for adsorpsjon og desorpsjon med temperatursving. Belegningsmetodene forbedret imidlertid ikke sorbentenes stabilitet.

Kinetikkstudien demonstrerte den raskeste adsorpsjons raten ved høyere CO_2 partialtrykk på grunn av en høyere drivkraft, og med en temperatur på 75 ℃ på grunn av en lavere diffusjonsbegrensning. En lavere PEI-mengde resulterte også i raskere adsorpsjonskinetikk. Eksperimentelle CO_2 adsorpsjonsdata ble analysert av 5 forskjellige kinetikk modeller for adsorpsjon. Modellenes evne til tilpassingen ble undersøkt, og det ble funnet ut at den fraksjons-order kinetiske modellen var i best overensstemmelse med den eksperimentelle adsorpsjonen av CO_2. Dette ble validert ved høy korrelasjonskoeffisient og lav rot-middel-kvadrat feil, i tillegg til en lav gjennomsnittlig absolutt avviksprosent mellom den modellerte modellen og det eksperimentelle CO_2 opptaket for forskjellige fysiske egenskaper til MSS, PEI-mengde, adsorpsjonstemperaturer of partialtrykk av CO_2.

Contents

List of Figures

List of Tables

List of Symbols

β_{DKM}	Ratio of k_{sur} and k_{bulk}
$\hat{y}_i$	Predicted data
σ	Surface tension
τ	Time required to reach equilibrium
θ	Contact angle
b	Number of observed predicted parameters
C	BET constant
d_p	Pore size
k	Kinetic rate constant
k_A	Adsorption rate constant for Avrami's kinetic model
k_{bulk}	Adsorption rate constants for bulk adsorption
k_{DKM}	Adsorption rate constant for dual kinetic model
k_F	Adsorption rate constant for fractional-order kinetic model
k_{PFO}	Adsorption rate constant for pseudo-first-order kinetic model
k_{PSO}	Adsorption rate constant for the pseudo-second-order kinetic model
k_{sur}	Adsorption rate constants for surface adsorption
m	Kinetic diffusion parameter
m_0	Weight of the sorbent

m_e	Weight of the sorbent at adsorption equilibrium
m_{PEI}	Mass of PEI
$m_{support}$	Mass of support
m_s	Amount of silica precursor needed to coat 1 g sorbent with one layer
MW_a	Weight of the adsorbate
n	Kinetic driving force parameter
N_A	Avogadro's number
P	Nitrogen partial pressure
p	Number of observed experimental data
P_0	Nitrogen the saturation pressure
p_{CO_2}	CO_2 partial pressure
q_{bulk}	Adsorption capacity inside the bulk
q_e	Adsorption capacity
q_{sur}	Adsorption capacity at the surface
q_t	Adsorption capacity at time t
R	Gas constant
r	Radius of sphere
r_p	Pore radius
S_{BET}	BET surface area
S_N	Surface area occupied by nitrogen
T	Temperature
t	Time
V	Molar volume
V_m	Volume of the adsorbed monolayer of N
V_p	Pore volume
x	Vector of unknown variables
X_N	Mass fraction of nitrogen per gram PEI
y_i	Observed experimental data

Acronyms

ADD Average Absolute percentage Deviation

BET Brunauer Emmett Teller Method

BJH Barret-Joyner-Halenda

CCS Carbon Capture and Storage

CCU Carbon Capture and Utilization

MCM Mobil Composition of Matter

MSS Mesoporous Silica Sphere

MW Molar Weight

PEI Polyethylenimine

RF Resorcinol Formaldehyde

RMSE Root Mean Square Error

SBA Santa Barbra Amorphous

SSE Sum of Square Error

SST Sum of Square Total

TEOS Tetraethyl Orthosilicate

TGA Thermogravimetric Analysis

TMOMS Trimethoxymethylsilane

Chapter 1

Introduction

1.1 Motivation

Air pollution of greenhouse gasses has a significant impact on the environment and the public health [1]. As we have reached the third decade of this millennium, it has become clear that today's generation must face a major challenge to reduce greenhouse gas emissions to the environment. At the same time, the industrialisation continues its unstoppable progress. Economic development, modernization, urbanization and rapid human population growth have led to an increasing global energy demand, and it is assumed to increase even more the coming years [2]. In 2018, fossil fuels such as oil, gas and coal contributed with 85% of the total energy demand in the world, while on the other hand, 11% of the total energy demand was generated from renewable energy sources, including biomass and waste [3].

Generation of energy is a major driving force to air pollution, and it is expected that fossil fuel will be used as an energy source the coming years in order to keep up with the increasing energy demand [2]. Emissions of greenhouse gas, such as carbon dioxide (CO_2), from an increasing number of fossil fuel power stations and its contribution to global warming has raised concerns [4]. Today, the average global atmospheric concentration of CO_2 is around 412 ppmv. This number has increased dramatically since the pre-industrial period when it was 280 ppmv [5]. The Paris Agreement aims to make a global response in order to keep the global temperature rise below 1.5 ℃ compared to pre-industrial temperatures. However, with the current global climate policies it is expect that the global temperature will increase with 2.8-3.2 ℃ [6]. A reduction of

greenhouse gases will require urgent and rapid political actions. One solution to combat global warming and climate change may be carbon capture and storage (CCS) [7].

The CO_2 emissions from a fossil fuel combustion processes can be captured either before burning the fuel (pre-combustion capture), after fuel burning (post-combustion capture) or by burning fuel in pure O_2 causing flue gas with a high concentration of CO_2 [8]. Compared to pre-combustion and oxy-fuel combustion capture, post-combustion capture units can be implemented to an already existing fossil fuel power station with little retrofitting. The unit will reduce the emissions by separation of CO_2 from flue gas, which will prevent CO_2 from being releasing to the environment [9]. CO_2 capture from flue gas is a research field with many recent publications, and the technology is rapidly developing. The most promising industrial process for CO_2 capture at pulverized coal-fired power stations is the aqueous amine process for regenerative absorption of CO_2 [10]. However, due to high volumetric flow rates of flue gas with low CO_2 partial pressures and a temperature range of 100-150 ℃, creates major concerns associated with this process. [11]. Due to the large cost and efficiency penalties involved when the process is applied for reducing greenhouse gas emissions, makes it not a sustainable process in an economic point of view [12]. Especially energy consumption is a critical factor in selecting the appropriate technology for CO_2 capture. Therefore, new CO_2 capture technologies are fast developing as a result of the many disadvantages with the current technology.

CO_2 capture on porous solid-supported amine sorbents is fast developing, and it is considered to be a promising alternative to the aqueous amine process. These sorbents consist of amine functional groups that are either grafted or immobilized to the surface of the support. The active amine sites will behave similarly to aqueous amine solution and adsorb large quantities of CO_2 and being regenerative. This CO_2 capture technique has a great advantage because of the lower energy consumption, easier regeneration and good cyclic adsorption/desperation stability. It has also been shown that solid amine sorbents have high CO_2 capacities at low partial pressures of CO_2 and low regeneration temperature. [13].

1.2   Objective

Capturing CO_2 form flue gas by solid-supported amine sorbents seems like a promising technology. It has already been reported about sorbents with excellent ability to capture CO_2 under flue gas conditions [11, 14]. Although it is a promising technology, little research has been done on mesoporous silica spheres (MSS) modified with polyethylenimine (PEI).

The main objective of this master thesis is to optimize PEI impregnated MSS for low-temperature CO_2 capture to achieve high CO_2 adsorption capacity, good cyclic stability and improve the adsorption kinetics. Kinetic adsorption models has been developed, and valuable kinetic parameters can be estimated by the fitting of the experimental adsorption data at different adsorption conditions. This can be used to understand the kinetics and the reaction mechanism of these sorbents, and also be used as a tool for realizing this CO_2 capture technology into a commercial scaled process.

Chapter 2

Literature Review

The background and the motivation for the performance and kinetic study of carbon capture on amine impregnated mesoporous silica spheres (MSS) became clear in the previous chapter. Carbon capture on solid sorbent is a promising technology which can provide an additional tool in the mitigation of climate change. This chapter explains the climate change challenges the world is facing and gives a broad overview of different technologies for low-temperature CO_2 capture reviewed in the literature.

2.1 Climate Changes

Climate change is caused primarily by global warming, which has harmful consequences on the environment as well as biological and human systems on this planet [15]. A global temperature rise leads to a warmer ocean, glaciers that are melting and rising sea levels. Greenhouses gases contributes to global warming and they are mainly water vapor (H_2O), carbon dioxide (CO_2), methane (CH_4), nitric oxide (NOx) and ozone (O_3) [16]. A rapid increase of the atmospheric concentration of greenhouse gases is a result of the unstoppable progress of the industrialisation and the global increasing energy demand. It is commonly known that human activities, such as energy generation from fossil fuels, increase the atmospheric concentration of greenhouse gasses [2]. The emissions from fossil energy sources will act like an addition of greenhouse gas to the Earth's self-balancing natural systems, which will put extra pressure on the Earth's system and influence the energy balance known as greenhouse effect [17].

Radiative forcing is a term used to measure the change in the Earth's energy balance, and it is described as the difference between the solar energy absorbed by the Earth and the energy radiated back to space [18]. Climate forcing occurs when there is a change to the Earth's radiative equilibrium, which will allow the global temperature to fall or rise over a more extended period. When Earth radiates less energy to space than it has received from incoming sunlight energy, the radiative forcing becomes positive, and this extra energy will cause temperature rise. A zero radiative forcing is a system in thermal equilibrium. The greenhouse gasses mentioned above influence the Earth's radiative forcing and is a driving force to make the total radiative forcing positive. And as the Intergovernmental Panel on Climate Change (IPCC) stated, the rapid increase of the average global atmospheric concentration of CO_2 is the most significant contributor for a positive radiative forcing [18].

2.2   Global Atmospheric Concentration of Carbon Dioxide

The average global atmospheric concentration of CO_2 has rapidly increased since the pre-industrial period. Measurements taken shows that CO_2 concentration in the atmosphere has increased from 280 to 412 ppmv, in less than 300 years [5]. The atmospheric CO_2 concentration over the last decades is illustrated in Figure 2.1.
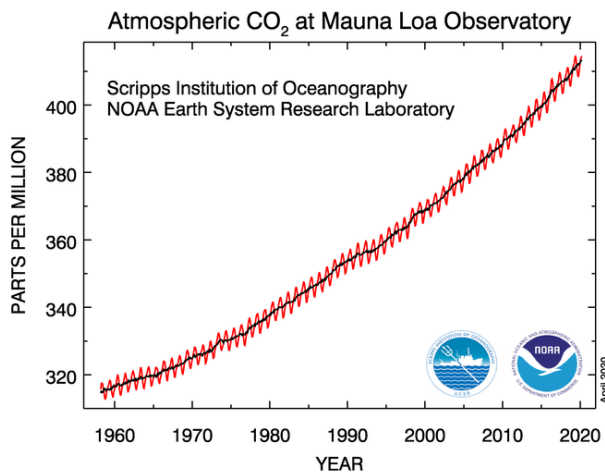
Figure 2.1: Atmospheric concentration of CO_2 from Mauna Loa as a function of years [19]

Human activities such as the burning of fossil fuels for energy generation, industrial processes and transportation are the major contributor to the increasing CO_2 emissions [2]. In 2014, these activities were responsible for 90% of the global CO_2 emissions. The total global emissions has increased to over 36 billion tonnes of CO_2 in 2017, compared to 2 billion tonnes of CO_2 in 1900 [20].

2.3 Sources of Carbon Dioxide

Economic development, modernization, urbanization and rapid human population growth have to lead to increasing global energy demand, and it is the main reason why the CO_2 concentration in the atmosphere has increased [2]. 85% of the world's total energy demand was generated by the combustion of fossil fuels in 2018, and the power and industry sectors are therefore responsible for a big part of the CO_2 emissions [3]. The CO_2 emissions in 2014 by sector or by source are illustrated in Figure 2.2, and it clearly shows that almost 70% of the world's CO_2 emissions came from the electricity and heat production sector, in addition to, the manufacturing industries and construction sector. The transport sector, where fossil fuels are combusted in smaller engines is the second-largest contributor to CO_2 emissions. Although they are smaller sources, such as a simple car engine, they are still responsible for 20% of the global CO_2 emissions. In order to reach the global target and keep global warming below 1.5 ℃, the emissions of CO_2 must be reduced drastically. Luckily, CO_2 capture plants are already in use, and the emissions are being captured.
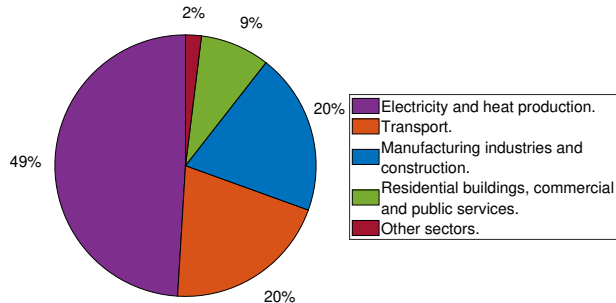
Figure 2.2: World's CO_2 emissions by sector [20].

2.4 Carbon Dioxide Reduction

Limitation of Earth's natural resources and global warming due to greenhouse gas emissions has raised concerns worldwide [4]. However, this awareness is also a driving force for innovation and development of new technology to make the already existing processes less polluting and more efficient. A study by Goeppert et al. [21] suggested three approaches to reduce the CO_2 emissions: Emitting less, sequestering or utilizing. Newly developed technology make current processes more energy-efficient, allows them to use different fuels or even switching towards renewable energy sources, which results in less CO_2 emissions. Capturing CO_2 from flue gas and store it, or utilize it, is also an approach to avoid release of large amounts of CO_2 into the atmosphere from the energy-demanding industry. This process capturing CO_2, transport it and utilize it or deposit it somewhere it will not emit into the atmosphere, usually in a geological formation [22].

2.4.1 Carbon Capture and Storage

As mention in the previous section, carbon capture and storage (CCS) is one of the most promising approaches in order to reduce greenhouse gas emissions to the atmosphere. The carbon is referred to as the CO_2, which is emitted from large point sources such as power generation from burning oil, coal or gas and manufacturing of cement and other industrial processes [3]. CCS-technology contains three basic steps: Separation of CO_2 from flue gas, transportation of CO_2 and storage under the Earth's surface. In this way, CCS can be referred to as carbon recycling as the CO_2 returns to were it came from, underground [22]. There are four main methods for CO_2 separation: Membrane separation, absorption by liquids, adsorption by solids and cryogenic distillation [23].

2.4.2 Carbon Capture and Utilization

So far, CO_2 has been mention as a threat to the environment and as the responsible component to global warming. CO_2 is also a vital gas to life on Earth and an important component for many industrial processes such as methanol production, fuel synthesis, bio-fuel and plastic production [24]. Carbon Capture and Utilization (CCU) aims to use the captured CO_2 as a resource and convert it into other products or substances with higher economic value instead of permanent geological storage of the component [25]. However, the carbon footprint for CCU does not result in zero emissions to the atmosphere, and a variety of important factors needs to be taken into account. Since the process to make new products will require more fuel, it should not exceed the amount of energy released from burning fuel. Also, production of products was CO_2 is one of the reactants demand much energy since the CO_2 molecule is a thermodynamically stable form of carbon [26]

2.5   Carbon Dioxide Capture Approaches

For a power generation plant, there are three main approaches for implementing a carbon capture unit: Pre-combustion, Oxy-fuel combustion and Post-combustion CO_2 capture. The optimal solution of carbon capture is based on the approach's advantages and disadvantages, in addition to, the flue gas conditions. CO_2 concentration, temperature and the pressure of the gas stream are some important conditions parameters [27].

Pre-combustion Carbon Dioxide Capture

Fuel reacts with water and oxygen in a pre-combustion CO_2 capture process. The carbon in the fuel is converted to CO and CO_2, and H_2 is produced simultaneously. Water-gas shift reaction form CO_2 and H_2 when CO reacts with water (Figure 2.3). The composition of the mixed gas will then be approximately and 20–40% CO_2 and 60–80% H_2 [28]. An advantages of pre-combustion CO_2 capture is the production of H_2, which is a so called green energy source. H_2 can be used in many areas such as Chemical industry, fuel batteries, aerospace industry etc., and the combustion of H_2 only generates water and no waste gas [29].
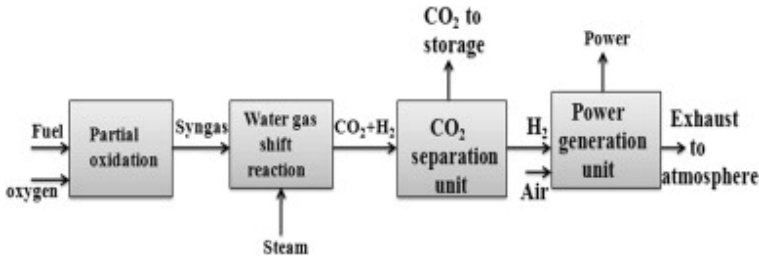
Figure 2.3: Principle of pre-combustion process [8].

Oxy-fuel Combustion Carbon Dioxide Capture

Fuel burns in pure oxygen in an oxy-fuel combustion CO_2 capture process. A consequence of burning fuel in pure oxygen is high CO_2 concentration in the flue gas, which make the purification of CO_2 much more accessible than, for example, in the post-combustion process [30]. The NOx concentration in the flue gas will also be lowered. Another advantage of Oxy-fuel combustion is the high temperature in the flue gas. In order to recover waste heat, the flue gas is often recycled back to the combustor, as shown in Figure 2.4. It is necessary to recover as much heat as possible since an oxy-fuel combustion CO_2 capture unit would reduce the efficiency of a coal-fired power station by 10-12%. The energy penalty caused by the separation of air, purification and compression of

CO_2 needs to be minimized by heat integration and process optimization [27].
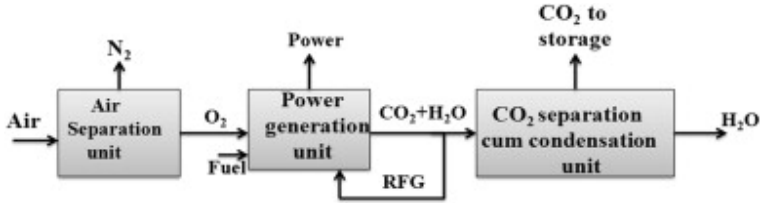
Figure 2.4: Principle of oxy-fuel-combustion process [8].

Post-combustion Carbon Dioxide Capture

Fuel burns in air in a post-combustion CO_2 capture process, and the concentration of CO_2 in the flue gas is typically around 4-14% [27]. Due to the low concentration, separation of CO_2 from flue gas is challenging and may result in great energy demand. For one of the most researched post-combustion CO_2 separation technologies, the regeneration of the absorption solvent, monoethanolamine (MEA), require around 80% of the total energy consumption, and it varies from 3.0 to 4.5 MJ/kg CO_2. However, the CO_2 capture unit can be added to existing power stations with little retrofitting compared to pre-combustion and oxy-fuel combustion CO_2 capture units, illustrated in Figure 2.5 [27]. A full scale post-combustion CO_2 capture unit for coal-fired power station is already in use in Canada [31].
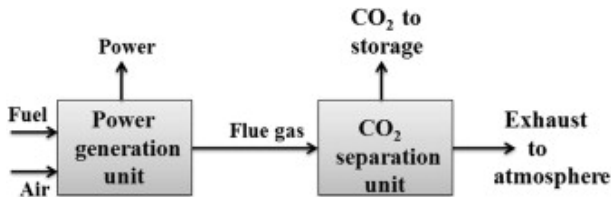
Figure 2.5: Principle of post-combustion process [8].

2.6   Carbon Dioxide Separation Technologies

It is essential to understand the aspect of the process conditions before going into specific materials and technologies that are capable of capturing CO_2. A sorbent used in a post-combustion CO_2 capture unit must be capable of capturing CO_2 at low temperatures (< 200 °C), low partial pressure of CO_2 and in the presence of moisture [11, 14]. In addition, it must also have high selectivity towards CO_2, good adsorption capacity and be highly stable. From an economic point of view,

the sorbent must be easily regenerated at low energy consumption in high CO_2 partial pressure, remain high stability, and finally, easy to scale up for industrial use. Summarizing the most important characteristics:

- High selectivity towards CO_2.

- Resistant to moisture.

- Acceptable adsorption capacity.

- Good cyclic stability.

- Fast kinetics.

- Easy to regenerate at low energy requirement.

- Scalable for industrial use.

There are several sorbent materials, both liquids and solids, that are capable of separate CO_2 from flue gas, and they can be divided into four groups: Aqueous absorbents, physical adsorbents, chemical adsorbents and membranes [10, 14, 32]. Today, most CCS-research tends to be dominated by aqueous amine-based chemical absorption technologies and Kohl at al. [10] gives an overview of this technology. Due to some disadvantages with this process, research on CO_2 capture by solid sorbent is fast developing and Wang et al. [32] discuss a great variety of solid sorbents. Selective membranes for CO_2 capture is a relatively new concept [8] and will, together with the other sorbents, be discussed bellow.

2.6.1 Aqueous Amine Absorption

Separation of CO_2 by chemical absorption is widely used in the chemical industry as well as in petroleum and coal-fired power plants. The process consists of an absorber where aqueous amine solution reacts with CO_2 from flue gas and a regenerator where the CO_2 is released. The absorber and regenerator are working continuously. There exists a variety of amine solutions for aqueous carbon capture, such as monoethanolamine (MEA), diethanolamine (DEA) and methyldiethanolamine (MDEA). MEA is often chosen as the absorbent because of its good CO_2 absorption capacity, high reaction rate with CO_2 and its relatively low cost [14, 33]. In the absorber, CO_2 and MEA react and form carbamic acid, RNHCOOH, as shown in reaction 2.1. Carbamic acid will further react with MEA and form carbonate, $RNHCOO^-$ (reaction 2.2) [34].

$$RNH_2 + CO_2 \rightleftharpoons RNHCOOH \tag{2.1}$$
$$RNH_2 + RNHCOOH \rightleftharpoons RNHCOO^- + RNH_3{}^+ \tag{2.2}$$

The reaction mentioned above is a reversible exothermic acid-base reaction between the amino-group and the CO_2 molecule. Therefore, regeneration of the CO_2-rich amine-solution can done by adding heat to the solution, forcing reaction 2.1 and 2.2 to go in opposite direction, and CO_2 being released. This process is currently the most efficient method for post-combustion CO2-capture [14]. The process for a typical amine absorption and regeneration system designed for a post-combustion CO_2 capture is illustrated in Figure 2.6.
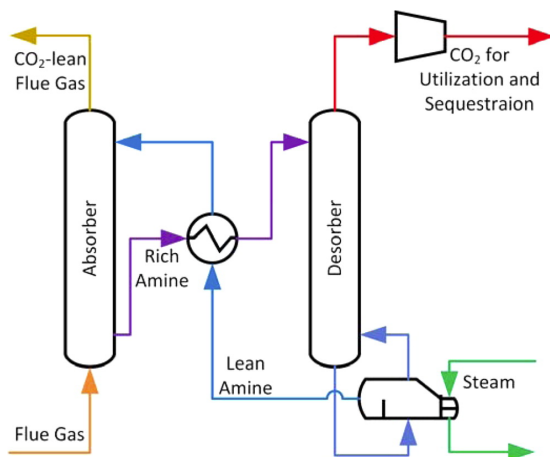
Figure 2.6: Amine absorption process for post-combustion CO2 capture [14].

CO_2 containing flue gas and lean amine solution reacts as the gas flows upwards and the solution flows downwards in the absorber. Amine-groups in the solution react with CO_2 from the flue gas, and the solution becomes CO_2-rich as it reaches the bottom of the absorber. The CO_2-rich amine solution gets heated by a heat exchanger before it enters the desorber column and CO_2-lean flue gas leaves the absorber-tower. In the desorber column, CO_2-rich amine solution gets heated up, and the adsorbed CO_2 is released from the solution and sent to compression. The regenerated amine solution is sent back to the absorber [14].

The downsides of aqueous amine absorption are closely related to the regeneration of the amine-solution. The 30 wt% MEA-solution has high CO_2-adsorption efficiency, but it requires a large amount of energy to heat the solution for

regeneration. The high temperature in the desorber may also cause thermal degradation by the formation of larger molecules in the absorbing solvent. The degradation will lower the CO_2 absorption capacity [14]. In addition, many other issues, such as equipment corrosion, amine loss due to solvent evaporation from the desorber causes environmental concerns may also occur when the temperature of the amine-solution is high [35].

2.6.2 Membrane Separation

Separation of CO_2 form flue gas using a selective membrane is a relatively new concept. Membranes can separate component by various mechanisms due to their semi-permeable barrier. These mechanisms may be ionic transport, molecular sieve and solution/diffusion or adsorption/diffusion. The material of the membrane can be porous or non-porous and made of organic material (polymers) or inorganic material (ceramic, carbon, metallic or zeolite). Membranes have a great advantage since it is energy-efficient, its straight forward application and it is environmentally compatible [8].

Gas absorption and gas separation are both illustrated in Figure 2.7 and are classified as the two membrane processes for CO_2 capture. Membranes developed for gas absorption consists of microporous solid material which is placed between the gas and the absorbent liquid flow, and work as a contacting device. Figure 2.7a shows the liquid phase absorbs CO_2 that has been separated from the flue and diffused through the membrane, which results in a high driving force at any instant. Due to the high driving force, gas absorption has a higher removal rate compared to gas separation, which consists of a porous material where one component diffuses faster through the membrane than the others. Permeability and selectivity are the main operational parameters when designing a gas separation membrane, and the difference in partial pressure and diffusivity of CO_2 molecules in the membrane is driving force for this separation process (Figure 2.7b) [8].

(a) Gas absoption membrane

(b) Gas separation membrane
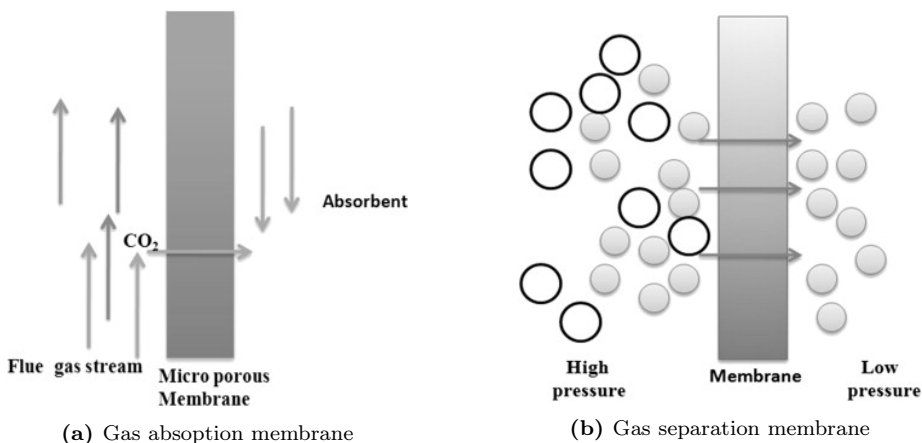
Figure 2.7: Working principles of CO_2 capturing membranes [8].

2.6.3   Physical Adsorption

The disadvantages with aqueous amine-based absorption process, such as high operational cost, a low contact area between gas and liquid and corrosion on equipment, has pushed the research on CO_2 capture to find other alternatives. CO_2 capture by solid sorbent is a relatively new concept, but this technology is fast developing, and many articles have already been published in the last decade. The CO_2 capturing sorbents may be organized according to their working temperatures: low-temperature (< 200℃), intermediate-temperature ($200 - 400$℃) and high-temperature (> 400℃) [36]. Most of the solid sorbent for physical CO_2 adsorption reported in the literature are mainly zeolites and activated carbon, but also ordered mesoporous silica and metal-organic frameworks have shown good carbon capture abilities. They are calcified as low-temperature sorbents [32, 37]. Due to their low costs, high surface area and the ease of regeneration, these sorbents are promising CO_2 capture candidates.

During physical adsorption, the attraction between the CO_2 molecule and the surface of the sorbent occur as they approach each other. This attraction is a result of van der Waals forces, but also electrostatic interactions can attract CO_2 molecules to the surface. Electrostatic interaction will only be significant if the sorbent has an ionic structure, while van der Waals forces will always be present [38]. Reaction 2.3 shows a general mechanism for physical adsorption of CO_2 on the surface of a solid sorbent and reaction 2.4 shows the attraction between a CO_2 molecule and a metal-ion (surface), which form an ion-dipole interaction.

$$CO_2 + Surface \;\rightleftharpoons\; (CO_2) \cdot Surface \qquad (2.3)$$

$$^{+\delta}O{=}C{=}O^{-\delta} \cdots ^{+\delta}(metal{-}ion) \qquad (2.4)$$
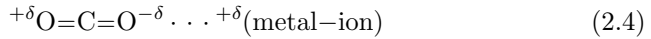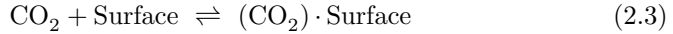
Activated Carbon

Activated carbon is a promising solid sorbent alternative for CO_2 capture due to their low cost, great availability, good thermal stability and low moisture sensitivity. Besides, these carbon-based sorbents have a high surface area which can absorb a great quantity of CO_2 molecules. However, in the temperature range of 50–120 ℃ activated carbon has shown poor CO_2 adsorption capacity, and these sorbents are designed to work best within high-pressure gasses. This indicate low selectivity toward CO_2 in operational conditions and high sensitivity in temperature [36]. To overcome these challenges, researchers are now focusing on improvement of CO_2 selectivity and adsorption capacity by improving pore structure and surface area of the sorbent, and also with chemical adjustments on the surface by increasing its alkalinity [37].

Zeolites

Zeolites are microporous, aluminosilicate minerals with a crystalline structure, and are commonly used as catalysts and adsorbents for industry applications. Their ability to adsorb specific components for gas purification has made zeolite a promising candidate for CO_2 capture from flue gas. Zeolites adsorb CO_2 by an ion-dipole interaction, illustrated in reaction 2.4, or bi-coordination creating strong bound carbonate specie. Zeolites have shown good ability to separate CO_2 from gases consist of multiple compounds and may be suited for pressure swing adsorption (PSA) process. However, the selectivity towards CO_2 over other gases, such as H_2, N_2, CH_4, is generally low and with increasing temperature above 30 ℃ their adsorption capacities rapidly decrease. To overcome these challenges, work on improving the zeolite's CO_2 capture performance is done by either changing the structure and composition, zeolite purity or exchange with alkali and alkaline-earth cations [32, 37].

Samanta et al. [11] and Yu et al. [37] have summarized the CO_2 capacity and operating conditions of various solid sorbents by physical adsorption, and some of them are listed in Table 2.1. The major drawback for most of the listed sorbents is low adsorption capacity due to low selectivity towards CO_2. Metal-organic framework and carbonaceous materials seem to reveal high adsorption capacities and could be promising CO_2 adsorbents. However, these sorbents are exposed to very low temperatures and high CO_2 partial pressure, which do not represent flue gas conditions. The silica-based sorbents have shown lower

CO_2 adsorption capacities and selectivity. However, these sorbents can be easily chemically modified due to their OH-rich surface. This modification enhances their CO_2 adsorption capacity and selectivity, and make them promising adsorbents for flue gas with low CO_2 partial pressure.

Table 2.1: Summary of CO_2 adsorption capacity and operating conditions for solid sorbents by physical adsorption [11, 37].

Sorbent					Operating conditions		
Type	S_{BET} $[m^2/g]$	V_p $[cm^3/g]$	d_p [nm]	Adsorption capacity [mmol/g]	Gas composition $[p_{CO_2}, bar]$	T [°C]	Method
AC	1762	-	-	1.66	-	25	TGA
Meso-Carbon	798	0.87	6.3	1.50	1.00	25	Ads. isotherm
SWCNT	1587	1.55	-	4.02	1.00	35	Ads. isotherm
MWCNT	407	0.45	23.5	1.73	0.50	20	Ads. isotherm
Graphene	1550	-	-	7.95	1.00	−78	Ads. isotherm
MCM-41	1229	1.15	2.7	0.14	0.15	75	TGA
MCM-41	1229	1.15	2.7	0.20	1.00	75	TGA
MCM-41	1229	1.15	2.7	0.62	1.00	25	TGA
MCM-41	1267	0.32	1.8	1.58	1.00	20	Ads. isotherm
SBA-15	950	1.31	6.6	0.11	0.15	75	TGA
As-SBA-15	345	0.71	8.9	0.05	1.00	75	TPD-TCD
SBA-15	725	1.12	9.3	0.04	1.00	75	TPD-TCD
SBA-15	802	1.31	7.7	0.50	0.10	25	Ads. isotherm
KIT-6	895	1.22	6.0	0.02	1.00	75	TGA
HMS	561	1.44	9.8	0.22	1.00	25	TGA
Meso-Al_2O_3	271	-	-	0.84	1.00	25	TGA
PMMA (Diaion)	470	1.20	14.0	3.40	1.00	45	TP-MS
NaX	-	-	-	5.71	1.00	32	TGA
NaY	-	-	-	5.50	1.00	32	TGA
NaM	-	-	-	2.95	1.00	25	TGA
Na-ZSM-5	-	-	-	0.75	1.00	30	GC
ZSM-5	-	-	-	0.32	0.10	40	GC

S = surface area; V_p = pore volume; d_p = pore size; p_{CO_2} = CO_2 partial pressure.

2.6.4 Chemical Adsorption

Chemical adsorption must not be associated with chemical absorption. Chemical absorption, like the aqueous amine absorption described in section 2.6.1, is a process where the bulk of a substance (i.e. aqueous amine) takes up another substance (i.e. CO_2). For chemical adsorption, accumulation and reaction of the substance occur on the surface, not in the bulk of the sorbent [39]. As mentioned in the preceding paragraph, researchers focus on the improvement of CO_2 selectivity and adsorption capacity by chemical modification of the surface and improve the physical properties of sorbent. Introducing a functional group into the pores of a porous material, such as silica-based or carbon-based material, will enhance its CO_2 adsorption capacity and selectivity. Due to the weak acidity of CO_2, researchers tend to focus on increasing the alkalinity of the surface by introducing alkaline chemicals, such as alkaline carbonates and amine group, as functional groups into the pores of the sorbents [14, 37].

Alkali metal

Dry alkali metal-based sorbents, represented as M_2CO_3, are suitable for CO_2 capture operations under low-temperature flue gas conditions due to their turnover temperatures through bicarbonate formation. M represents the alkali metal. At temperatures below 100 ℃, the alkali metal-carbonates form bicarbonate in the presence of H_2O and CO_2. During regeneration, an increase in temperature to 120-200 ℃ causes the bicarbonate to decompose and release a mixture of CO_2 and H_2O. Carbonation and decarbonisation of an alkali-metal carbonate-based sorbent are illustrated in reaction 2.5.

$$M_2CO_3 + H_2O + CO_2 \rightleftharpoons 2MHCO_3 \tag{2.5}$$

Research done on alkali metal-based sorbents has shown that CO_2 adsorption capacity of the K_2CO_3-based sorbents tends to be higher than Na_2CO_3-based and Li_2CO_3-based ones in the temperature range of 40-160 ℃[40, 41]. A study by Hayashi et al. [42] presented how temperature effects the efficiency of CO_2 uptake for the alkali carbonates at flue gas conditions of 13.8% CO_2 with 10% H_2O, see Figure 2.8. Li_2CO_3 was the most ineffective alkali carbonate, even at low temperatures. Na_2CO_3 showed good efficiency at lower temperatures, but decreased rapidly as the temperature got above 60 ℃ and $NaHCO_3$ unfavorably decomposed. For K_2CO_3, the efficiency also decreased at higher temperatures. However, it remained at 82% capacity at 100 ℃ .
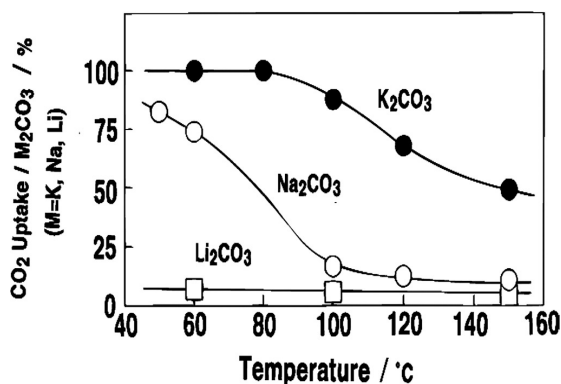
Figure 2.8: Effect of temperature on the efficiency of CO_2 uptake by alkali metal-based sorbents [42].

Despite the fact that alkali metal-based sorbents has shown promising CO_2 capture abilities, these sorbents tends to decrease its CO_2 capacity for cyclic

regeneration. Studies summed up by Samata et al. [11] shows that the surface of porous support plays an important role in enhancing cyclic stability. Okunev et al. [43] investigated different porous material loaded with K_2CO_3 and how it influence the CO_2 regeneration. The cyclic stability of the sorbents decreased in the sequence alumina > activated carbon > vermiculite > silica gel . In addition, a study by Lee et al. [44] found out that formation of $KAl(CO_3)_2(OH)_2$, $K_2Mg(CO_3)_2$ and $K_2Mg(CO_3)_2 \cdot 4\,(H_2O)$ occurred on the surface of Al_2O_3 and MgO support after regeneration at low temperatures ($<$ 200 °C). This indicated that K_2CO_3 were not completely converted to its original phase, which lowered the CO_2 capacity of the sorbents. For activated carbon and TiO_2 support loaded with K_2CO_3, regeneration was not a problem at even lower temperatures (130-150 °C).

Amine Adsorption

Like alkali metal-based sorbents, this kind of sorbents consists of a highly porous support material and a functional alkaline-group. In this case, the sorbent is loaded with basic organic amines, which will react with CO_2 from flue gas at low temperatures and enhance the CO_2 capacity of the sorbent. Due to the chemical reaction between CO_2 and the amine-group, it is of interest to know how the active amine-groups influence rate of CO_2 adsorption and the kinetics [11, 14]. The mechanism describing the interaction between the CO_2 molecules and the amine depends on the structure of the active amine-group. The structure of amines can be classified as primary amine, secondary amine and tertiary amine, and quaternary amine is sometimes included as well, depending on how many hydrogen atoms that are bonded to the nitrogen atom. Figure 2.9 shows the four amine functional groups. The reaction mechanism for primary and secondary amines consists of two steps. First, the carbon atom gets attacked by the lone pair of electrons on the active amine group and form zwitterions. In the second step, the zwitterion gets deprotonated by another amine-group and form carbamate. Tertiary amines and CO_2, however, do not react and form carbamate. Instead, they undergo a basic catalyzed hydration mechanism, which is then fixated by electrostatic attraction and van der Walls forces to form bicarbonate [45].

Primary amine   Secondary amine   Tertiary amine   Quaternary amine
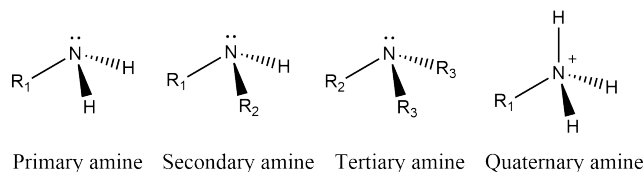
Figure 2.9: Amine functional groups.

Compared to the aqueous amine process, little research has been done on solid amine sorbents for carbon capture. Therefore, this technology is at a much less developed stage for industrial usages, and most of the research tends to be dominated by the development and characterisation of suitable support, and CO_2 adsorption capacity analysis of amine-functionalized sorbents. Mesoporous silica is a relatively recent development in nanotechnology and has shown great ability as support for active amine-groups due to their large pore volumes and high surface area. Large pore volume is favoured as it prevents the pores from becoming plugged by large the amine loadings [14]. The loading of amines into the pores of the support determines CO_2 adsorption capacities, and physical properties such as surface area and pore volume become critical factors. A large pore volume will handle a higher amine loading and give a higher CO_2 uptake. However, if the pore size of the support is too large, the amine may be lost during regeneration. Today, Mobil Composition of Matter (MCM-41) and Santa Barbara Amorphous (SBA-15) are the most common mesoporous silica on the marked [11].

Many types of amines are used to enhance the CO_2 adsorption capacity of a sorbent, and most research tends to be dominating by polyethylenimine (PEI), tetraethylenepentamine (TEPA) and diethanolamine (DEA) on silica or carbon support [11, 14]. Table 2.2 shows CO_2 capacity and operating conditions of various amine-based solid sorbents by chemical adsorption. Compared to physical adsorption, these sorbents show an overall higher CO_2 adsorption capacity. Even at low CO_2 partial pressure, amine impregnated sorbents tends to show good adsorption capacities and therefore have a higher selectivity towards CO_2 than unimpregnated sorbents.

Table 2.2: Summary of CO_2 adsorption capacity and operating conditions for amine-based solid sorbents [11].

Sorbent				Operating condition		
Support	Amine	Amine Loading [wt%]	Adsorption capacity [mmol/g](humid)	Gas composition [p_{CO_2}, bar]	T [°C]	No. of cycles
MCM-41	PEI	75	3.02	1.00	75	
MCM-41	PEI	50	2.05	0.10	75	
PE-MCM-41	DEA	77	2.93	0.05	25	
PE-MCM-41	DEA	73	2.81 (2.89)	0.05	25	
MCM-41	PEI	50	(3.08)	0.13	75	10
MCM-41	TEPA	50	4.54	0.05	75	6
SBA-15	TEPA	50	3.23	0.05	75	6
SBA-15	DEA + TEPA	50	3.61	0.05	75	6
SBA-15	PEI	50	3.18	0.15	75	
SBA-15	PEI	50	1.36	0.12	75	
SBA-15	APTES		(2.01)	0.10	25	
KIT-6	PEI	50	1.95	0.05	75	
monolith	PEI	65	3.75	0.05	75	5
mesoporous silica	PEI	40	2.40	1.00	75	
MC400/10	TEPA	83	5.57 (7.93)	0.10	75	50
precipitated silica	PEI	67	4.55	1.00	100	
R-IAS	E-100		(4.19)	0.10	25	
PMMA	TEPA	41	(14.03)	0.15	70	
PMMA	DBU	29	(3.00)	0.10	25	1
PMMA	DBU	29	(2.34)	0.10	65	6
PMMA (Diaion)	PEI	40	2.40 (3.53)	0.10	45	
SiO2 (CARiACT)	PEI	40	2.55 (3.65)	0.10	45	
Zeolite 13X	MEA	10	1.00	0.15	30	
Zeolite Y60	TEPA	50	(4.27)	0.15	60	20
β-zeolite	TEPA	38	2.08	0.10	30	

p_{CO_2} = CO_2 partial pressure.

Mesoporous silica was discovered in the late 1970s, and it has got much attention for its excellent physical properties such as ordered pore structures, large pore volume and high surface area [46]. Mesoporous silica spheres (MSS) is a new type of support and may be used for CO_2 capture. It has promising physical properties which can handle a large amount of amine loading and large amine molecules. From Table 2.2 it can be seen that PEI impregnated mesoporous silica (SBA-15) had a high CO_2 adsorption capacity of up to 3.18 mmol/g under dry conditions and low CO_2 partial pressure.

2.7   Adsorption Kinetics of Sorbents

Several different support material and amines have been reviewed in the preceding paragraphs. It has become clear that most of the research tends to be dominated by the development and characterisation of suitable sorbent, and its CO_2 capturing performance in the form of adsorption capacity. However, little research has been done on cyclic stability and adsorption kinetics. It is of great interest to find the adsorption/desorption kinetics of a sorbent for industrial applications. Kinetic parameters allow determination of time needed for completion of the adsorption and desorption process, also known as the residence

time. When residence time of a sorbent is known, the performance of a flow-through process, such as a fixed-bed reactor, can be determined and optimized [47].

Different kinetic models and the corresponding kinetics of the sorbents have been reported in the literature. Already in 1898, Lagergren developed the pseudo-first-order model for adsorption kinetics [48]. This model was the first adsorption capacity based rate equation for sorption in a liquid/solid system. Serna-Guerrero et al. [49] investigated adsorption of CO_2 on amine-functionalized mesoporous silica in 2011. It was the first to develop a kinetic model suitable for CO_2 adsorption on these sorbents. A year later, Heydari-Gorji et al. made a more general model to describe the kinetics of CO_2 adsorption on amine-modified mesoporous silica using a fractional-order kinetic model [47]. The kinetic models will be described in the Theory section. Table 2.3 summarize the different kinetic studies done on amine-modified sorbents [47, 49, 50, 51]. The studies showed that amine loading, CO_2 partial pressure, adsorption and desorption temperatures are critical parameters for CO_2 adsorption kinetics.

Table 2.3: Summary of CO_2 adsorption kinetics parameters and operating conditions for amine based solid sorbents.

Support	Amine (wt%)	T [℃]	Gas composition [p_{CO_2}, bar]	Kinetic model	n	m	k
MCM-41	PEI(30)	50	1.00	Fractional-order	1.74	0.53	0.09 [a]
MCM-41	PEI(30)	75	1.00	Fractional-order	2.00	1.54	1.24 [a]
MCM-41	PEI(30)	75	0.10	Fractional-order	1.38	0.98	1.42 [a]
MCM-41	PEI(30)	75	0.05	Fractional-order	1.20	0.88	0.74 [a]
MCM-41	PEI(50)	50	1.00	Fractional-order	1.45	0.34	0.003 [a]
MCM-41	PEI(50)	75	1.00	Fractional-order	1.80	0.96	0.23 [a]
MCM-41	PEI(55)	75	1.00	Fractional-order	1.78	0.69	0.134 [a]
MCM-41	PEI(55)	75	0.10	Fractional-order	1.30	0.61	0.18 [a]
MCM-41	PEI(55)	75	0.05	Fractional-order	1.20	0.68	0.30 [a]
SBA-15	TEPA(60)	30	0.10	Fractional-order	2.22	2.00	0.18 [b]
SBA-15	TEPA(60)	50	0.10	Fractional-order	0.039	1.55	0.039 [b]
SBA-15	TEPA(60)	75	0.10	Fractional-order	1.64	1.27	0.001 [b]
MMSV	PEI(40)	75	1.00	Pseudo-second-order	-	-	1.02 [c]
MMSV	PEI(50)	75	1.00	Pseudo-second-order	-	-	0.46 [c]
MMSV	PEI(60)	75	1.00	Pseudo-second-order	-	-	0.18 [c]
MCM-41	PEI(50)	25	0.05	Pseudo-first-order	-	-	$2.53 \cdot 10^{-4}$ [d]
MCM-41	PEI(50)	75	0.05	Pseudo-first-order	-	-	$6.81 \cdot 10^{-3}$ [d]
MCM-41	PEI(50)	25	0.05	Avrami	0.97	-	$2.35 \cdot 10^{-4}$ [d]
MCM-41	PEI(50)	75	0.05	Avrami	0.52	-	$2.96 \cdot 10^{-3}$ [d]

[a]$[g^{n-1} \ min^{-m} cg^{n-1}]$; [b]$[mmol^{1-m} \ g^{m-1} \ s^{-n}]$; [c]$[g \ mmol^{-1} \ min^{-1}]$; [d]$[s^{-1}]$

Chapter 3

Theory

In the previous chapter, carbon capture approaches and technologies were briefly described, in addition to, the importance of this technology in order to combat climate changes, and what materials used to separate CO_2 from flue gas. Amine-modified mesoporous silica sphere (MMS) were briefly motioned as a potentially suitable sorbent for CO_2 capture. To the best of the author's knowledge, no articles have been published to describe the performance and kinetics of CO_2 adsorption using amine-modified MMS. This thesis aims to identify and optimize the performance of the sorbents and purpose a kinetic model which is in good agreement with the CO_2 adsorption kinetics. This chapter explains the theory behind the synthesis of MMS, its physical properties and how to enhance CO_2 capture performance. For the modelling part, it will give a general explanation of the models and the modelling approaches.

3.1 Synthesis of Mesoporous Silica Spheres

Ströber et al. were the first group to develop a method for synthesis and growth control of nonporous monodispersed silica spheres from a water-alcohol and ammonia–tetraalkoxysilane system in 1968 [52]. Due to numerous applications in chemical areas, different preparation methods of monodisperse silica spheres are under continuous development. A resorcinol formaldehyde polymerisation with silica nanoparticles method can be used to produce MSS [53]. Previous master students from the catalyst group made most of the MSS support used in this master thesis. Since the objective of this thesis does not include development of MSS with excellent physical properties, the theory will not focus too much

on the MSS synthesis. However, one batch of MSS support is synthesised by the author of this thesis.

3.1.1 Resorcinol Formaldehyde Polymerisation

Resorcinol formaldehyde (RF) polymer has shown excellent properties as a carbon template in mesoporous silica synthesis as the polymer provide excellent large surface area, high porosity, large pore volume and good mechanical strength to the final silica support [53, 54]. The reaction mechanism for the RF polymerisation occurs in two steps: Resorcinol reacts with formaldehyde in a substitution reaction and form substituted hydroxymethylresorcinol. RF polymer is then formed by step-growth polymerisation where two hydroxymethyl-groups react and from an ether bridge (–CH2–O–CH2–) between the two hydroxymethylresorcinol molecules in a condensation reaction. Hydroxymethyl-groups may also react and form a methylene bridge (–CH2–) with non substituted resorcinol [54]. The reaction mechanism for the synthesis of RF polymer is illustrated in Figure 3.1
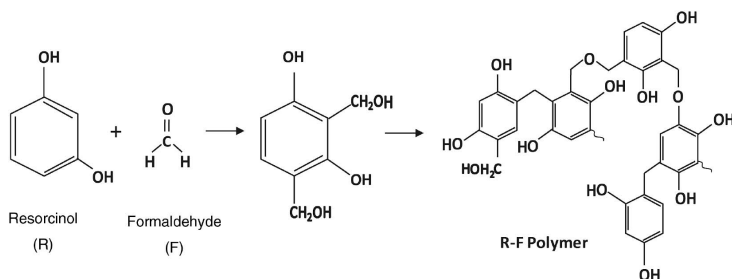
Figure 3.1: Reaction mechanism of rescorcinol-formaldehyde polymerisation [55].

Since the polymer particle size can be adjusted, the RF polymerisation is a critical step as it influences the physical properties of the silica support. During RF polymerisation, the size of clusters appears to be thermodynamically controlled. These clusters will undergo subsequent aggregation and form networks, which results in wet gels by further polymerisation [54]. Also, Lin et al. [56] showed in 1997 that it is necessary to have slightly alkaline conditions to obtain large pore volumes and high surface areas of the resulting gels. Adding colloidal silica nanoparticles to the RF solution provides alkaline condition, causing a much faster gelation rate for RF polymerisation and will also influence the RF polymer size (and shape). The pH adjustments help to control the polymer particle size and shape during the emulsification process [57].

3.1.2 Hard Templating Synthesis

In order to obtain a controlled mesoporous material, the hard templating synthetic procedure is a commonly used method due to its well known straightforward technique. In this method, the desired material (silica precursor) is structured by a template, RF polymer, which create a silica network with RF polymer inside its pores. Since the silica/RF polymer is a gel-phase, spheres can easily be formed by inverse emulsion sol-gel polymerization in an oil medium. The final mesoporous material is completed after the RF polymer template is removed. Carbon template can be removed at high temperatures where it reacts with oxygen and forms CO_2. Voids occur where the template used to be [58]. In other words, the pore system of the silica support is formed by the interstices between the colloidal silica nanoparticles [59].

In addition to its relatively easy straightforward technique, the hard templating method has another great advantage, which is pore size and pore volume controlling. The porosity can be controlled by two approaches: Either adjust the mass ratio of RF polymer and silica nanoparticles or change the size of silica nanoparticles (precursor). The pore size of the final product will increase with an increasing mass ratio of RF polymer and silica nanoparticles. Besides, larger silica nanoparticles create smaller pore size, but results in a higher pore volume of the mesoporous silica spheres [57].

3.2 Performance Enhancement

In order to enhance CO_2 adsorption capacity and cyclic adsorption/desorption stability of sorbents, a catalyst precursor can be impregnated into the pores, and layers of silica coating can protect the surface. Filling the pores with an amine will increase the number of active sites for CO_2 to react on, and layers of surface-coating may prevent lost of catalyst precursor during cyclic regeneration [60, 61].

3.2.1 Impregnation of Amine

As described in the literature review chapter, various amines have been tested as a catalyst precursor in mesoporous materials. Mesoporous silica modified with polyethylenimine (PEI) showed a high CO_2 adsorption capacity, and therefore a promising candidate for CO_2 capture, which will be further investigated in this thesis. There are different procedures on how to modify mesoporous materials with amines. Xu et al. [60] found out in 2003 that the wet impregnation method gave a higher adsorption capacity of the sorbent than, i.e. sorbent impregnated by the mechanic mixing method. In addition, most of the research done on amine-modified solid sorbents tends to be dominated by wet impregnation method as their impregnation procedure [11, 14, 45, 47, 50, 51].

The principle behind the wet impregnation method is that a specific volume of a solution containing the catalyst precursor comes in contact with the surface of the catalyst support. The imbibed solvent is then removed from the sorbent after a certain time of drying, leaving the final sorbent free from liquids [62]. Solvents also prevent air from being trapped inside the pores of the support during impregnation. If the pore size is large pressurized air can escape from the pores without bursting the structure of the support. However, for smaller pore sizes, the high capillary effect of the liquid will entrap the air inside the pores, resulting in high air pressure and may break the pore structure of the support [63].

Wet impregnation can also relate to diffusional impregnation since two phenomena are controlling the distribution of the precursor inside the pores of the sorbent: Fick's Law and adsorption capacity. Fick's Law describes the diffusion of the precursor into the pores of the sorbent, and the adsorption capacity of the surface and the adsorption equilibrium constant controls the total adsorption of the precursor onto the support [63]. Figure 3.2 illustrates the phenomena controlling the precursor distribution.
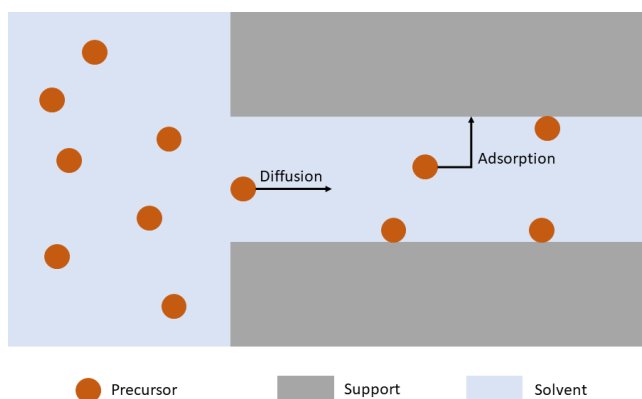
Figure 3.2: Physical transport phenomena involved in wet impregnation of a pore. The precursor migrates from solvent into the pore from the left to the right [63].

The balance between diffusion and adsorption determines the distribution of the precursor on the surface of the porous support during wet impregnation. The concentration of precursor in the solution decreases when they adsorb on the support surface. When the concentration decreases, the diffusion of the precursor decreases as well because of a lower driving force. With a high precursor concentration in the solution outside the support, it is possible to enhanced diffusion. Also, to obtain adsorption equilibrium in a sorbent of radius r, the time τ required is proportional to r^2, which means that by doubling the size of

the sorbent, the time to reach equilibrium quadruples. The wet impregnation method under diffusional conditions is a slow process as may take several hours [63].

3.2.2 Chemical Reaction Between Carbon Dioxide and Amine

Active amine groups are used as catalyst precursor to enhance the CO_2 adsorption capacity of solid sorbents [11, 14]. For this thesis, branched PEI is impregnated into mesoporous silica spheres support.

Polyethylenimine

PEI comes in many varieties, and can be large polymer with repeating units of amino groups linked together with carbon aliphatic CH_2CH_2 bridges. Branched PEI 800 MW (Figure 3.3) contains primary, secondary and tertiary amino groups in approximately 25/50/25 ratio [64], in contrast to linear PEI, which only contain secondary amines. Both branched and linear PEI can be used for carbon capture.
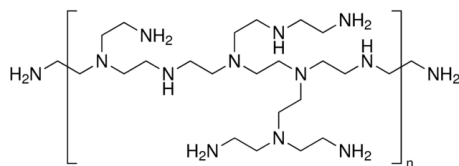
Figure 3.3: Chemical structure of branched polyethylenimine [64].

Chemical Reaction Mechanism

Under dry conditions, previous studies have reviled that CO_2 adsorption by amine impregnated solid sorbent follow an anionic and cationic mechanism. CO_2 reacts with either a free primary amine or secondary amine and form an intermediate product called zwitterion [65]. This intermediate has both positively charged and negatively charged groups, but with an overall charge of zero. Next, the zwitterion reacts with another free amino group to form the carbamate, which is a basic-catalyzed deprotonation of the zwitterion [9]. On the other hand, tertiary amines need to be in presence in moisture to react with CO_2. Tertiary amines do not have a free proton, like primary and secondary amines, which contribute to the deprotonation step. Instead, protonated amines and OH^- are formed when tertiary amines react with water and bicarbonate-ion is formed when the OH^- attacks the CO_2 molecule under alkaline conditions. Protonated amines and bicarbonate ions will then create an ionic bond [9]. However, due to interactions between the intermediate zwitterions and tertiary

amines, tertiary amines may take part in the carbon capture reactions under dry conditions. The reaction mechanisms for primary, secondary and tertiary amines are shown in Figure 3.4.
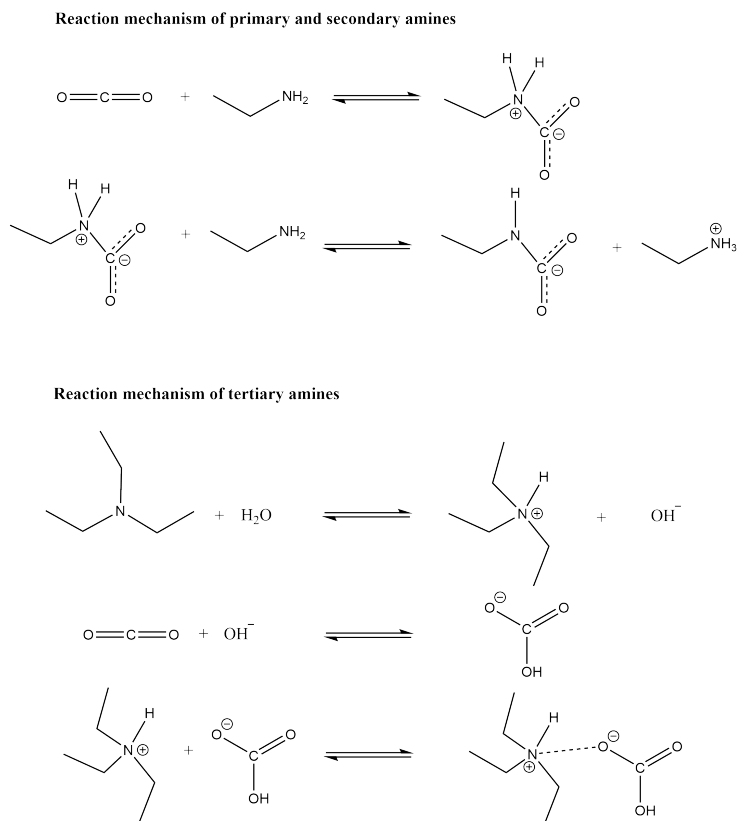
Figure 3.4: Reaction mechanisms between primary, secondary and tertiary amine, and CO_2.

Since two amine groups are needed to form carbamate, the equilibrium CO_2 adsorption capacities are limited to an amine efficiency of 1 mmol CO_2/2 mmol N in a reaction between CO_2 and a primary or secondary amine. In the presence of moisture, tertiary amines may reach an amine efficiency of 1 mmol CO_2/mmol N [66].

3.2.3   Sorbent Coating - a Protective Layer

The loss of catalytic activity, selectivity and stability over time, also known as catalyst deactivation, is a problem that causes concerns in industrial catalytic processes. Billions of dollars are paid by the industry each year for catalyst

replacement and process shutdown due to catalyst deactivation [67]. Therefore, it is a great interest to develop methods to enhance the catalytic activity, selectivity and stability.

Amine impregnated solid sorbents tends to suffer from cyclic adsorption/desorption stability issues due to the loss of amine through evaporation [11, 14]. A higher number of adsorption/desorption cycles and a high operating desorption temperature results in more reduced stability of CO_2 adsorption capacity. Silicate, such as Tetraethyl ortosilicate (TEOS), has been used to coat layer(s) of SiO_2 on carbon nanofiber (CNF)/carbon felt (CF) catalyst in order to improve its stability during Fischer–Tropsch synthesis [61].

In order to have a better understanding of the SiO_2-coating on the sorbent surface, the coating-mechanism needs to be explained step-by-step by the formation of intermediate products at different coating stages. In general, the generation of SiO_2 from a silicate occurs during the Stöber process, which can be described as:

$$\equiv Si-O-R_1 + H_2O \rightleftharpoons \equiv Si-OH + R_1-OH \tag{3.1}$$

$$\equiv Si-OH + OH-Si \equiv \rightleftharpoons \equiv Si-O-Si \equiv + H_2O \tag{3.2}$$
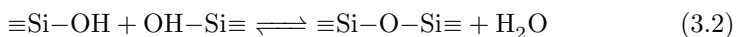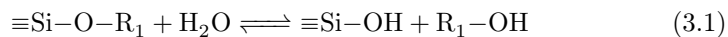
Reaction 3.1 describes the hydrolysis of silicate to form silanols and reaction 3.2 describes the condensation of silanols which generate silica. In this case, R_1 is either a methyl or ethyl group. OH^--ion attacks the silicon atom in both cases, which indicate that the two reactions are nucleophilic, and generation of SiO_2 will only occur in alkaline conditions with sufficient amount of OH-ions. During the condensation, generated silica will directly nucleate on the surface. A simplified mechanism for the SiO_2 coating on a surface, based on observations by Chen et al. [68], is given in Figure 3.5.

(a) Silanols diffusion to surface   **(b)** Nucleation of SiO_2.   **(c)** Growth of SiO_2.
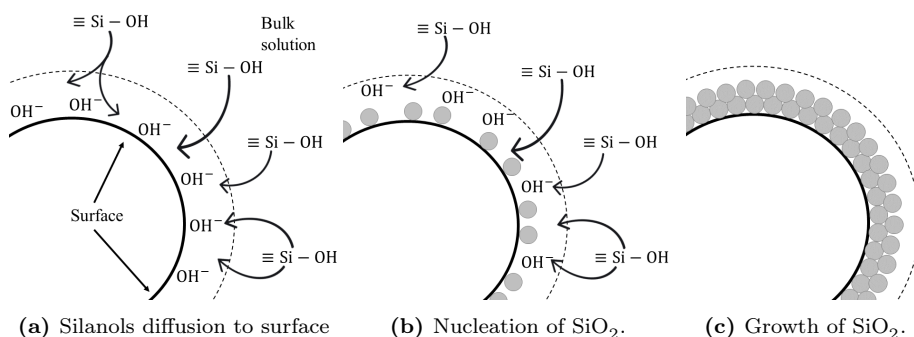
Figure 3.5: SiO_2 coating process on silica surface

As mention above, silicates are used as a precursor for SiO_2 through hydrolysis and condensation reactions. TEOS and trimethoxymethylsilane (TMOMS) are used as a precursor to cover the sorbent with silica in this thesis. TEOS has an excellent chemical structure for surface coating due to its four ethyl-groups attached to oxygen atoms surrounding the central Si-atom (Figure 3.6a). TMOMS has three methyl groups attached to oxygen atoms surrounding the central Si-atom, in addition to a methyl-group bounded directly to the Si-atom, see figure 3.6b. The amount of TEOS or TMOMS needed to cover on a gram of amine impregnated sorbent with one layer of SiO_2 was calculated using equation A.6 in appendices.

(a) Tetraethyl ortosilicate.   **(b)** Trimethoxymethylsilane
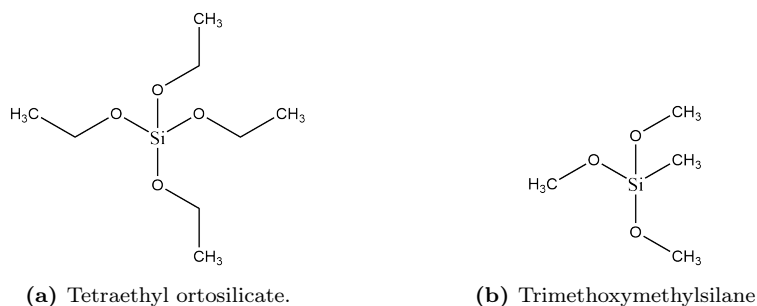
Figure 3.6: Chemical structures of silicate precursors.

3.3   Characterisation

The physical properties of the support and the sorbent, such as surface area, pore volume and pore size, affect its mechanical strength, CO_2 adsorption capacity, and its ability of PEI modification and silica coating. Different characterisation techniques can be done to measure these critical parameters.

3.3.1 Nitrogen Physisorption

Nitrogen physisorption is a method where the surface area, pore volume and pore size of porous materials can be measured by adsorption of nitrogen molecules on a solid surface. Catalysts are usually small particles since an efficient catalyst wants a large surface area. Therefore, it is of interest to know the surface area per unit of weight in order to get a better understanding of how good the dispersion of the active sites will be at the surface of the catalyst support. To prevent poor stability and sintering of catalyst during reactions, most of the heterogeneous catalyst on the market consists of inert support with active particles inside its pores [63, 59].

Silica support may offer pores with high internal surface area, thus the area inside the pores. In order to obtain internal surface area, it is essential to understand the difference between roughness and porosity of a surface: A surface is porous if most of the pores are deeper than they are wide, see Figure 3.7. Porous materials will have both internal and external surface area, while materials with roughness surfaces will only have external surface area [59].

(a) Porosity   **(b)** Roughness

Figure 3.7: The difference between porosity and roughness.

The principle of measuring surface area is simple: Take an inert gas, such as nitrogen or argon, physisorbed the gas molecules onto the surface of the material and determine how many molecules are needed to cover the surface with a monolayer. N_2 molecules will adsorb on the surface, and each molecule will occupy 0.162 nm^2 at 77 K. The surface area and pore size distribution follows directly. However, adsorption of N_2 molecules can occur beyond the monolayer and form multilayers [59]. In order to explain the relationship between the adsorbed nitrogen at given partial pressure and the adsorbed monolayer, it is necessary to review the Brunauer Emmett and Teller isotherm (BET isotherm) equation:

$$\frac{P}{V(P_0 - P)} = \frac{1}{V_m C} + \frac{(C-1)}{V_m C} \frac{P}{P_0} \tag{3.3}$$

where P and P_0 is the nitrogen partial pressure and the saturation pressure at 77 K, respectively. V_m is the volume of the adsorbed monolayer of N_2, and C is the BET constant. There are limitations to the BET method, and it is only valid under some assumptions including dynamic equilibrium between absorptive and adsorbate, molecules adsorb on similar adsorption site in the first layer, no adsorbate-adsorbate interactions and densely packed layers [59]. Depending on the interactions between the adsorbent and adsorbate, a plot of $\frac{P}{V(P_0P)}$ against $\frac{P}{P_0}$ will result in one of six different adsorption isotherms, see Figure 3.8a. Some of the isotherms have a point B. Before reaching this point, the surface is partially occupied by the N_2 molecules until the monolayer is filled (at point B). At higher pressures, a second layer starts to form, followed by multilayer formation. The adsorption isotherm allows calculation of specific surface area of a catalyst by showing the volume of gas adsorbed at monolayer, V_m and knowing the fact how much area a gas-molecule occupies. In addition, IUPAC has classified each of the isotherms [69]:

- Type I isotherms indicate microporous solids (pore size $\leq$ 2 nm)

- Type II isotherms indicate macroporous solids (pore size $\geq$ 50 nm)

- Type IV isotherms indicate mesoporous solids (pore size 2-50 nm)

- Type VI isotherms indicate argon or krypton graphitised on carbon.

Type III and Type V isotherms, however, are not very common. In addition, Type IV isotherm can further be analysed by its hysteresis loops, as shown in Figure 3.8. The loops occur due to capillary condensation in mesopores, and it appears in the multilayer range [69]. UPAC has also classified the hysteresis as following:

- H1 indicate mesoporous samples with uniform pores.

- H2 indicate complex network of pore structure for carbon activated samples.

- H3 and H4 indicate not well-defined mesoporous structure.

(a) Physisortion isotherms
(b) Hysterisis loops
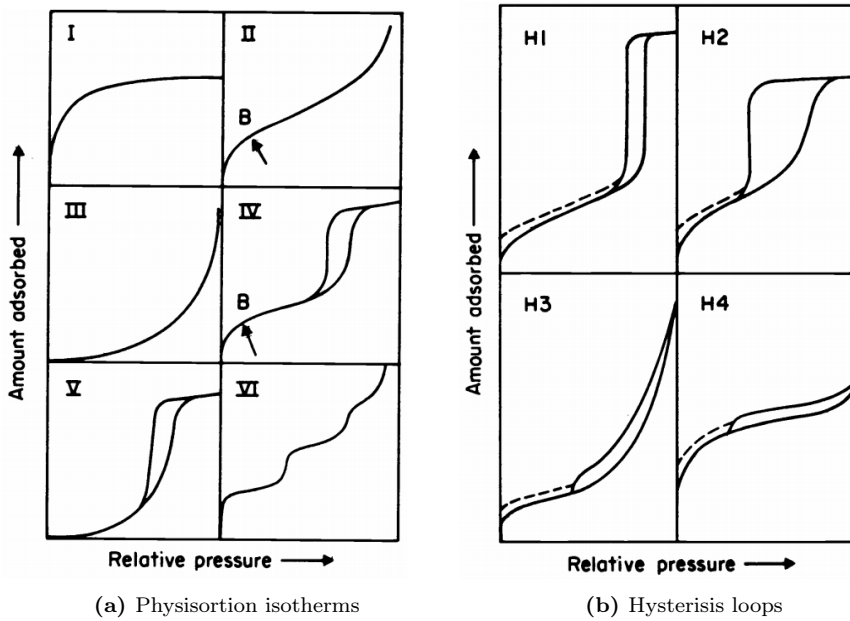
Figure 3.8: Six different types of adsorption isotherms and four types of hysteresis loops [69].

Barrett, Joyner and Halenda (BJH) model can be used for pore size distribution of a catalyst at high relative pressure to the adsorption- or desorption curve of the isotherms [70]. In small pores, the gas molecules may condense due to capillarity condensation. The condensation phenomenon is explained by the Kelvin equation:

$$ln\frac{P}{P_0} = -\frac{2\sigma V cos(\theta)}{r_p RT} \tag{3.4}$$

σ, V and θ is the surface tension of nitrogen, molar volume of nitrogen and the contact angle at 77 K, respectively, r_p is the pore radius, R is the gas constant, and T is the temperature. Rearranging equation 3.4 for r, makes it possible to find the pore size distribution, and then which types of pores: micropores, mesopores or macropores [59]. Although the BJH method is one of the most used models for calculation of pore size distribution, several assumptions need to be taken into account. Ertl et al. [70] listed the following assumptions:

- The Kelvin equation is applicable over the mesopore range.

- The meniscus curvature is controlled by pore size.

- The pores are rigid and of uniform shape.

- The distribution is confined to the mesopore range.

- There are no pore-blocking effects.

- Adsorption on the pore walls conforms to standard isotherm.

3.3.2   Thermogravimetric Analysis

Thermogravimetric analysis (TGA) is a method to measure the amount and rate of weight changes in a sample. TGA is done in a controlled atmosphere, and the results can be weight change as a function of time at isothermal conditions or as a function of increasing temperature. Due to decomposition, dehydration or oxidation of a sample, a TGA instrument can characterise the sample's weight change, in addition to, detecting phase changes. A typical maximum and minimum temperature range is usually from 25 ℃ to around 1000 ℃[71, 72].

Nitrogen and argon are typical inert gases used as balance gas, which enters into the TGA instrument to create an inert atmosphere around the balance. In order to obtain an oxidizing or reducing atmosphere, oxygen or hydrogen can be used instead of inert gases, respectively. Parallel to the balance gas, there is a sample gas entering from the bottom of the quartz tube, see Figure 3.9 and 3.10. This sample gas contains component(s) which can be absorbed by the sample, in this case, CO_2. Changing the flow rate of the balance gas and sample gas, while keeping the total flow rate constant, makes it possible to measure weight change at a different partial pressure of the adsorbate [71].
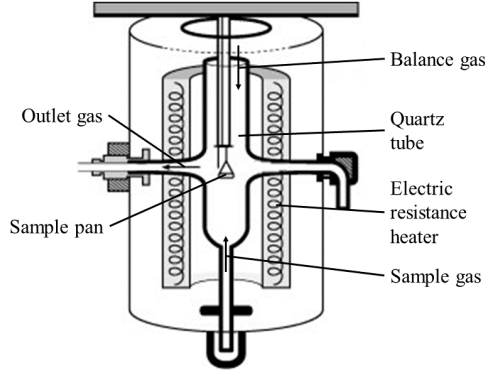
Figure 3.9: An apparatus schematic illustration of TGA Q500 [73].

TGA instruments measure and record temperature, sample mass and time. Therefore, the balance is one of the most crucial components as it records minimal changes in sample weight (< 0.0001 mg) during the analysis [72]. Figure 3.10 shows that the sample pan holder is connected to the balance from above. An adsorption and desorption analysis in a TGA instrument measure the mass of adsorbate the sorbent is capable of adsorbing at a given temperature, and how proper the regeneration of the sorbent is. Knowing the weight of the sorbent before adsorption (m_0) and the weight at adsorption equilibrium (m_e), makes it is possible to calculate the adsorption capacity of the sorbent, q_e:

$$q_e = \frac{(m_{e,i} - m_{0,i}) \cdot 1000}{m_{0,1} \cdot MW_a} \qquad i \in N \qquad (3.5)$$

where MW_a is the molar weight of the adsorbate, and N represent the number of the adsorption and desorption cycles. Stability measurement of adsorption capacities for solid sorbent, can be found by equation 3.6, where the $q_{e,1}$ and $q_{e,i}$ are adsorption capacities of cycle 1 and cycle i, respectively.

$$S_{CO2,i} = \frac{q_{e,i}}{q_{e,1}} \qquad i \in N \qquad (3.6)$$
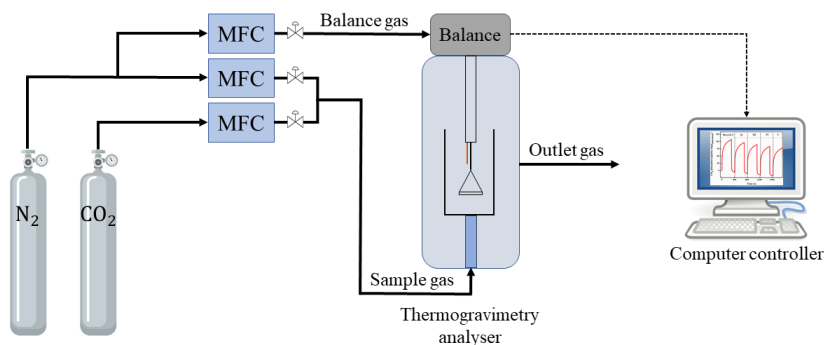
Figure 3.10: Schematic diagram of a TGA setup.

3.4   Kinetics

In real industrial application, fast adsorption kinetics are of high priory among the properties expected from an excellent solid sorbent for CO_2 capture. It is essential to understand and evaluate the kinetics of sorbents and the overall mass transfer in the CO_2 adsorption process. Both adsorption and desorption kinetics are necessary in order to do simulations and make a rational design of gas treating units for CO_2 capture [50].

Several molecular processes are coinciding during CO_2 adsorption on solid sorbents. Usually, a realistic diffusion-reaction process between CO_2 and a sorbent can be divided into five steps: CO_2 external diffusion, film diffusion, pore diffusion, solid diffusion and the chemical reaction with active amine sites [74]. Figure 3.11 illustrate all five steps. Detailed reaction mechanism models have been developed for kinetic modelling [75]. However, these models tend to be too complex for simulation and process optimization. In this master thesis, different kinetic models for CO_2 adsorption processes are compared against each other in order to see how good they fit experimental CO_2 adsorption of PEI-impregnated MSS.
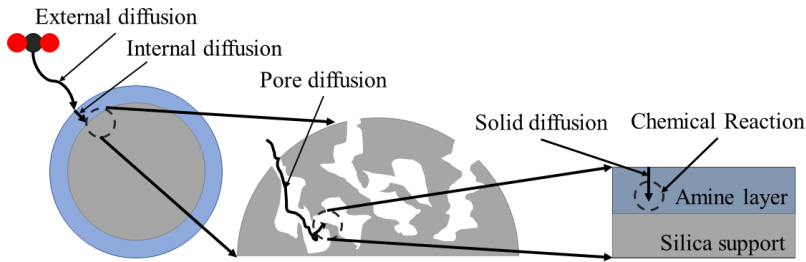
Figure 3.11: Five diffusion and reaction steps during CO_2 adsorption onto amine modified mesoporous silica.

3.4.1 Kinetic Models for Carbon Dioxide Adsorption

Pseudo-First-order Model

Back in 1898, Lagergren developed the pseudo-first-order model for adsorption kinetics [48]. This model was the first adsorption capacity based rate equation for sorption in a liquid/solid system, and it is still commonly used do describe adsorption rates. The model is given by equation 3.7:

$$\frac{\partial q_t}{\partial t} = k_{PFO}(q_e - q_t) \tag{3.7}$$

k_{PFO} is the adsorption rate constant for pseudo-first-order model, and q_e and q_t are the adsorption capacities at adsorption equilibrium and at time t, respectively. An integration of equation 3.7 with boundary conditions: $q_t = 0$ at $t = 0$ and $q_t = q_e$ at $t = \infty$, gives the integrated form:

$$q_t = q_e(1 - e^{-k_{PFO}t}) \tag{3.8}$$

Pseudo-Second-order Model

The pseudo-second-order model was presented and discussed by Ho et al. in 1999 [76]. CO_2 molecules occupy active amine sites during an adsorption process, and this model assumes that the number of occupied active sites is proportional to the adsorption capacity. The model is given by equation 3.9:

$$\frac{\partial q_t}{\partial t} = k_{PSO}(q_e - q_t)^2 \tag{3.9}$$

k_{PSO} is the adsorption rate constant for the pseudo-second-order model. Integration of equation 3.9 with the same boundary conditions as mention above gives the following expression:

$$q_t = \frac{q_e t}{\frac{1}{k_{PSO} q_e} + t} \tag{3.10}$$

Avrami's Model

A modification of Avrami's kinetic model of particle nucleation by Lopes et al. [77], resulted in a kinetic model for adsorption in 2003. This model provides a fractional reaction order, n, which can be used to describe the complex adsorption mechanisms associated with the multiple adsorption pathways that occur. The model is given by equation 3.11:

$$\frac{\partial q_t}{\partial t} = k_A^n t^{n-1}(q_e - q_t) \tag{3.11}$$

Where k_A is the adsorption rate constant. An integration of equation with the same boundary conditions as mention above gives the following expression

$$q_t = q_e(1 - e^{-(k_A t)^n}) \tag{3.12}$$

Modified Fractional-Order Model

A more general fractional-order kinetic model was developed by Heydari et al. [47], which had a goal to describe the adsorption rate of CO2 using chemical adsorption with active amine sites as a function of time. In this model, the nth power of the driving force and m^{th} power of the adsorption time is directly proportional to the absorption rate, and it is expressed by equation 3.13:

$$\frac{\partial q_t}{\partial t} = k_F t^{m-1}(q_e - q_t)^n \tag{3.13}$$

where k_F is the adsorption rate constant. For $n = 1$, equation 3.13 reduces to Avrami's equation, and reduces to pseudo-first-order or pseudo-second-order kinetic models when m = 1 and n = 1 or 2, respectively. Integration of equation with the same boundary conditions as mention above gives the following expression:

$$q_t = q_e - \frac{1}{\left[\,((n-1)k_F/m)t^m + (1/q_e^{n-1})\,\right]^{1/(n-1)}} \tag{3.14}$$

Dual Kinetic Model

The dual kinetic model was recently developed by Ohs et al. [78], and this model assumes that CO_2 uptake by the sorbent is a function of the current CO_2 loading. The total sum of adsorbed CO_2 at the surface, q_{sur}, and inside the bulk, q_{bulk}, defines the overall adsorption q_t. The model is given by equation 3.15:

$$\frac{\partial q_t}{\partial t} = \frac{\partial q_{sur}}{\partial t} + \frac{\partial q_{bulk}}{\partial t} \tag{3.15}$$

Furthermore, both q_{sur} and q_{bulk} represent adsorption capacities, but at different locations within the amine layer. A fractional-order kinetic model is used to describe q_{sur}, while the kinetic model for q_{bulk} take into account that CO_2 molecules may also react with the non-surface active amine sites (bulk amine layer). Therefore, it is assumed that the adsorption can be described as a reaction of a higher order. With this information, equation 3.15 can be presented as:

$$\frac{\partial q_t}{\partial t} = k_{sur}(q_e - q_t)^n + k_{bulk}q_t(q_e - q_t)^n \tag{3.16}$$

where k_{sur} and k_{bulk} are the adsorption rate constants for surface and bulk adsorption, respectively. Unlike Avrami's and fractional-order model, this model is not a time-dependent definition of the adsorption as there is no time parameter t in the model equation. Instead, the current CO_2 loading and the driving force are the main kinetic factors for this model. To derive the dual kinetic model, equation 3.16 can be rearranged to:

$$\frac{\partial q_t}{\partial t} = k_{DKM}(1 + \beta_{DKM} \cdot q_t)(q_e - q_t)^n \tag{3.17}$$

where k_{DKM} is the rate constant for the dual kinetic model and β_{DKM} is the ratio of k_{sur} and k_{bulk}. Integration of equation 3.17 with the same boundary conditions as mention above gives a complex solution. An ordinary differential equation (ODE) solver is therefor necessary to solve this equation, which will be introduced in the next chapter.

3.4.2   Modelling Approach

A good modelling approach is required when fitting experimental data of an adsorption process into a kinetic model. Model fitting may be a complex and challenging task due to several molecular processes coinciding, and it is necessary to simplify the model as much as possible without having a significant impact on actual physics describing the process. For these models, the ordinary differential equations (ODE) mentioned in the previous subsection are integrated with boundary conditions in order to find an equation describing the time-dependent CO_2 adsorption capacity, q_t, as a function of time. For complicated ODEs, an integration will lead to complex solutions. ODEs, like the dual kinetic model, can be solved with MATLAB's ODE solver function `ODE45`, which is MATLAB's standard solver for ODE's. In this solver use Runge-Kutta method, and for efficient computation, the time step is a variable. Equation 3.18 describes the problem the ODE solver will handle:

$$\frac{dx}{dt} = f(t, x), \qquad\qquad x(t_0) = x_0 \qquad (3.18)$$

x is a vector of unknown variables to be found, t is independent variable and $f(t, x)$ is the function of t and x. With given the initial conditions $x = x_0$ at $t = 0$, the mathematical problem is specified and $f(t, x)$ can then be found [79].

The kinetic and fractional-order parameters, k, n and m, can be obtained by utilizing the `lsqnonlin` function in MATLAB, which solves nonlinear least-squares (nonlinear data-fitting) problems of experimental data. In addition, MATLAB toolbox offers a Levenberg-Marquardt optimization algorithm which can be used in curve fitting of non-linear problems. Especially when fitting model functions to data, i.e., non-linear parameter estimation, minimization problems like these give excellent curve fitting. Compared to the Gauss-Newton algorithm, Levenberg-Marquardt optimization algorithm is more robust. Even if the starting point is far away for the minimum, it will find a solution in many cases [80, 81]. Appendix D shows the general MATLAB pseudo-codes used to solve these kinetic models.

Chapter 4

Experimental

4.1 Synthesis of Mesoporous Silica Spheres

The synthesis of MSS was based on a method developed by Wang et al. [57] using resorcinol and formaldehyde polymerisation and colloidal silica with inverse sol-gel emulsion in an oil medium. The synthesis can be divided into three steps: Resorcinol and formaldehyde polymerisation, washing and separation, and hard-templating removal.

4.1.1 Resorcinol and Formaldehyde Polymerisation

Span 80 (0.3 mL, Sigma-Aldrich) was added to Paraffin oil (300 mL, Sigma-Aldrich) and the solution was stirred with a rotation speed of 200 rpm and heated to 85 ℃. In parallel, resorcinol (12.96 g, 99%, Sigma-Aldrich) and formaldehyde solution (17.4 mL, 36.5-38% in H_2O. Sigma-Aldrich) were dissolved in distilled water (21 mL) with a rotation speed of 200 rpm in room temperature. Next, colloidal silica (21.4 mL, LUXOX SM@40) was added dropwise to RF-solution under stirring. After 40 minutes of mixing, the solution was added to the Paraffin oil and Span 80 solution. First, the mixture was stirred with a rotation speed of 200 rpm at 85 ℃ for 1 hour, then it was set in a catalyst preparation oven at 80 ℃ for 2 days.

4.1.2 Washing and Separation

After ageing, the hybrid hydrogel spheres were separated from the paraffin oil by filtration and washed with acetone. Acetone was added to the filtrated

spheres (the residue), and the mixture was then exposed to ultrasonic irradiation (Elmasonic S 60 H) for 1 hour. The spheres were then separated from the solvent by filtration. The filtration and washing step was repeated three times. Finally, the spheres were dried at 80 ℃ for 24 hours to obtain silica–carbon spheres.

4.1.3   Hard-Templating Removal

After drying, the silica–carbon spheres were exposed to 750 ℃ and air flow in a high temperature furnace. Heating rate were set to 1 ℃ per minute, and the temperature were set to be isothermal for 4 hours after reaching 750 ℃, before slowly cooling down.

4.2   Modification of Mesoporous Silica Spheres

4.2.1   Wet impregnation with PEI

Methanol (2 mL, Sigma-Aldrich) was added to the desired amount (equation A.2) of polyethylenimine (Sigma-Aldrich, branched MW 800). The solution was stirred with a rotation speed of 600 rpm at 35 ℃ for 30 minutes. A desired amount of MSS was added to the solution and stirred at 200 rpm at 40 ℃. When there was no visible liquid left (approximately 1.5 to 2 hours), the impregnated MSS were then dried at 40 ℃ overnight.

4.2.2   Sorbent Coating

In order to find the right amount of the coating precursor, from now on called X gram, equation A.6 was used. The equation gave the amount of silica precursor needed to cover 1 gram of sorbent with one layer of SiO_2. 2 different coating methods were tested:

Method 1

The desired amount of TEOS (X g, Sigma-Aldrich) was mixed with ethanol ($2X$ g, 96%, Sigma-Aldrich) for 7 minutes at room temperature with a rotation speed of 600 rpm. Distilled water (1.5 mL water/1 g sorbent) was then added to the solution and mixed for 30 minutes with a rotation speed of 600 rpm at 35 ℃. The desired amount of MMS was then added into the solution and the rotation speed was set to 50 rpm. After 1 minute, the pH of the mixture was controlled. If pH was less than 10, ammonia solution (25% AnalaR NORMAPUR®, VWR International) was added dropwise until pH reached 10. The mixture was stirred for 1 hour before it was separated by filtration and washed with distilled water. The sorbent was then dried at 45 ℃ for 6 hours.

The same procedure was done with colloidal silica (X g, LUXOX SM@40), instead of TEOS. However, due to the structure of colloidal silica, $\equiv$Si$-$OH, it was not necessary to preform a hydrolysis step. Therefore, colloidal silica was added directly to the mixture of distilled water ($3X$ g) and a desired amount of MMS.

Method 2

Distilled water (1 mL) and trimetoxylmetylsilane (X g, 98% Sigma-Aldrich) were mixed for 1 minute with a rotation speed of 600 rpm at room temperature. A desired amount of MMS was then added into the solution, and the rotation speed was set to 50 rpm. After 1 minute, the pH of the solution was controlled. If pH was less than 10, ammonia solution (25% AnalaR NORMAPUR®, VWR International) was added dropwise until pH reached 10. The mixture was stirred for 3 minutes before it was separated by filtration. The sorbent was then dried at 45 ℃ for 6 hours.

4.3 Catalyst Characterisation

4.3.1 Nitrogen Physisorption

Determination of surface area, pore volume and pore size of MSS support and modified MSS were done by physisorption of nitrogen. Samples of MSS were weighted (aimed for a total of $30m^2$ sample) and degassed in VACPREP 061 Degasser overnight at 200 ℃. Modified MSS was degassed at 60 ℃. The nitrogen physisorption of the degassed samples was subsequently performed the following day using TriStar 3000 Surface Area and Porosity Analyser. The installed program: *BJH Adsorption, 42 points, using Nitrogen* under *analysis condition*, was used during the physical properties analysis.

4.3.2 Thermogravimetric Analysis

CO_2 adsorption capacity and stability of amine-modified MSS were measured using a thermogravimetric apparatus (Thermogravimetric Analyser TA Instrument Q500). CO_2 gas balanced with N_2 gas was used to obtain different CO_2 partial pressures for the adsorption measurements under atmospheric pressure (see equation A.1). In a typical run, amine-modified MSS (around 12-16 mg) were placed in a platinum sample pan and loaded onto the sample pan holder in the TGA instrument. Each analysis started with a pre-treatment step for removal of unwanted compounds and moisture: The sample was exposed to pure N_2 gas with a total gas flow rate of 100 mL/min at room temperature for 30 minutes. The temperature was then raised to 100 ℃ and kept constant for 2 hours. After the pre-treatment, the temperature was set to wanted adsorption temperature and kept isothermal for 10 minutes. The feed of the sample gas was

switched to CO_2 containing gas. The adsorption conditions were kept constant for the whole adsorption step. After adsorption, the temperature was set to desired desorption temperature before the sample gas was switched back to pure N_2 gas. The desorption conditions were kept constant for the whole desorption step. The adsorption/desorption step was repeated N times for cyclic stability analysis. For all analysis, the total gas flow rate (sample gas + balance gas) was 100 mL/min, and the heating and cooling rate were set to 10 ℃/min.

Chapter 5

Results

The following chapter presents experimental results of characterisation, performance and the kinetics adsorption modelling of modified mesoporous silica spheres. All results are discussed in Chapter 6.

5.1 Nitrogen Physisortion

Nitrogen physisorption was used in order to characterise the physical properties of 5 batches with MSS support, impregnated MSS and coated MSS. BET and BJH method was used to estimate surface area, pore volume and pore size. All physical properties of these samples are listed in Table 5.1. MSS-1 to MSS-4 have all been synthesised by previous master students, in addition to, PEI impregnation of MSS-2 and MSS-4 [53]. The author of this thesis synthesised MSS-5.

The largest surface area was observed for MSS-4, while MSS-5 provided the smallest surface area of the tested MSS support. However, the supports have similar pore volumes, and the pore sizes were all being in the mesoporous size range. After impregnation of PEI, both the surface areas and pore volumes for all samples had shrunk. The largest surface area was observed for MSS-5 with 25 wt% PEI, while MSS-1 and MSS-2 provided the smallest surface areas of the tested amine impregnated MSS sorbents. Sorbent with equal amine loading (40 wt%) showed similar surface areas and pore volumes, but the pore sizes varied from 10 to 116 nm. After coating, the surface areas and pore volumes for the coated MSS-3 and MSS-5 samples had increased. MSS-2 showed similar properties as before coating. The largest surface was observed for MSS-3 with

40 wt% PEI, while MSS-2 provided the lowest surface area of the coated amine impregnated MSS. Silica coated MSS-3 and MSS-5, showed similar pore volumes and pore sizes. Due to shortage of amine impregnated MSS-1 and coated amine impregnated MSS-4 sorbents, MSS-1 samples were not coated, and nitrogen physisorption characterisation was not done on coated amine impregnated MSS-4.

Table 5.1: BET surface area, pore volume and pore size of MSS support, PEI-impregnated MSS and surface coated MSS from 5 different batches. Surface areas are estimated through the BET-method and BJH-model are used for pore volumes and pore sizes with nitrogen physisorption.

	Sorbent				
Silica support	PEI-loading	Coating-loading	BET Surface area	Pore volume	Pore size
Sample	[wt%]	[N layers]	[m^2/g]	[cm^3/g]	[nm]
MSS-1	-	-	117	0.46	14
MSS-2	-	-	98	0.49	17
MSS-3	-	-	114	0.45	14
MSS-4	-	-	137	0.51	14
MSS-5	-	-	73	0.40	22
MSS-1	40	-	2	0.03	116
MSS-1	30	-	9	0.12	56
MSS-2	40	-	2	0.02	102
MSS-3	40	-	3	0.01	35
MSS-4	40	-	4	0.01	10
MSS-5	40	-	5	0.03	34
MSS-5	25	-	16	0.10	29
MSS-2	40	1^a	3	0.04	112
MSS-3	40	1^b	51	0.32	18
MSS-5	40	2^c	36	0.23	24
MSS-5	25	2^c	42	0.27	22

[a] TEOS; [b] Colloidal silica; [c] TMOMS;

5.2 Catalyst Performance

5.2.1 Effect of Adsorption Temperature and Carbon Dioxide Partial Pressure

Thermalgravimetric analysis (TGA) was carried out in order to investigate the performance of the sorbents. MSS-3/40PEI showed a maximum CO_2 adsorption capacity around 75 °C after three different adsorption temperatures at 50 °C, 75 °C and 100 °C were investigated in 5% CO_2 gas (shown in Figure 5.1a). In addition, MSS-1/40PEI were exposed to different CO_2 partial pressures at 75 °C in order to see how it affected the CO_2 adsorption measurements. As seen in Figure 5.1b, at low CO_2 partial pressures, the adsorption capacity increased rapidly with small increment in CO_2 partial pressures. In the higher CO_2 partial pressure region, the sorbent became saturated.
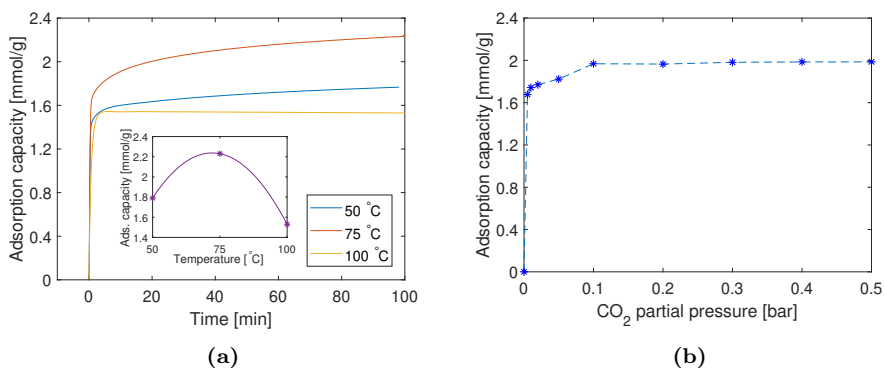
Figure 5.1: (a) Comparison of adsorption temperatures in 5% CO_2 gas on MSS-3/40PEI and (b) under different partial pressure of CO_2 at 75 °C on MSS-1/40PEI.

5.2.2 Carbon Dioxide Adsorption Capacity and Cyclic Stability

CO_2 adsorption capacities of the PEI impregnated MSS were compared and investigated in 5% CO_2 gas balanced with N_2 gas at 75 °C. For desorption, pure N_2 gas at 75 °C was used. A more detailed method is described in section 4.3.2. The CO_2 adsorption capacities for all sorbents are calculated by equation 3.5, and given in Figure 5.2. Among the modified MSS with the same PEI loading (40 wt%), MSS-3/40PEI was found to give the highest CO_2 adsorption capacity with 2.24 mmol/g, closely followed by MSS-5/40PEI.
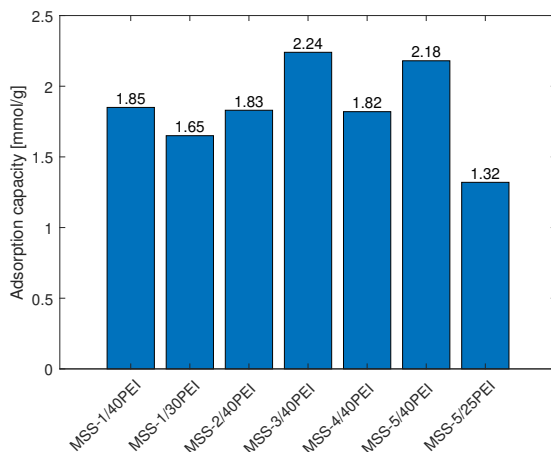
Figure 5.2: Comparison of CO_2 adsorption capacity on different batches of meso-porous silica spheres impregnated with PEI at 75 °C in 5% partial pressure CO_2 gas.

For practical application, the sorbents should also have a long term stable cyclic adsorption/desorption performance, not only a high CO_2 adsorption capacity. Ten adsorption/desorption cycles were done on each sorbent in order to get an idea of the cyclic stability. Equation 3.6 was used in order to find the cyclic stability, and Figure 5.3 presents the cyclic stability of the sorbent as a function of cycles. Cycle 1 was not included because of the high temperature used in the pretreatment step (see section 4.3.2). It was found that none of the sorbents lost more than 2% of capacity after nine cycles. MSS-3/40PEI lost 0.3% of the capacity, while MSS-1/40PEI increased its capacity with 0.3%. Lower PEI loading resulted in less stable sorbent.

For MSS-1 and MSS-4 sorbents, both adsorption and desorption lasted for 100 minutes each. However, due to time constraints, MSS-2, MSS-3 and MSS-5 sorbents had shorter adsorption/desorption cycles (60/60 minutes).
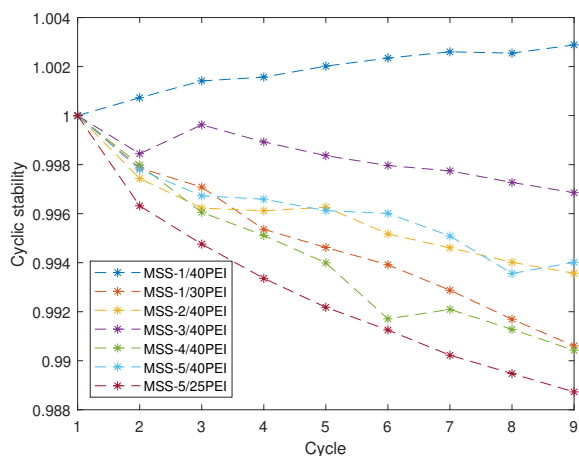
Figure 5.3: Comparison of cyclic adsorption/desorption stability on different batches of MSS impregnated with PEI at 75 ℃ in 5% CO_2 partial pressure gas. Desorption was done in pure N_2 gas at 75 ℃.

To further investigate the stability of MSS-1/40PEI, a 19 cyclic adsorption/desorption test was done. The long term stability of the sorbent is presented in Figure 5.4. The results indicated that MSS-1/40PEI maintained extremely stable, even after 19 cycles.
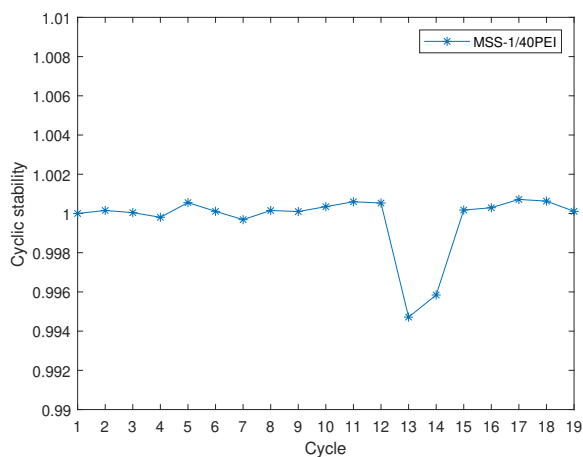
Figure 5.4: A 19 cyclic adsorption/desorption stability on MSS-1/40PEI at 75 ℃ in 5% partial pressure CO_2 gas.

The table below sums up the 3 of the most critical parameters for an amine-modified sorbent performance: adsorption capacity, cyclic adsorption/desorption stability and amine efficiency. Amine efficiency was fond by equation A.3. All sorbents showed relatively low amine efficiency.

Table 5.2: CO_2 adsorption capacities, 9 cyclic adsorption/desorption stability and amine efficiency of PEI impregnated MSS using 5% CO_2 partial pressure gas at 75 ℃.

Sorbent	Adsorption capacity [mmol/g]	Stability [%]	Amine efficiency [$mmol_{CO_2}/2mmol_N$]
MSS-1/40PEI	1.85	100.29	0.100
MSS-1/30PEI	1.65	99.06	0.118
MSS-2/40PEI	1.83	99.36	0.099
MSS-3/40PEI	2.24	99.69	0.121
MSS-4/40PEI	1.82	99.04	0.098
MSS-5/40PEI	2.18	99.40	0.117
MSS-5/25PEI	1.32	98.87	0.114

5.2.3 Desorption Behaviour

An evaluation of the desorption behaviour was done by a series of experiments performed on MSS-2/40PEI using different desorption temperatures in the range of 75-120 ℃ and pure N_2 gas. Figure 5.5 shows the relative dynamic desorption behaviour for three different temperatures. The sorbent was completely regenerated within 60 minutes of desorption at 75 ℃. An increase in desorption temperature to 100 ℃ resulted in faster desorption, and the sorbent was completely regenerated within 18.7 minutes. The regeneration was completed after 4.7 minutes at 120 ℃. It was also observed from Figure 5.5 that a desorption temperature of 100 ℃ and 120 ℃ resulted in a loss of the sorbents mass: 0.2 wt% and 0.9 wt%, respectively after one desorption step of 60 minutes.

Desorption at 120 ℃ in 70% CO_2 gas balanced in argon gas, was also carried out. This experiment was done in TGA Linseis. It was of interest to see the desorption behaviour in a high concentration of CO_2. However, the result showed it was challenging to do desorption under these conditions, see Figure B.26 in Appendix B.2.2.
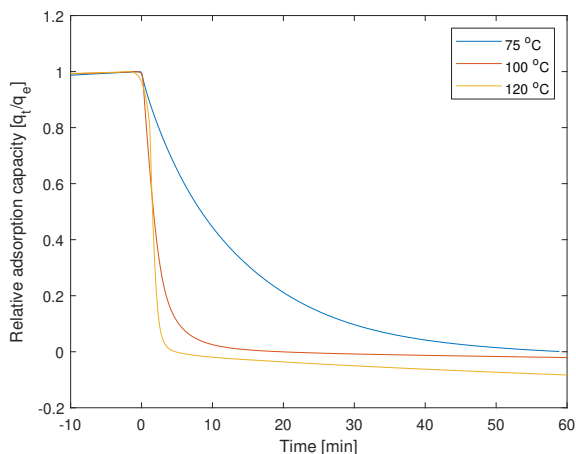
Figure 5.5: Comparison of relative desorption behavior of MSS-2/40PEI at three different desorption temperatures in pure N_2.

5.3 Silica Coating

Two silica coating methods, described in section 4.2.2, were tested on MSS-3/40PEI, MSS-5/40PEI and MSS-5/25PEI. A previous master student did silica coating on MSS-2/40PEI and MSS-4/40PEI with a different coating method. The physical properties of the coated sorbents are listed in Table 5.1. However, no physical properties characterisation on silica-coated MSS-4/40PEI was done due to shortages of samples. Ten adsorption/desorption cycles were done on each coated sorbent and the corresponding un-coated sorbent in order to investigate the effect of silica coating. Table 5.3 presents the silica coating method used, CO_2 adsorption capacity and cyclic stability of the silica-coated PEI-impregnated MSS and their corresponding un-coated sorbents. The adsorption and desorption steps lasted for 100 minutes each. However, due to time constraints, un-coated MSS-2/40PEI at 75 ℃ and both coated and un-coated MSS-5/25PEI had shorter adsorption and desorption time (60/60 minutes).

SiO_2-coated sorbents tended to show weaker adsorption capacities than the corresponded un-coated sorbent. At lower desorption temperature (75 ℃), the cyclic stability of both SiO_2-coated and un-coated sorbent was similar, but with an increasing desorption temperature to 100 ℃ and 120 ℃, the cyclic stability of SiO_2-coated sorbents tended to be weaker than un-coated sorbents, which was the opposite result of the hypothesis.

The cyclic stability testing of SiO_2-coated MSS-3 using method 1 with TEOS

and Col. SiO_2 were stopped after 8th and 3rd cycle, respectively, as they showed extremely low CO_2 adsorption capacities (0.04 mmol/g). MSS-3 was later coated with Col. SiO_2 using less time for condensation, called method 1^a in Table 5.3. The cyclic stability testing of SiO_2-coated MSS-5 using method 2 with TMOMS gave the same trend as method 1^a.

Table 5.3: Comparison of CO_2 adsorption capacity and nine cyclic adsorption/desorption stability of PEI impregnated MSS both with and without silica cover, coated with different methods. All experiments were done under given operating conditions with a total gas flow of 100 mL/min.

| Sorbent | | | | | | Operating conditions | | | | |
Silica support Sample	PEI-loading [wt%]	SiO2 precursor	Coating [N Layers]	Method	Adsorption capacity Coated (un-coated) [mmol/g]	Gas$_{ads}$ $p_{CO_2}:p_{N_2}$ [bar]	Gas$_{des}$ $p_{CO_2}:p_{N_2}$ [bar]	T_{ads} [°C]	T_{des} [°C]	9th Cycle Stability Coated (un-coated) [%]
MSS-2	40	TEOS	1	-	1.67 (1.83)	0.05 : 0.95	0.00 : 1.00	75	75	99.1 (99.4)
MSS-2	40	TEOS	1	-	1.61 (2.07)	0.05 : 0.95	0.00 : 1.00	75	100	97.0 (97.7)
MSS-2	40	TEOS	1	-	1.76 (2.24)	0.05 : 0.95	0.00 : 1.00	75	120	91.9 (93.5)
MSS-3	40	TEOS	1	1	0.04 (2.07)	0.05 : 0.95	0.00 : 1.00	75	120	90.3 (94.2)
MSS-3	40	Col. SiO$_2$	1	1	0.04 (2.07)	0.05 : 0.95	0.00 : 1.00	75	120	112.9 (94.2)
MSS-3	40	Col. SiO$_2$	1	1^a	0.91 (2.07)	0.05 : 0.95	0.00 : 1.00	75	120	91.0 (94.2)
MSS-4	40	TEOS	1	-	1.15 (2.13)	0.05 : 0.95	0.00 : 1.00	75	120	90.5 (94.4)
MSS-5	40	TMOMS	2	2	0.79 (2.14)	0.05 : 0.95	0.00 : 1.00	75	120	91.3 (95.1)
MSS-5	25	TMOMS	2	2	0.63 (1.38)	0.05 : 0.95	0.00 : 1.00	75	120	92.7 (91.9)

^{a}Shorter mixing time (10 min)

5.4   Kinetic Modelling

Figure 5.6 illustrate the relative dynamic adsorption and desorption behaviour in order to illustrate and compare the adsorption/desorption kinetics of all PEI-impregnated sorbents. Adsorption and desorption behaviour with actual values are given in Figure B.15 in Appendix B.2.1. The sorbents were exposed to 5% CO_2 gas balanced in pure N_2 gas at 75 ℃ for adsorption and pure N_2 gas at same temperature were used for desorption.
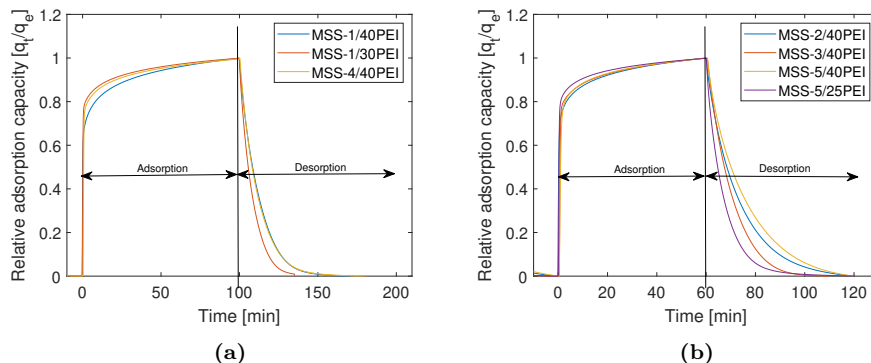
Figure 5.6: Dynamic relative adsorption and desorption profiles for PEI impregnated (a) MSS-1 and MSS-4, and (b) MSS-2, MSS-3 and MSS-5 at 75℃ in 5% CO_2 gas for adsorption and 100% N_2 gas for desorption.

MSS-1/40PEI used 29.4 minutes to reach 90% of its equilibrium CO_2 adsorption capacity, which in this case spent the longest time. On the other hand, MSS-5/25PEI spent the shortest time to reach 90% of its equilibrium capacity after 8.8 minutes. Table 5.4 shows the time it took to reach 90% of the CO_2 adsorption capacity for each sorbents. It was also observed in Figure 5.6 that the desorption process was much slower than the adsorption process. A lower PEI loading resulted in a faster regeneration time of the sorbents. MSS-1/30PEI was regenerated after 40.3 minutes, while MSS-1/40PEI spent the longest time for regeneration of all samples, 67.9 minutes. MSS-3/40PEI used the shortest time for regeneration of the sorbent impregnated with 40 wt% PEI. Table 5.4 shows the regeneration time for all sorbents.

Table 5.4: The time used to reach 90% of the sorbent CO_2 adsorption capacity in 5% CO_2 at 75 ℃, and 100% regeneration in pure N_2 at 75 ℃.

Sorbent			
Silica Support	PEI-loading	$t_{ads,90\%}$	$t_{des,100\%}$
Sample	[wt%]	[min]	[min]
MSS-1	40	29.4	67.9
MSS-1	30	17.5	40.3
MSS-2	40	14.8	58.9
MSS-3	40	13.2	47.5
MSS-4	40	21.3	64.5
MSS-5	40	12.6	59.4
MSS-5	25	8.9	43.0

5.4.1 Kinetic Models

The adsorption kinetics of sorbents exposed to different CO_2 partial pressures and temperatures were investigated in order to find an appropriate kinetic model. The experimental data was fitted and compared to five different kinetic models using `lsqnonlin` and `fitnlm` function from MATLAB. The nonlinear data-fitting made it possible to obtain the kinetic parameters (k, n, m and β), Root Mean Square Error ($RMSE$) and coefficient of determinations (R^2). All these variables for the different kinetic models are listed in Tables 5.5, 5.6, 5.7, 5.8 and 5.9. The kinetics of all 5 MSS batches were investigated since it was of interest to see how the physical properties influenced the adsorption process of different sorbents with same PEI loading.

The kinetic modelling was divided into long term and short term adsorption kinetics. Long term adsorption was full-length adsorption, while short term took only the first 3 minutes into account. Due to time constraints, MSS-2, MSS-3 and MSS-5 had long term adsorption for 60 minutes, while MSS-1, MSS-4 had 100 minutes long term adsorption. The impact of shorter adsorption time will be discussed in section 6.4.

Pseudo-First-order Kinetic Model Fitting

Pseudo-first-order kinetic model was described by equation 3.7, and the integrated form with boundary conditions, equation 3.8, was used as the objective function for kinetic modelling. `lsqnonlin` was used as the solver to minimize the objective function. `fitnlm` was used in order to find $RMSE$ and R^2 of the generated adsorption profiles, while ADD was found by equation A.8 in Appendix A.5. For long term adsorption, the model gave poor fitting according to relatively high ADD and $RMSE$, and extremely low R^2. For short term adsorption, both $RMSE$ and R^2 improved, but ADD stayed more or less the

same or even increased. No sorbent stood out in particular, but MSS-1/40PEI exposed to 50% CO_2 gave by far the poorest fitting.

Table 5.5: Values of pseudo-first-order kinetic model parameters, it's errors and correlation coefficient for long term adsorption (100/60 minutes) and short term adsorption (first 3 minutes) model fitting of PEI impregnated MSS.

Sorbent	T	p_{CO2}	Long term				Short term			
			k_{PFO}	ADD	$RMSE$	R^2	k_{PFO}	ADD	$RMSE$	R^2
	[°C]	[bar]	[min^{-1}]	[%]			[min^{-1}]	[%]		
MSS-1/40PEI	75	0.02	0.27	8.01	0.152	0.265	1.46	29.33	0.052	0.978
MSS-1/40PEI	75	0.05	0.37	8.31	0.165	-0.391	2.56	8.96	0.049	0.978
MSS-1/40PEI	75	0.50	0.34	8.75	0.189	-0.431	5.37	10.85	0.078	0.880
MSS-1/30PEI	75	0.05	1.18	5.96	0.113	0.048	2.95	8.30	0.045	0.983
MSS-2/40PEI	75	0.05	0.78	7.29	0.145	0.164	2.65	5.36	0.040	0.985
MSS-3/40PEI	75	0.05	1.32	6.46	0.163	0.120	3.01	2.81	0.052	0.980
MSS-3/40PEI	50	0.05	2.04	4.81	0.098	0.010	3.46	6.03	0.050	0.970
MSS-4/40PEI	75	0.05	1.01	6.46	0.133	-0.028	2.88	6.33	0.036	0.990
MSS-5/40PEI	75	0.05	0.83	6.21	0.147	0.419	1.81	3.89	0.038	0.991
MSS-5/25PEI	75	0.05	1.57	5.39	0.080	0.369	2.82	9.75	0.046	0.963

Pseudo-Second-order Kinetic Model Fitting

Pseudo-second-order kinetic model was described by equation 3.9, and the integrated form with boundary conditions, equation 3.10, was used as the objective function. The same procedure, as described above, was used to in order to find $RMSE$, R^2 and ADD of the generated adsorption profiles. For long term adsorption, the model gave slightly better fitting then pseudo-first-order kinetic model, with a lower ADD and $RMSE$, and higher R^2. For short term adsorption, ADD increased tremulously, while a smaller increment of $RMSE$ was observed. R^2 increased for all sorbents for short term adsorption. No sorbent stood out in particular.

Table 5.6: Values of pseudo-second-order kinetic model parameters, it's errors and correlation coefficient for long term adsorption (100/60 minutes) and short term adsorption (first 3 minutes) of PEI impregnated MSS.

Sorbent	T	p_{CO2}	Long term				Short term			
			k_{PSO}	ADD	$RMSE$	R^2	k_{PSO}	ADD	$RMSE$	R^2
	[°C]	[bar]	[g mmol^{-1}min^{-1}]	[%]			[g mmol^{-1}min^{-1}]	[%]		
MSS-1/40PEI	75	0.02	0.30	3.37	0.071	0.842	2.24	16.60	0.122	0.883
MSS-1/40PEI	75	0.05	0.35	4.05	0.088	0.704	4.32	17.11	0.095	0.918
MSS-1/40PEI	75	0.50	0.31	4.51	0.108	0.534	8.10	12.17	0.049	0.952
MSS-1/30PEI	75	0.05	0.80	3.94	0.068	0.652	5.07	17.70	0.114	0.889
MSS-2/40PEI	75	0.05	0.69	3.66	0.073	0.789	4.19	12.77	0.084	0.934
MSS-3/40PEI	75	0.05	0.77	4.20	0.091	0.724	3.70	6.84	0.095	0.931
MSS-3/40PEI	50	0.05	1.28	3.65	0.066	0.549	5.08	11.78	0.091	0.902
MSS-4/40PEI	75	0.05	0.64	4.24	0.079	0.638	4.62	14.39	0.150	0.909
MSS-5/40PEI	75	0.05	0.64	3.15	0.066	0.882	2.23	11.06	0.110	0.927
MSS-5/25PEI	75	0.05	1.66	2.97	0.045	0.804	5.53	17.37	0.078	0.892

Avrami's Kinetic Model Fitting

Avrami's kinetic model was described by equation 3.11, and the integrated form with boundary conditions, equation 3.12, was used as the objective function. The same procedure, as described above, was used in order to find $RMSE$, R^2 and ADD of the generated adsorption profiles. For long term adsorption, the model gave a fitting with relatively low ADD and $RMSE$, and all R^2 were above 0.900, except MSS-5/25PEI. For short term adsorption, ADD increased, while $RMSE$ stayed more or less the same. R^2 increased slightly for almost all sorbents, except MSS-1/40PEI exposed to 50% CO_2 gas, which also showed poorest ADD. No sorbent stood out in particular.

Table 5.7: Values of Avrami's kinetic model parameters and it's errors for long term adsorption (100/60 minutes) and short term adsorption (first 3 minutes) model fitting of PEI impregnated MSS.

| Sorbent | T | p_{CO2} | Long term | | | | | Short term | | | | |
| | | | k_A | n | ADD | $RMSE$ | R^2 | k_A | n | ADD | $RMSE$ | R^2 |
	[°C]	[bar]	[min^{-1}]		[%]			[min^{-1}]		[%]		
MSS-1/40PEI	75	0.02	0.41	0.35	2.86	0.036	0.958	1.44	1.17	13.10	0.047	0.983
MSS-1/40PEI	75	0.05	0.61	0.31	2.00	0.036	0.950	2.55	1.04	8.77	0.049	0.978
MSS-1/40PEI	75	0.50	0.67	0.29	4.50	0.042	0.931	5.57	0.60	15.82	0.064	0.921
MSS-1/30PEI	75	0.05	1.72	0.27	1.70	0.034	0.917	2.88	1.34	6.11	0.030	0.992
MSS-2/40PEI	75	0.05	1.16	0.32	1.86	0.035	0.951	2.70	0.89	5.64	0.037	0.988
MSS-3/40PEI	75	0.05	1.88	0.29	1.76	0.049	0.922	3.02	0.95	2.98	0.052	0.980
MSS-3/40PEI	50	0.05	3.95	0.24	1.93	0.038	0.851	3.44	1.17	4.87	0.049	0.972
MSS-4/40PEI	75	0.05	1.49	0.27	1.66	0.035	0.928	2.83	1.15	5.65	0.032	0.992
MSS-5/40PEI	75	0.05	1.15	0.34	2.01	0.047	0.939	1.83	0.91	4.24	0.034	0.993
MSS-5/25PEI	75	0.05	2.23	0.30	2.90	0.033	0.889	2.82	1.32	6.65	0.042	0.969

Fractional-Order Kinetic Model Fitting

Fractional-order kinetic model was described by equation 3.13, and the integrated form with boundary conditions, equation 3.14, was used as the objective function. The same procedure, as described above, was used in order to find $RMSE$, R^2 and ADD of the generated adsorption profiles. For long term adsorption, the model gave the overall best fitting of all tested kinetic models in this work, which can be seen from the overall lowest ADD and $RMSE$, and highest R^2 obtained by this model. For short term adsorption, ADD increased slightly, while $RMSE$ decreased. R^2 showed extremely high values, close to 1 for almost all sorbents. No sorbent stood out in particular.

Table 5.8: Values of fractional-order kinetic model parameters and it's errors for long term adsorption (100/60 minutes) and short term adsorption (first 3 minutes) of 7 different PEI impregnated MSS.

Sorbent	T	p_{CO2}	k_F	n	m	ADD	RMSE	R^2	k_F	n	m	ADD	RMSE	R^2
	[°C]	[bar]	[a]			[%]			[a]			[%]		
MSS-1/40PEI	75	0.02	0.23	0.77	0.29	2.79	0.036	0.959	12.92	2.49	2.48	4.66	0.014	0.999
MSS-1/40PEI	75	0.05	0.16	0.34	0.15	1.17	0.029	0.967	55.12	2.73	2.48	4.66	0.014	0.998
MSS-1/40PEI	75	0.50	0.13	0.08	0.10	1.24	0.021	0.982	55.00	2.69	2.69	5.39	0.032	0.979
MSS-1/30PEI	75	0.05	0.20	0.64	0.18	1.43	0.033	0.919	29.40	1.97	2.13	4.69	0.013	0.998
MSS-2/40PEI	75	0.05	0.28	0.81	0.26	1.70	0.035	0.952	9.12	1.91	1.53	3.39	0.015	0.998
MSS-3/40PEI	75	0.05	0.36	1.04	0.30	1.78	0.049	0.922	12.69	2.14	1.75	1.41	0.026	0.995
MSS-3/40PEI	50	0.05	2.68	3.02	1.04	1.70	0.032	0.896	16.76	1.87	1.85	4.07	0.033	0.988
MSS-4/40PEI	75	0.05	0.18	0.47	0.15	1.21	0.033	0.935	14.99	1.86	1.80	4.43	0.016	0.998
MSS-5/40PEI	75	0.05	1.00	3.07	1.28	1.90	0.040	0.957	3.12	1.62	1.34	2.41	0.013	0.999
MSS-5/25PEI	75	0.05	3.62	2.95	1.07	1.92	0.029	0.923	65.07	2.48	2.41	2.22	0.018	0.994

[a] $\mathrm{mmol}^{1-n}\ \mathrm{g}^{n-1}\ \mathrm{min}^{-m}$

Dual Kinetic Model Fitting

The dual kinetic model was described by equation 3.15. However, in this case, the objective function was not an integrated form with boundary conditions, but the ODE described by equation 3.17 was used instead. $RMSE$ and R^2 was found by equation A.7 and A.12, and ADD was found by equation A.8, all listed in A.5. For long term adsorption, the model gave good fitting of all sorbents with a relatively low ADD and $RMSE$, but not a very satisfying R^2 was obtained by this model. For short term adsorption, no specific trend was observed for ADD, while $RMSE$ slightly decreased or stayed the same. R^2 showed extremely high values, close to 1 for some sorbents. No sorbent stood out in particular.

Table 5.9: Values of dual kinetic model parameters for long term adsorption (100/60 minutes) and short term adsorption (first 3 minutes) of PEI impregnated MSS.

Sorbent	T	p_{CO2}	k_{DKM}	n	β	ADD	RMSE	R^2	k_{DKM}	n	β	ADD	RMSE	R^2
	[°C]	[%]	[a]		[g mmol^{-1}]	[%]			[a]		[g mmol^{-1}]	[%]		
MSS-1/40PEI	75	2	0.19	3.08	2.40	3.15	0.054	0.907	0.75	1.45	3.05	2.96	0.031	0.992
MSS-1/40PEI	75	5	0.28	3.31	2.09	3.12	0.059	0.864	1.24	1.64	3.44	2.96	0.025	0.994
MSS-1/40PEI	75	50	0.35	3.47	1.29	3.58	0.073	0.790	2.64	2.38	3.92	5.95	0.033	0.975
MSS-1/30PEI	75	5	0.68	3.25	2.35	2.13	0.038	0.895	1.29	1.32	3.17	2.20	0.021	0.996
MSS-2/40PEI	75	5	0.42	3.12	2.29	2.45	0.047	0.914	1.23	1.69	2.98	1.18	0.013	0.998
MSS-3/40PEI	75	5	0.30	3.08	2.26	2.59	0.053	0.920	0.84	1.55	2.92	4.68	0.037	0.992
MSS-3/40PEI	50	5	0.91	3.26	2.43	1.68	0.031	0.900	1.43	1.65	3.16	3.06	0.029	0.990
MSS-4/40PEI	75	5	0.53	3.27	1.94	2.23	0.043	0.890	1.22	1.46	3.11	1.17	0.015	0.998
MSS-5/40PEI	75	5	0.22	2.93	2.36	1.99	0.047	0.947	0.64	1.62	2.63	0.68	0.011	0.999
MSS-5/25PEI	75	5	1.35	2.96	2.98	2.30	0.027	0.927	1.52	1.57	3.71	6.33	0.029	0.984

[a] $\mathrm{mmol}^{1-n}\ \mathrm{g}^{n-1}\ \mathrm{min}^{-1}$

Figure 5.7, 5.8, 5.9, 5.10, 5.11, 5.12 and 5.13 illustrate the fitting of each model to each sorbents under the same conditions: 5% CO_2 gas balanced in N_2 at 75 °C. Based on the figures, the fractional-order showed the overall best fitting of

the evaluated kinetic models. Besides, fractional-order often had the highest R^2 and the lowest $RMSE$ and ADD. The short term kinetic modelling gave an overall better fitting than long term kinetic modelling. The figures for long term adsorption show only the first 10 minutes of the total adoration process as this was the most interesting part of the adsorption kinetics. Full adsorption length for long term adsorption can be seen in Appendix C.2.

The figures bellow showed an underestimation of the experimental adsorption in the initial phase for both the pseudo-first-order and pseudo-second-order kinetic model until they both overestimated the CO_2 uptake. The figures also showed an overestimation of the CO_2 uptake for both Avrami and fractional-order in the initial phase of long term adsorption for PEI impregnated MSS-1, MSS-2, MSS-3 and MSS-4. The models also underestimated the CO_2 uptake until around 4-5 minutes when the models gave proper fitting until the end of the adsorption step. Dual kinetic model, however, showed proper fitting in the initial phase but gave an overestimation after around 2 minutes for long term adoption. For short term adsorption, the figures illustrated proper fitting for all models in the initial adsorption step, except the pseudo-second-order model. It was observed that the model underestimated the CO_2 uptake for all sorbents. The next seven pages show the comparison of the above mentioned kinetic models on experimental CO_2 adsorption for each sorbent.
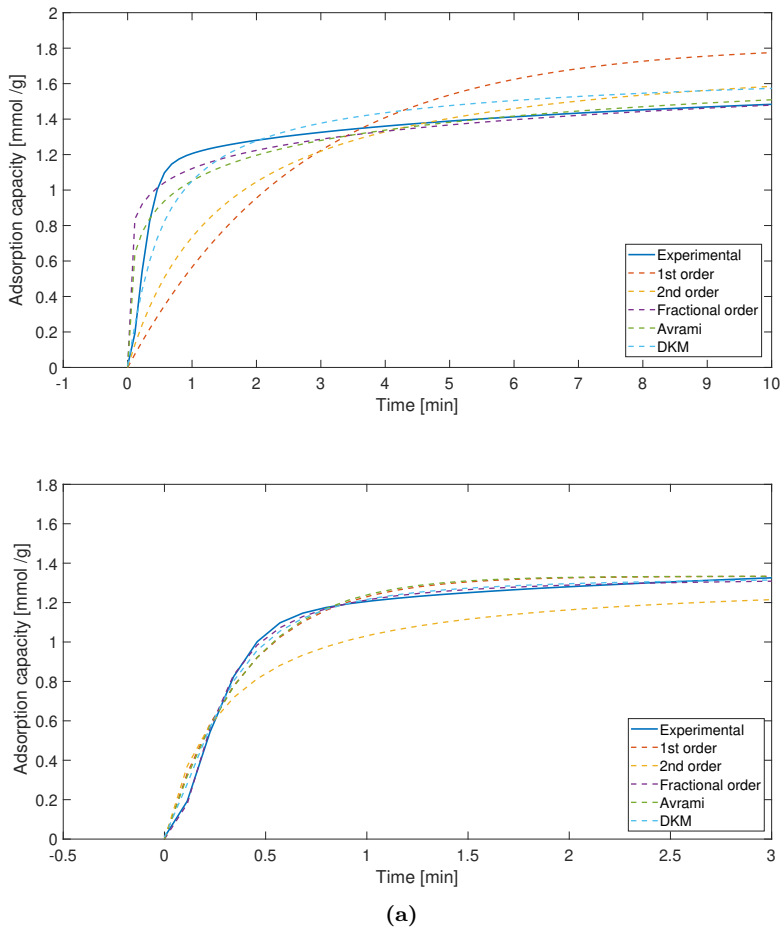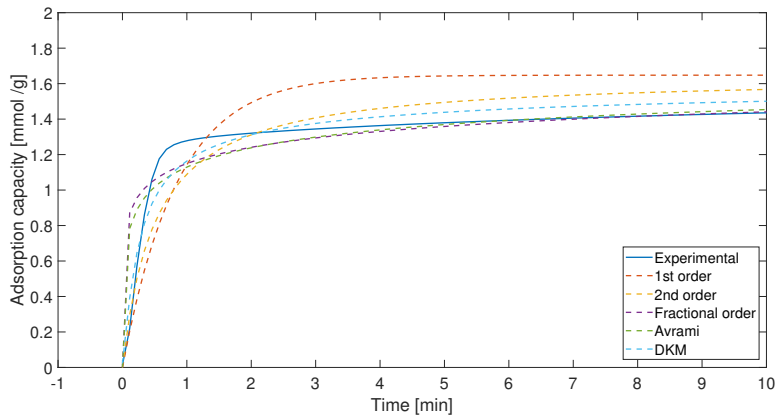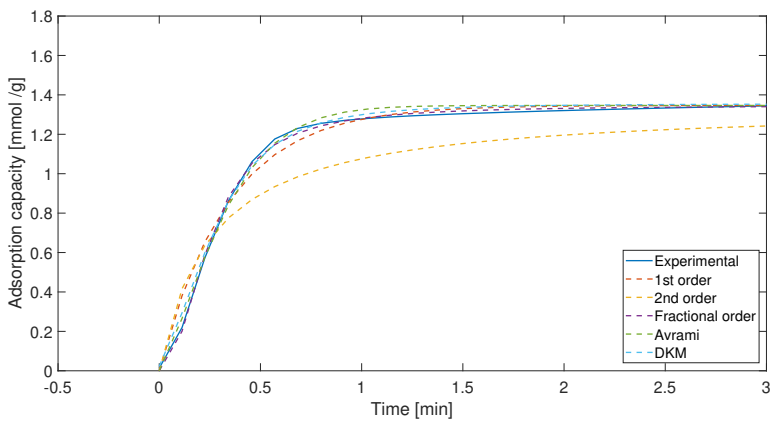
Figure 5.7: Comparison of kinetic models on experimental CO_2 adsorption on MSS-1/40PEI exposed to 5% CO_2 gas balanced with N_2 at 75 ℃ for both (a) long term adsorption (100 min) and (b) short therm adsorption (3 min).
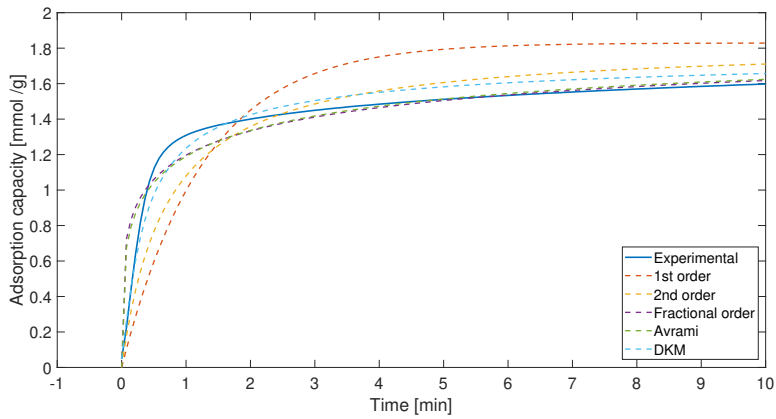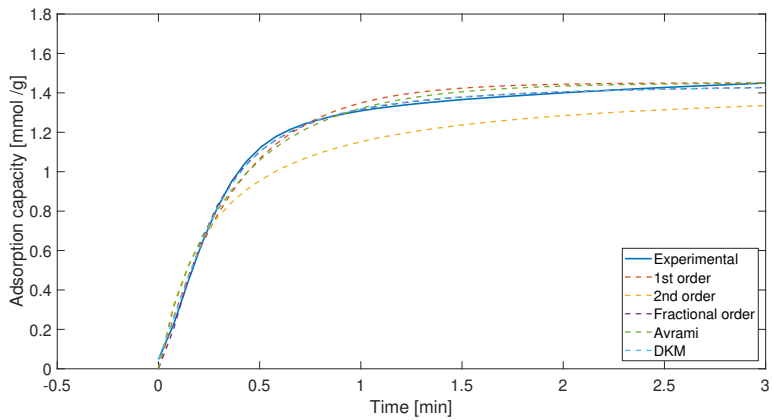
(a)

(b)

Figure 5.8: Comparison of kinetic models on experimental CO_2 adsorption on MSS-1/30PEI exposed 5% CO_2 gas balanced with N_2 at 75 ℃ for both (a) long term adsorption (100 min) and (b) short term adsorption (3 min).
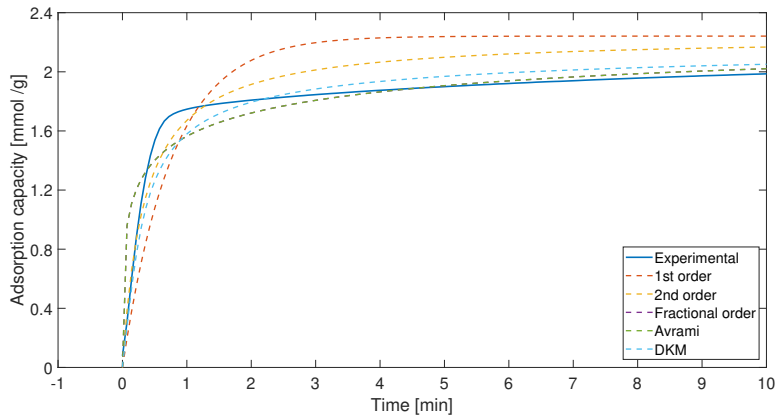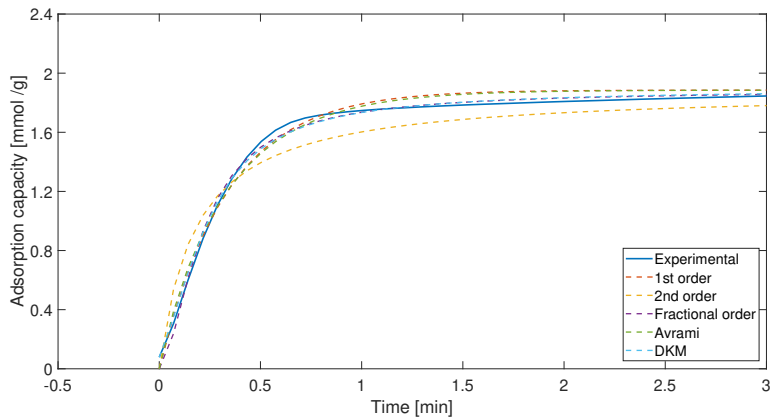
(a)

(b)

Figure 5.9: Comparison of kinetic models on experimental CO_2 adsorption on MSS-2/40PEI exposed 5% CO_2 gas balanced with N_2 at 75 ℃ for both (a) long term adsorption (60 min) and (b) short term adsorption (3 min).

(a)

(b)

Figure 5.10: Comparison of kinetic models on experimental CO_2 adsorption on MSS-3/40PEI exposed 5% CO_2 gas balanced with N_2 at 75 ℃ for both (a) long term adsorption (60 min) and (b) short term adsorption (3 min).
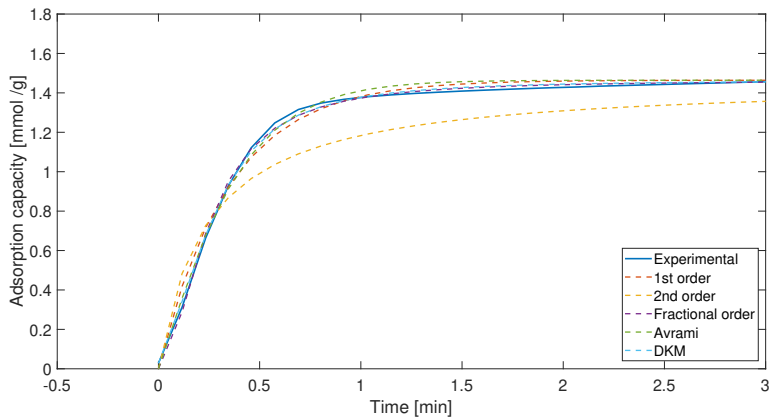
(a)

(b)

Figure 5.11: Comparison of kinetic models on experimental CO_2 adsorption on MSS-4/40PEI exposed 5% CO_2 gas balanced with N_2 at 75 ℃ for both (a) long term adsorption (100 min) and (b) short term adsorption (3 min).
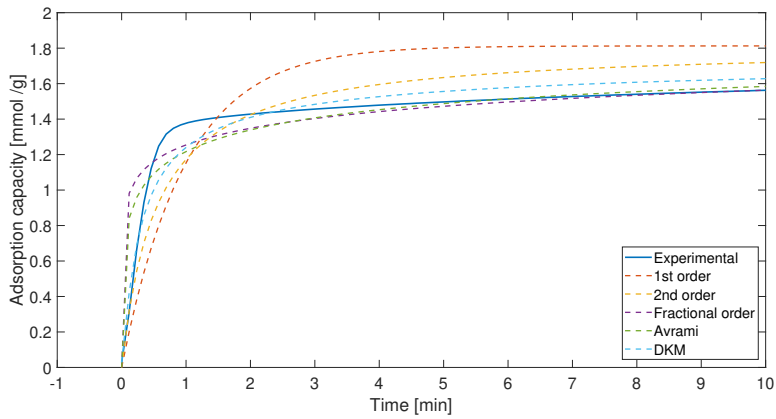
Figure 5.12: Comparison of kinetic models on experimental CO_2 adsorption on MSS-5/40PEI exposed 5% CO_2 gas balanced with N_2 at 75 ℃ for both (a) long term adsorption (60 min) and (b) short therm adsorption (3 min).
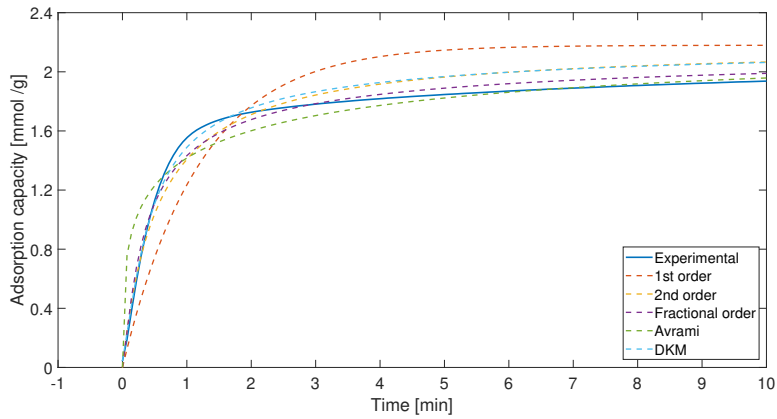
(a)

(b)

Figure 5.13: Comparison of kinetic models on experimental CO_2 adsorption on MSS-5/25PEI exposed 5% CO_2 gas balanced with N_2 at 75 °C for both (a) long term adsorption (60 min) and (b) short therm adsorption (3 min).
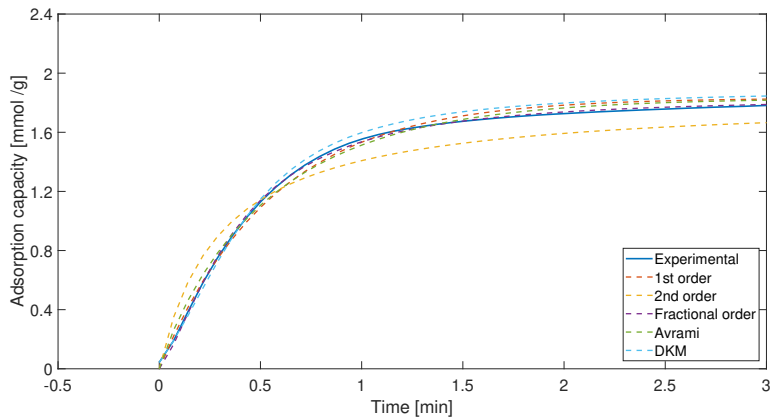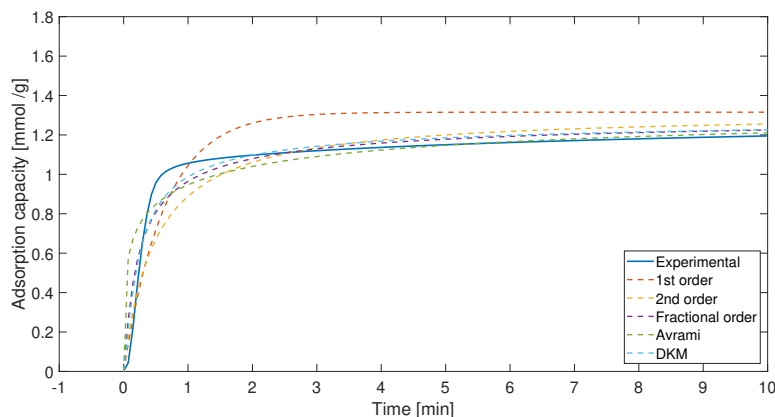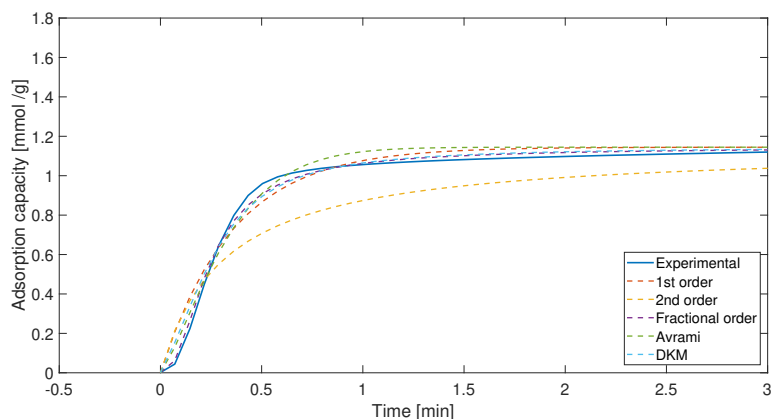
5.4.2   Dependence of Adsorption Conditions on Kinetic Parameters

MSS-1/40PEI was exposed to different CO_2 partial pressures in order to evaluate the performance of the sorbent, see Figure C.1. Since the fractional-order kinetic model showed the best fitting in the previous section, a model fitting of experimental CO_2 adsorption with 2%, 5% and 50% CO_2 gas balanced in N_2 were done, and Figure 5.14 presents the results. It was found that the fractional-order kinetic model showed the best fitting at lower CO_2 partial pressures for short term adsorption (Figure 5.14b). However, at long term adsorption, a

higher CO_2 partial pressure gave best fitting (Figure 5.14a) for the same kinetic model. All kinetic parameters and errors are listed in Tables 5.8.
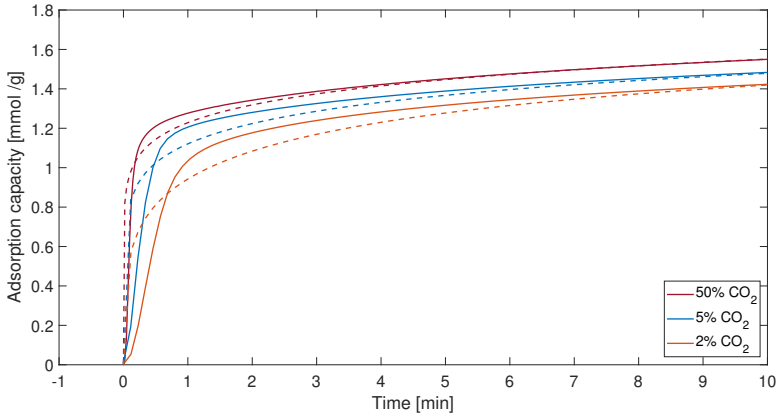
(a)
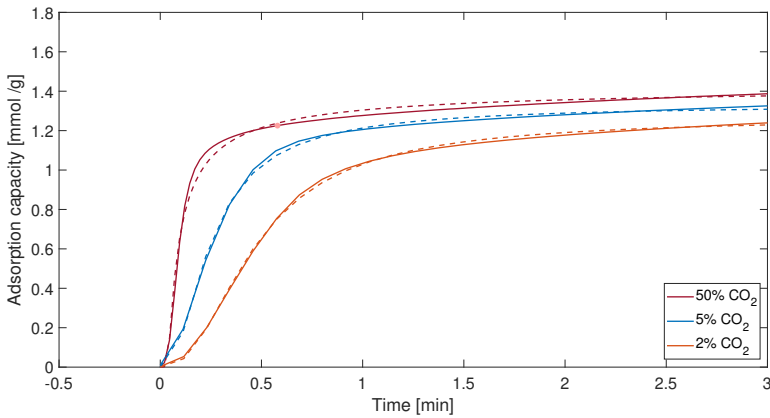
(b)

Figure 5.14: Comparison of different CO_2 partial pressure adsorption fitting of fractional order kinetic model on MSS-1/40PEI at 75 ℃ for both (a) long term adsorption (100 min) and (b) short term adsorption (3 min). The dashed lines represent the modelled adsorption profiles generated by the fractional-order kinetic model.

MSS-3/40PEI was exposed to different adsorption temperatures in order find the optimum temperature for maximum CO_2 uptake, see Figure 5.1a. Figure 5.15 shows experimental and generated profiles of CO_2 adsorption at 75 ℃ and 50 ℃ in 5% CO_2 partial pressures using fractional-order kinetic model. Adsorption at 100 ℃ was not included in the kinetic study as desorption was observed in the adsorption step at 5% CO_2 gas. See Figure 5.1a,
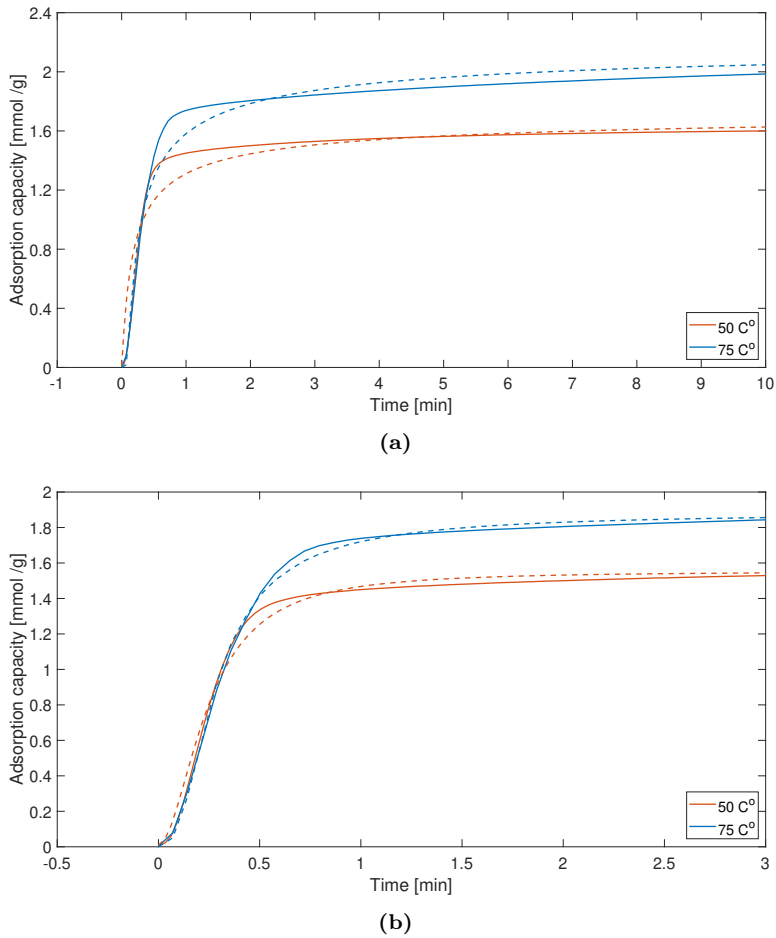
(a)

(b)

Figure 5.15: Comparison of different adsorption temperatures model fitting with fractional order kinetic model on MSS-3/40PEI in 5% CO_2 gas for both (a) long term adsorption (60 min) and (b) short term adsorption (3 min). The dashed lines represent the modelled adsorption profiles generated by the fractional-order kinetic model.

Chapter 6

Discussion

6.1 Nitrogen Physisortion

Nitrogen physisorption at 77 K with BET and BJH method were used as characterisation technique to analyse the different sorbents physical properties.

6.1.1 Mesoporous Silica Spheres

Results from the nitrogen physisorption experiments, presented in Table 5.1, showed that MSS-1 and MSS-3 have a similar surface area in the range of 114 to 117 m^2/g. MSS-4 showed the highest surface area of 137 m^2/g, while MSS-5 had the lowest surface area of all tested samples with 73 m^2/g. Sample MSS-1, MSS-2, MSS-3 and MSS-4 were synthesised by a previous master student and it was reported that they were synthesised with a carbon-source and colloidal silica solution weight ratio (C/SI) of 20/25. However, the calcination temperature was different. MSS-1 was calcined at 550 ℃, MSS-2 at 650 ℃ and MSS-4 at 750 ℃ [53]. MSS-3 had not a reported calcination temperature, but taking the physical properties into account; it may be reasonable to assume equal calcination temperature as MSS-1. MSS-5 was synthesised by the author of this master thesis with a C/SI of 20/28 and calcined at 750 ℃. It was shown that a relatively small change in C/SI had a great impact on the physical properties of the final MSS.

The average pore size of the MSS samples were all in the range of a mesoporous size (2-50 nm). MSS-1 to MSS-4 were in the range from 14-17 nm, while MSS-5 had the largest average pore size of with 22 nm. MSS-4 obtained highest pore

volume, with 0.51 cm^3/g, while MSS-5 showed pores of 0.40 cm^3/g. Judged by these results, a lower C/SI ratio gave a lower surface area and pore volume, and larger average pore size.

Judged by the shape of the isotherms from Figure B.1 to B.4, sample MSS-1, MSS-2, MSS-3 and MSS-5 had all type IV isotherms. It was also reported that MSS-4 had type IV isotherm [53]. Besides, it was assumed by the shape of the isotherms that the hysteresis of all samples had type H1. H1 type indicated that the pores were arranged with uniform size and shape within the aggregated silica nanoparticles, which form the spherical shape for the support. The pore size distribution of the samples, which can be seen in the same figures, have peaks indicating the most abundant pore sizes of the supports. It was found that the peaks were corresponding well to the average pore diameter for MSS support presented in Table 5.1. The peaks of MSS-2 and MSS-5 were slightly less than the average pore diameter of 17 nm and 22 nm, respectively. The curve at larger pore sizes and a smaller peak at 40 nm for the pore distribution plots of MSS-2 and MSS-5 might explain why the peaks did not correspond to the average pore diameter as god as for MSS-1 and MSS-3.

6.1.2   PEI Impregnated Mesoporous Silica Spheres

The physical properties of PEI impregnated MSS were challenging to analyse using BET and BHJ method with nitrogen physisorption. However, filling the pores with PEI resulted in an expected decrease of both the surface areas and pore volumes for all samples. The largest surface area was observed for MSS-5 with 25 wt% PEI, while MSS-1 and MSS-2 with 40 wt% provided the lowest surface areas. Samples with lower PEI loading showed a higher pore volume than samples impregnated with 40 wt% PEI. The increase was expected since an increment of PEI would occupy more of the pore volume of the support.

The average pore size for PEI impregnated MSS varied a lot, where MSS-4/40PEI reported the smallest pores size of 10 nm, while MSS-1/40PEI reported a pore size of 116 nm. The results were challenging to analyse. The BJH method might have been invalid for PEI impregnated MSS since at least two assumptions in the BJH method were not satisfied: PEI can block the pores, which is not present for BJH method, and pores may not be rigid and uniform in shape. Besides, MSS-1/40PEI, MSS-1/30PEI and MSS-2/40PEI consisted mainly of macropores, in which Kelvin equation was not valid for calculations [82].

6.1.3   Silica Covered Mesoporous Silica Spheres

In order to see any changes in the physical properties of PEI impregnated MSS before and after silica cover, another nitrogen physisorption analysis at 77 K with BET and BJH method was done on the silica-coated MSS. As mention,

silica-coated MSS-2/40PEI and MSS-4/40PEI were made by a previous master student [53] with another coating method, and due to a shortage of coated MSS-4/40PEI, it was not possible to run a BET and BHJ analysis. Little changes in physical properties after silica-coating of MSS-2/40PEI was observed by the results present in Table 5.1. In Wang's master thesis *"a small amount"* of ethanol was added to TEOS before it was mixed with PEI impregnated MSS. No hydrolysis step was taken into account nor condensation of silanols on the surface of the MSS. Based on the results from the BET analysis, it might be possible that TEOS molecules covered the surface. However, due to no hydrolysis and condensation step, it is hard to imagine the formation of a silica layer based on the detailed coating method described in this thesis.

Silica-coated PEI impregnated MSS-3 and MSS-5 showed significant changes in physical properties. Silica-coated MSS-3/40PEI with TEOS was not included in Table 5.1, which will be discussed in section 6.3. The samples increased its surface area, and pore volume, after the coating method of silica was done. Ethanol and water were used for the coating method, described in section 4.4.2. PEI is easily soluble in ethanol and mixable in water [64], diffusion of PEI out of the pores during the coating method might be the reason why an increment in both surface area and pore volume occurred. Besides, it was observed that a larger volume of the samples was loaded to the sample pan before testing the adsorption capacity in TGA, compared to samples without silica cover. The samples must have had a weight loss during the coating method, which indicated that PEI might have diffused out the pores.

6.2 Catalyst Performance

Thermalgravimetric analysis (TGA) was carried out in order to investigate the performance of the sorbents. In this section, optimum adsorption temperature and different CO_2 partial pressure will be discussed, in addition to, CO_2 adsorption capacities and cyclic stability of the PEI impregnated MSS.

6.2.1 Effect of Adsorption Temperature and Carbon Dioxide Partial Pressure

Figure 5.1a shows the adsorption profile of MSS-3/40PEI exposed to 5% CO_2 gas in N_2 at different temperatures for 100 minutes. It was found that the adsorption capacity of the sample increased with increasing temperature until it reached 75 ℃. Although the chemical reaction between PEI and CO_2 was exothermic and thermodynamic favoured at a lower temperature (25 ℃), kinetic limitations causing slow adsorption rate might be the reason for low CO_2 adsorption capacity at low temperatures. Assuming that the pores have been filled with PEI, MSS-3/40PEI was considered as a highly loaded sorbent, and

the adsorption behaviour at temperatures lower than 75 ℃ was therefore limited by slow diffusive mass transfer of CO_2 [83, 84]. The fact that pores were filled with PEI limited the accessibility to free active amine sites.

An increase in temperature to 75 ℃ reduced the diffusional resistance and resulted in reduced kinetic limitation and higher CO_2 adsorption capacity. The reduced diffusion resistance was clearly shown in Figure 5.1a as adsorption at 50 ℃ rapidly reached a lower CO_2 adsorption capacity compared to adsorption at 75 ℃, which reached a much higher CO_2 adsorption capacity. Both temperatures showed a diffusion limiting region after the fast initial adsorption. However, a lower diffusion resistance for 75 ℃ resulted in a much higher CO_2 adsorption capacity after 100 minutes. The CO_2 capacity decreased when the temperature was beyond 75 ℃. The low maximum capacity at 100 ℃ may indicate that CO_2 adsorption capacity was favoured by thermodynamic equilibrium instead of chemical reaction kinetics between CO_2 and PEI impregnated MSS. Diffusion resistance may not have been the limiting factor, and the decreasing uptake was rather reliable with the thermodynamic limitation [84].

As the optimum adsorption temperature was chosen for PEI impregnated MSS, the sorbent was exposed to different CO_2 partial pressures at 75 ℃ for CO_2 adsorption measurement, which is shown in Figure 5.1b. In the low CO_2 partial pressures region (0-0.05 bar) the adsorption capacity increased rapidly with a small increment in CO_2 partial pressure. The sorbent was saturated from 0.10-0.50 bar CO_2 partial pressure. No measurements beyond 0.50 bar were done, as the TGA TA Q500 had a maximum limitation of 0.50 bar CO_2 partial pressure with a total gas flow of 100 ml/min. However, since the sorbent reached its saturation at around 0.10 bar, it would not affect the result.

6.2.2 Carbon Dioxide Adsorption Capacities and Cyclic Stability

CO_2 adsorption capacities of all PEI impregnated MSS were compared in 5% CO_2 gas balanced in N_2 at 75 ℃ and are presented in Figure 5.2. These conditions were chosen in order to simulate temperature and partial pressure conditions of flue gas inside an adsorber column. It is important to mention that due to time constraints, PEI impregnated MSS-1 and MSS-4 sorbents had a 100 minutes adsorption time, while PEI impregnated MSS-2, MSS-3 and MSS-5 had 60 minutes. However, shorter adsorption time will not affect the maximum capacity of the sorbent too much as they all had reached approximately 98% of maximum adsorption capacity after 60 minutes. All sorbents showed relatively good adsorption capacity taking the low CO_2 partial pressure into account. However, in comparison with PEI-impregnated SBA-15 and other mesoporous silica materials mentioned in the literature, MSS has potential for improvement.

MSS-3/40PEI was found to give the highest CO_2 uptake of the PEI impregnated MSS with the same loading of amine, i.e. 40 wt%. Although the physical properties were similar, the MSS-3/40PEI adsorbed 0.39 mmol CO_2 more per gram than MSS-1/40PEI. The visible µm sized spheres of MSS-1 tended do deform during impregnation of PEI. The deformation might indicate that pores could be blocked, and therefore prevent adsorption of CO_2. Little deformation of MSS-3 was observed during impregnation of PEI nor for MSS-2 and MSS-4 [53]. No deformation indicated better physical strength of the spheres. MSS-1, MSS-2 and MSS-4 loaded with 40 wt% PEI showed all similar CO_2 adsorption capacities even though the physical properties of the MSS support were slightly different. The similar capacities might be an indication that the pores were filled with PEI, and an external layer of PEI might cover the external surface of the spheres. After CO_2 already had reacted with the PEI layer on the surface of the spheres, new additional CO_2 molecules were limited by slow diffusive mass transfer [83, 84], and experienced limited accessibility to free active amine sites. Besides, the viscosity of PEI was assumed to increase as the formation of carbamate occurred [85], and thus enhanced diffusion resistance of CO_2 molecules.

Lower PEI loading of 30 wt% and 25% was impregnated for MSS-1 and MSS-5, respectively. Besides, 50 wt% PEI impregnation was done on MSS-1, but the physical properties of the support did not handle such high loading, which ended up in very poor adsorption capacity [86]. However, it was of interest to compare PEI loadings to adsorption capacity and kinetics, and especially amine efficiency (mmol CO_2/mmol 2N).

An interesting observation was the high CO_2 adsorption capacities for MSS-3/40PEI and MSS-5/40PEI. Although they had the smallest pore volumes, and MSS-5/40PEI had the smallest surface area, both sorbents showed the highest capacities. The low adsorption capacity may indicate a differently organised pore structure of MSS-2 and MSS-4, compared to MSS-3 and MSS-5, preventing diffusion of PEI into the pores. These sorbents were made in 2019, and age might have an impact on the adsorption capacity. MSS-5 had higher silica content, which resulted in smaller pore volume and surface area, but also indicated good mechanical strength of the support that could handle the wet impregnation method better.

For practical application the sorbent should also have excellent regenerability and stability in adsorption-desorption cycles, not only a high CO_2 adsorption capacity. Figure 5.3 shows the cycle stability performance of PEI impregnated MSS. It became clear that the cyclic stability of the PEI impregnated MSS were excellent when the adsorption/desorption temperature was 75 ℃. It was done 10 adsorption/desorption cycles, but the cyclic stability testing started at

cycle two since the high temperature used in the pre-treatment step could have an effect on adsorption capacity of the first cycle. The stability of each cycle was found by equation 3.6. The stability for almost all sorbents, except MSS-1/40PEI, decreased after 9 cycles. Loss of PEI might explain the small decay of the sorbets adsorption capacity. However, literature has reported that the surface of porous silica and amine groups create strong interactions between each other [87]. Formation of $Si-O-N^+H_3R$ and/or $Si-O-N^+H_2R$ may have been formed by chemical interaction between the silanol groups on the surface silica support and the amine groups in PEI. The interaction worked as an anchor for PEI-molecules inside the pores of the support and led to a good cycling stability.

During the cyclic testing, a baseline shift of the adsorption capacity occurred, which can be seen from the figures in Appendix B.2.2. The baseline shift was more visible at higher desorption temperatures, which indicated a loss of organic matter (PEI). However, the stability of the sorbent remained good. During adsorption, the viscosity of PEI increased as the formation of carbamate occurred and made some active amine sites unavailable fro CO_2 to react with due to high diffusion resistance. When some PEI evaporated from the external surface during desorption, unused available active amine sites may have been reachable for CO_2 the following adsorption step. According to the low amine efficiency, there was a large number of available active amine after an adsorption step.

6.2.3   Desorption Behaviour

It was observed by Figure 5.6a and 5.6b that sorbents with lower amine loading regenerated faster due to the lower diffusion barrier. Another way to tune the regeneration speed was by adjusting the desorption temperature, as can be seen in Figure 5.5. An increase in desorption temperature made the sorbent regenerate much faster, but also led to a loss of organic matter. Therefore, desorption temperature was considered as a critical parameter for both adsorption capacity and cyclic stability. As a general rule, this thesis aimed for a complete and fast regeneration at lowest possible desperation temperature, while the sorbent maintained its integrity. To evaluate the desorption behavior, three different desorption temperatures (75 ℃, 100 ℃ and 120 ℃) in pure N_2 gas were examined on MSS-2/40PEI. This sorbent was chosen due to the relatively large quantity of both PEI impregnated and silica covered samples which will be discussed in the next section. The sorbent was completely regenerated just before 60 minutes at 75 ℃. Due to strong interactions between CO_2 and amine, and high diffusion barrier, this process was time-consuming. Increasing the desorption temperature to 100 ℃ resulted in faster release of CO_2, and the sorbent was completely regenerated after 18 minutes. At 120 ℃, the sorbent was completely regenerated just after 4 minutes. However, after 60 minutes of desorption at 100 ℃ and 120 ℃, the sorbent had lost 0.2 wt% and 0.9 wt% of its original weight, respectively, which was assumed to be of organic matter (PEI).

6.3   Silica Coating

As mentioned in the desorption behaviour section, it was essential to maintain the integrity of the sorbent and to prevent amine loss, in addition to, achieve a complete and fast regeneration at lowest possible desperation temperature. Desorption at 100 ℃ and 120 ℃ led to a loss of PEI, and it was therefore of interest to develop a method to cover the sorbents with a protective silica layer. The methods used are described in section 4.2.2 and Wang's master thesis [53]. Psychical properties of coated sorbents are presented in Table 5.1, while a comparison of the performance of the coated sorbents and the corresponding un-coated sorbents is presented in Table 5.3.

First, MSS-2/40PEI and its corresponding coated sorbents were examined and compared for nine cyclic adsorption/desorption tests at three different desorption temperatures (75 ℃, 100 ℃ and 120 ℃). These samples, in addition to MSS-4/40PEI and its corresponding coated sorbents, were prepared by Wang [53]. It was shown from Table 5.1 that the stability of the sorbent was almost identical after nine adsorptions/desorption cycles at 75 ℃ desorption. On the other hand, an increase in desorption temperature led to more reduced stability of silica-coated sorbent compared to the un-coated sorbent. The same result was observed for MSS-4/40PEI and its corresponding coated sorbents. While the un-coated sorbent maintained a relatively good cyclic stability at high desorption temperature, the coated sorbent showed more reduced stability which was the opposite as expected. As discussed in section 6.1.3, the method had no hydrolysis step nor condensation of silanols on the surface of the MSS. Due to a lower CO_2 adsorption capacity for the coated samples, it might be a possibility that TEOS molecules covered the surfaces. However, with no hydrolysis or condensation step, it is hard to imagine the formation of a silica layer based on the coating method described in the thesis. Hence, it was of interest to develop a new method.

The coating methods used in this work was based on the hydrolysis of the silica precursor (TEOS and TMOMS) and condensation of silanols on the surface of MSS. TEOS and colloidal silica were used as silica precursor for coating method 1. MSS-3/40PEI were the sorbent to be covered due to a shortage of MSS-2 and MSS-4 support. The adsorption capacity for covered sorbents dropped from 2.07 mmol/g to 0.04 mmol/g. The decrease of adsorption capacity might indicate that the structure of the support got deformed during condensation and PEI loaded pores were blocked, or PEI diffusion out of the pores during condensation and washing. PEI diffusion was considered as the most likely reason for the drop of adsorption capacity. As discussed in section 6.1.3, a larger volume of silica-coated sorbents was loaded to the sample pan in order to reach the wanted mass, compared to sorbents without silica-coating. Hence, the samples must have had a weight loss during the coating method, which could be an indication that PEI

might have diffused out the pores. The cyclic adsorption/desorption tests for MSS-3/40PEI/TEOS and MSS-3/40PEI/Col.SiO$_2$ were cancelled after 8 and 3 cycles, respectively. A shorter condensation time was carried out in order to see if it affected the diffusion of PEI. For this case, the adsorption capacity dropped from 2.07 mmol/g to 0.91 mmol/g, and the stability also decreased.

A second method (method 2) was developed in order to try to reduce the loss of PEI during condensation. TMOMS were used as the silica precursor since it was more soluble in water compared to TEOS. Ethanol, which may have led to a lower diffusion limitation for PEI to escape out of the pores, could be excluded from method 2. A new sorbent, MSS-5/40PEI, was used for this method since all MSS-3 were used for modification method 1. Table 5.3 showed no improvement for either stability nor capacity. The pore size of MSS-5 was measured to be lager than for the other supports. Large pore size may have an impact on the diffusion of PEI during condensation. The condensation step in method 2 lasted for only 3 minutes, which indicate that a great quantity of PEI was lost in a short time.

The low pore volumes of the supports and relatively large loading of PEI was another parameter that could affect the poor coating results. All supports had been loaded with 40 wt% of PEI for comparison reasons. The results obtained from TKP4580 - Chemical Engineering, Specialization Project autumn 2019 showed that MSS impregnated with 40 wt% of PEI gave the highest CO$_2$ adsorption capacity [86]. However, the amine efficiency of the same MSS impregnated with 30 wt% PEI was higher. Low amine efficiency indicated un-used active amine sites for support loaded with for 40 wt% PEI, and that there could be an external layer of PEI covering the sorbent. In order to investigate if external PEI-layer could affect the coating method, MSS-5 were impregnated with as low as 25 wt% PEI. The results for Table 5.3 showed more reduced CO$_2$ adsorption capacity, but the stability improved with almost 1 %. The lower capacity may indicate loss of PEI, but it might also be due to blockages of amine sites by the protecting silica layer. However, this improvement of stability was not as good as expected. It was therefore suggested to do more research on silica-coating of sorbents with lager pore volumes and higher surface area, which could handle a higher PEI loading.

6.4 Kinetic Modeling

The dynamic adsorption/desorption behaviour for relative CO$_2$ adsorption capacities for all sorbents are presented in Figure 5.6a and 5.6b. Dynamic adsorption/desorption with real numbers are presented in Figure 5.6 in Appendix B.2.1. The relative adsorption/desorption curve made it possible to observe the rate of adsorption for each sorbent and compare them. MSS-1/40PEI showed

the poorest adsorption rate as the curve flattened out relatively fast compared to MSS-4/40PEI. With lower PEI loading, a faster adsorption rate was obtained. From Table 5.1, a lower PEI loading resulted in a larger surface area covered with PEI for CO_2 to react on, which explains the faster adsorption rate in the initial phase. Also, the pore volume was lager as the pores contained less amount of amine, which may have led to reduced diffusive mass transfer limitation [47]. For regeneration of saturated sorbents, the temperature was set 75 °C in pure N_2 gas. The most noticeable observation was that desorption was a much slower process than adsorption. In addition, a lower loading of PEI resulted in a faster desorption process, which was the same trend also observed for the adsorption process. MSS-3 showed similar adsorption rate behaviour as MSS-2 and MSS-5 with equal PEI loading and same adsorption time. However, the desorption process for MSS-3 was faster than MSS-2 and MSS-5. The different desorption behaviour might indicate different pore structure of the support.

6.4.1   Evaluation of the Kinetic Models

Figure 5.7 to 5.13 illustrate the CO_2 adsorption capacity vs time in 5% CO_2 gas balanced with N_2 at 75 °C for each sorbents, and the corresponding generated adsorption profiles by five different kinetic models. All sorbents showed a steep adsorption curve during the initial adsorption stage. The generated adsorption profiles fitted quite poorly if long term adsorption (100/60 minutes) were taken into account. Especially pseudo-first-order and pseudo-second-order kinetic models showed poor $RMSE$ and R^2, and a relatively large ADD, which can bee seen in Table 5.5 and 5.6 for long term adsorption. Introducing the Avrami, fractional-order and dual kinetic models, the corresponding adsorption profiles showed better agreement to the experimental adsorption compared to the two other models. However, the kinetic models did not give a satisfying $RMSE$ and R^2, but the ADD was acceptable, especially for the fractional-order model. See Table 5.7, 5.8 and 5.9. As the curve of experimental adsorption capacity flattened, the Avrami, the fractional-order and dual kinetic models were all in excellent agreement (See Appendix C.2). The good agreement after initial adsorption explained why ADD was low, even though the kinetic models did not fit properly at the beginning of the adsorption process.

It was found that fractional-order gave the overall best model fitting. A possible explanation was the interaction between amine-impregnated sorbent and CO_2 which may not be a single chemical adsorption process, but rather a more complex chemical adsorption process [74, 88]. First, CO_2 diffused to the surface of the adsorbent before reacting quickly with the active amine sites, as illustrated in Figure 3.11, and the sorbents reached 80% of the maximum adsorption capacity fast. Then, the adsorption rate became slower as the driving force of the adsorption weakened and CO_2 diffusion resistance was increased, due to carbamate formation.

A typical trend observed for the long term adsorption kinetic modelling of pseudo-first-order and pseudo-second-order was a lower adsorption rate compared to the experiment adsorption the first 1-3 minutes. Then, an overestimation occurred until experimental adsorption had reach equilibrium. Avrami and fractional-order kinetic model usually followed the same trend. They had a steeper adsorption slope in the very beginning before an underestimation occurred until after around 4-6 minutes were experimental adsorption and generated models agreed very well. The dual kinetic model fitted the experimental adsorption values very well at the beginning of the first minute before it underestimated the adsorption capacity until around 2 minutes. Then, it overestimated the experimental adsorption. The long term adsorption kinetic modelling showed that it was challenging to fit kinetic models to experimental adsorption.

For the short term adsorption kinetic modelling, where only the first 3 minutes of adsorption were taken into account, the trend was slightly different. Here, all kinetic models, except pseudo-second-order, fitted the experiment adsorption very well, which can be seen from figures 5.7 to 5.13. The good agreement was also verified by low $RMSE$ and extremely high R^2, which can be found in Table 5.5 to 5.9. However, the ADD tended to show higher values than for long term adsorption. Since short term adsorption kinetic modelling only took the beginning of each adsorption into account, the experimental adsorption capacity with flat curves after 3 minutes was not included. It was in this region the Avrami, fractional-order and dual kinetic models were in excellent agreement with experimental data for long term adsorption. The fractional-order kinetic model was found to give the best fitting of the initial adsorption step, which was the most challenging step for kinetic model fitting. The values form Table 5.8 showed low $RMSE$ and extremely high R^2, which indicated strong agreement of the model and experimental data. Figure 5.7a, 5.8b and 5.11b showed a small change in adsorption rate after approximately 0.1 minute. Even here, the fractional-order model followed the experimental graph, while the other models did not.

6.4.2 Dependence of Adsorption Conditions on Kinetic Parameters

Judged by the values from the kinetic modelling tables, it was not easy to decide which of the sorbents that were the fastest or most preferable for industrial usage. However, the parameters n and m in fractional-order equation (equation 3.13) indicated the driving force and diffusion resistance, respectively [47]. A large value of n indicated that the driving force (number of unoccupied amine sites) was dominating the adsorption. In other words, n indicated the pseudo-order of the reaction between the active amine sites and CO_2 molecules. For MSS-3/40PEI it was shown by Table 5.8 that an increase in adsorption tem-

perature increased n, for short term adsorption. A faster absorption rate at 75 ℃ was also visible from Figure 5.15. The value of n, shown in Table 5.8, was more stable even with an increment of CO_2 partial pressure from 2% to 50%. However, the fitting of the fractional-order model was slightly poorer for high CO_2 partial pressure at short term adsorption. The presence of concentrated CO_2 might have influenced the adsorption from undergoing isothermally due to thermal effects [50]. The poorer adsorption fitting, shown in Figure 5.14b, could be a result since the specific isotherm requirements were not fulfilled. Based on the short term adsorption from Table 5.8, the lower partial pressure of CO_2 (2% CO_2 gas) provided extremely accurate adsorption profiles by the fractional-order model. It was shown that n increased with increasing adsorption temperature or increasing partial pressure of CO_2 in the gas, which indicated a lower reaction order if the adsorption temperature or CO_2 concentration decreased.

The observation of n's dependence on adsorption temperature or CO_2 concentration was in good agreement with Heydari-Gorji et al. kinetic study of PEI impregnated MCM-41 [47], and the model in this thesis predicted that a high driving force, gave a high k_F value and a n between 1 and 3. How fast the adsorption was, could be given by the parameter m. No clear trend was found with a different partial pressure of CO_2. However, a lower amine loading increased the value of m for MSS-5 sorbents at short term adsorption, as expected. For MSS-1 support, this was not the case, and the trend of m was unclear. Since visible deformation of the MSS-1 occurred during the impregnation process, it is hard to compare MSS-1 with different amine loading as the impregnation was done in two separate batches. In addition, the time used to impregnate a lower amine loading was shorter than the time required to impregnate higher amine loadings. The difference in impregnation time may have affected the damaging structure of the support.

The fractional-order kinetic model did not give a very systematic relationship between the model parameters and the CO_2 partial pressure in the feed gas. However, the dual kinetic model showed a clear trend for the kinetic parameters that could describe the CO_2 adsorption capacity at different CO_2 partial pressure in the feed gas. An increasing CO_2 partial pressure resulted in increasing k_{DMK} and n, and a decreasing β for long term adsorption and increasing β for the short term adsorption. However, the fitting was slightly better for the fractional-order model. The clear trend by the kinetic parameter under different CO_2 partial pressures provided a great advantage to the dual kinetic model for usages in process analysis with different feed compositions [78].

Chapter 7

Conclusion

A series of 5 mesoporous silica spheres (MSS) with different physical properties, synthesised by carbon hard template method, were modified with polyethylenimine (PEI) by wet impregnation method with different amine loadings. A new method for silica coating of the sorbents was also proposed. This study contributed to a systematic investigation of CO_2 adsorption and desorption behaviour of MSS sorbents in order to understand the effects of physical properties of the support, PEI loadings, temperatures and CO_2 partial pressure on both CO_2 absorption capacity, cyclic stability and kinetics.

After wet impregnation, the porous channels of MSS was filled with PEI in order to increase the CO_2 uptake. The thermalgravimetric analysis results showed that CO_2 adsorption capacity increased with higher amine loadings, and the supports ability to capture CO_2 with the same PEI loading (40 wt%) followed the order: MSS-3 > MSS-5 > MSS-1 > MSS-2 > MSS-4. Among the tested sorbents, MSS-3/40PEI showed a maximum CO_2 adsorption capacity of 2.24 mmol/g at 75 ℃ in 5% CO_2 gas. At 50 ℃ in 5% CO_2 gas, the adsorption capacity decreased due to strong diffusion limitations. MSS-1/40PEI showed the best cyclic adsorption/desorption stability, but a poorer adsorption capacity of 1.85 mmol/g. Cyclic stability decreased with lower amine loading on the same support.

In order to prevent loss of amine, new silica coating methods were investigated. However, the results indicated that PEI diffused out of the pores of the support during the coating procedure, which resulted in much weaker CO_2 adsorption capacity and cyclic stability compared to un-coated sorbents. It was suggested

that external PEI, which covered the external surface of the MSS, may have created problems during the condensation reaction of silanols on the surface of the sorbents.

A comparison of 5 kinetic models were investigated using the piecewise non-linear least square analysis. The fractional-order kinetic model was found to give the overall best fitting of the CO_2 adsorption behaviour with various PEI loadings and under different adsorption conditions, such as various CO_2 partial pressure and adsorption temperatures. Good agreement between the experimental results and the kinetic model was verified with a low value of $RMSE$ and R^2 close to one. The fractional-order model could be used to describe the dynamics of CO_2 adsorption on PEI impregnated MSS in simulated low-temperature dry flue gas conditions. Since the kinetics had to be described by fractional orders, it was evident that the adsorption process could not be described as single chemical adsorption, but rather a more complex chemical adsorption process.

Finally, the insight and the development of the adsorption kinetics for these sorbents may be used as a tool for designing a packed-bed adsorber for CO_2 capture. The support of the sorbent might need some improvements regarding physical properties and mechanical strength, but the potential of this sorbent for CO_2 capture was very promising.

Chapter 8

Future work

The global pandemic caused by the Covid-19 virus affected the practical lab-work of this master thesis since stricter regulations took effect. Therefore, some of the scheduled work had to be cancelled, and could be interesting recommendations for future work.

It should be of high priority to modify the synthesis of mesoporous silica spheres in order to improve their physical properties and mechanical strength. The surface area and pore volume were small compared to commercial SBA-15 and other mesoporous silica. A larger surface area and pore volume are favoured as it may handle a more significant loading of amine in which may increase the CO_2 adsorption capacity and cyclic stability. Improvement of the mechanical strength of the spheres is also necessary in order to handle the impregnation of amine. The silica spheres tested in this thesis showed weak mechanical strength in which may result in a collapse of pores.

Improvement of the physical properties may lead to less amine on the external surface and better dispersion of amine inside the pores. These improvements may have a positive effect on the silica coating method used in this thesis. It should be investigated, as there might be less interaction with external PEI and silica coating layer.

In order to obtain more realistic adsorption and desorption conditions of CO_2 from simulated flue gas at low-temperature, more parameters should be included. Adding humidity and other components, such as oxygen, to the simulated flue gas creates a more realistic environment inside an adsorbed column

for CO_2 capture, and it is essential to obtain more realistic adsorption kinetic data towards a real carbon capture process. Humidity will enhance the CO_2 adsorption capacity, as described in section 3.2.2. More realistic desorption conditions at higher temperatures and pure CO_2 gas should be investigated in order to obtain more realistic desorption data.

Bibliography

[1] B. Chen and H. Kan, "Air pollution and population health: a global challenge," *Environmental Health and Preventive Medicine*, vol. 13, pp. 94–101, Mar. 2008.

[2] M. Asif and T. Muneer, "Energy supply, its demand and security issues for developed and emerging economies," *Renewable and Sustainable Energy Reviews*, vol. 11, pp. 1388–1413, Sept. 2007.

[3] H. Ritchie and M. Roser, "Energy consumption by source," Nov. 2019. Library Catalog: www.ourworldindata.org/energy, viewed: 04.04.2020.

[4] H. Thee, N. J. Nicholas, K. H. Smith, G. da Silva, S. E. Kentish, and G. W. Stevens, "A kinetic study of CO_2 capture with potassium carbonate solutions promoted with various amino acids: Glycine, sarcosine and proline," *International Journal of Greenhouse Gas Control*, vol. 20, pp. 212–222, Jan. 2014.

[5] NOAA US Department of Commerce, "ESRL Global Monitoring Division - Global Greenhouse Gas Reference Network," Apr. 2020. Library Catalog: https://www.esrl.noaa.gov/gmd/ccgg/trends/global.html, viewed 04.04.2020.

[6] Climate Action Tracker, "Temperatures, Addressing global warming," Oct. 2019. Library Cat-alog: www.climateactiontracker.org/global/temperatures/, viewed: 04.04.2020.

[7] M. Mercedes Maroto-Valer, *Developments and innovation in carbon dioxide CO2 capture and storage technology*, vol. 1 of *Energy*. Oxford: Woodhead

Publ, 1 ed., 2010.

[8] M. K. Mondal, H. K. Balsora, and P. Varshney, "Progress and trends in CO2 capture/separation technologies: A review," *Energy*, vol. 46, pp. 431–441, Oct. 2012.

[9] S. Choi, J. Drese, and C. Jones, "Adsorbent Materials for Carbon Dioxide Capture from Large Anthropogenic Point Sources," *ChemSusChem*, vol. 2, pp. 796–854, Sept. 2009.

[10] A. L. Kohl and R. Nielsen, *Gas Purification.* Houston Texas: Gulf Publishing Company, 5 ed., Aug. 1997.

[11] A. Samanta, A. Zhao, G. K. H. Shimizu, P. Sarkar, and R. Gupta, "Post-Combustion CO2 Capture Using Solid Sorbents: A Review," *Industrial & Engineering Chemistry Research*, vol. 51, pp. 1438–1463, Feb. 2012.

[12] N. Dave, T. Do, G. Puxty, R. Rowland, P. H. M. Feron, and M. I. Attalla, "CO2 capture by aqueous amines and aqueous ammonia–A Comparison," *Energy Procedia*, vol. 1, pp. 949–954, Feb. 2009.

[13] A.-H. Lu and S. Dai, eds., *Porous Materials for Carbon Dioxide Capture.* Green Chemistry and Sustainable Technology, Berlin Heidelberg: Springer-Verlag, 1 ed., 2014.

[14] B. Dutcher, M. Fan, and A. G. Russell, "Amine-Based CO2 Capture Technology Development from the Beginning of 2013—A Review," *ACS Applied Materials & Interfaces*, vol. 7, pp. 2137–2148, Feb. 2015.

[15] C. B. Field and V. R. Barros, eds., *Intergovernmental Panel on Climate Change 2014: Impacts, adaptation, and vulnerability.* New York, NY: Cambridge University Press, 2014.

[16] ORD US EPA, "Greenhouse Gases," Nov. 2017. Library Catalog: https://www.epa.gov/report-environment/greenhouse-gases, viewed: 23.04.2020.

[17] X.-L. Yue and Q.-X. Gao, "Contributions of natural systems and human activity to greenhouse gas emissions," *Advances in Climate Change Research*, vol. 9, pp. 243–252, Dec. 2018.

[18] T. F. Stocker and D. Qin, *Intergovernmental Panel on Climate Change 2013: The Physical Science Basis 2013.* New York, NY: Cambridge University Press, 2013.

[19] NOAA US Department of Commerce, "Global Monitoring Laboratory - Global Greenhouse Gas Reference Network," June 2020. Library Catalog: https://www.esrl.noaa.gov/gmd/ccgg/trends/mlo.html, viewed: 15.04.2020.

[20] H. Ritchie and M. Roser, "CO2 and Greenhouse Gas Emissions," May 2017. https://ourworldindata.org/co2-and-other-greenhouse-gas-emissions, Viewed: 15.04.2020.

[21] A. Goeppert, M. Czaun, G. K. Surya Prakash, and G. A. Olah, "Air as the renewable carbon source of the future: an overview of CO2 capture from the atmosphere," *Energy & Environmental Science*, vol. 5, no. 7, p. 7833, 2012.

[22] SINTEF, "This is what you need to know about CCS – Carbon Capture and Storage." Library Catalog: http://www.sintef.no/en/latest-news/this-is-what-you-need-to-know-about-ccs-carbon-capture-and-storage/, viewed: 28.04.2020.

[23] D. Aaron and C. Tsouris, "Separation of CO2 from Flue Gas: A Review," *Separation Science and Technology*, vol. 40, pp. 321–348, Jan. 2005.

[24] J. A. . Moulijn, M. Makkee, and A. v. Diepen, *Chemical process technology.* Chichester: Wiley, 2nd ed. ed., 2013.

[25] H. Naims, "Economics of carbon dioxide capture and utilization—a supply and demand perspective," *Environmental Science and Pollution Research*, vol. 23, pp. 22226–22241, Nov. 2016.

[26] E. Fujita and C. Creutz, *Carbon Dioxide as a Feedstock, Chapter 5.* National Academies Press (US), 2001. Library Catalog: https://www.ncbi.nlm.nih.gov/books/NBK44146/, viewed: 30.05.2020.

[27] C. Song, Q. Liu, S. Deng, H. Li, and Y. Kitamura, "Cryogenic-based CO2 capture technologies: State-of-the-art developments and current challenges," *Renewable and Sustainable Energy Reviews*, vol. 101, pp. 265–278, Mar. 2019.

[28] J. Xu, Z. Wang, C. Zhang, S. Zhao, Z. Qiao, P. Li, J. Wang, and S. Wang, "Parametric analysis and potential prediction of membrane processes for hydrogen production and pre-combustion CO2 capture," *Chemical Engineering Science*, vol. 135, pp. 202–216, Oct. 2015.

[29] X. Deng, H. Wang, H. Huang, and M. Ouyang, "Hydrogen flow chart in

China," *International Journal of Hydrogen Energy*, vol. 35, pp. 6475–6481, July 2010.

[30] R. Stanger, T. Wall, R. Spörl, M. Paneru, S. Grathwohl, M. Weidmann, G. Scheffknecht, D. McDonald, K. Myöhänen, J. Ritvanen, S. Rahiala, T. Hyppänen, J. Mletzko, A. Kather, and S. Santos, "Oxyfuel combustion for CO2 capture in power plants," *International Journal of Greenhouse Gas Control*, vol. 40, pp. 55–125, Sept. 2015.

[31] K. Stéphenne, "Start-up of World's First Commercial Post-combustion Coal Fired CCS Project: Contribution of Shell Cansolv to SaskPower Boundary Dam ICCS Project," *Energy Procedia*, vol. 63, pp. 6106–6110, Jan. 2014.

[32] J. Wang, L. Huang, R. Yang, Z. Zhang, J. Wu, Y. Gao, Q. Wang, D. O'Hare, and Z. Zhong, "Recent advances in solid sorbents for CO 2 capture and new development trends," *Energy & Environmental Science*, vol. 7, no. 11, pp. 3478–3518, 2014.

[33] N. El Hadri, D. V. Quang, E. L. V. Goetheer, and M. R. M. Abu Zahra, "Aqueous amine solution characterization for post-combustion CO2 capture process," *Applied Energy*, vol. 185, pp. 1433–1449, Jan. 2017.

[34] B. Lv, B. Guo, Z. Zhou, and G. Jing, "Mechanisms of CO2 Capture into Monoethanolamine Solution with Different CO2 Loading during the Absorption/Desorption Processes," *Environmental Science & Technology*, vol. 49, pp. 10728–10735, Sept. 2015.

[35] Y. Liu, W. Fan, K. Wang, and J. Wang, "Studies of CO2 absorption/regeneration performances of novel aqueous monothanlamine (MEA)-based solutions," *Journal of Cleaner Production*, vol. 112, pp. 4012–4021, Jan. 2016.

[36] Q. Wang, J. Luo, Z. Zhong, and A. Borgna, "CO2 capture by solid adsorbents and their applications: current status and new trends," *Energy & Environmental Science*, vol. 4, no. 1, pp. 42–55, 2011.

[37] C.-H. Yu, C.-H. Huang, and C.-S. Tan, "A Review of CO2 Capture by Absorption and Adsorption," *Aerosol and Air Quality Research*, vol. 12, no. 5, pp. 745–769, 2012.

[38] D. M. Ruthven, *Principles of Adsorption and Adsorption Processes*. New York, NY: John Wiley & Sons, 1 ed., June 1984.

[39] H. S. Fogler, *Elements of chemical reaction engineering*. Prentice Hall in-

ternational series in the physical and chemical engineering sciences, Boston: Prentice Hall, 5th ed. ed., 2016.

[40] L. Nie, Y. Mu, J. Jin, J. Chen, and J. Mi, "Recent developments and consideration issues in solid adsorbents for CO2 capture from flue gas," *Chinese Journal of Chemical Engineering*, vol. 26, pp. 2303–2317, Nov. 2018.

[41] C. Zhao, X. Chen, E. J. Anthony, X. Jiang, L. Duan, Y. Wu, W. Dong, and C. Zhao, "Capturing CO2 in flue gas from fossil fuel-fired power plants using dry regenerable alkali metal-based sorbent," *Progress in Energy and Combustion Science*, vol. 39, pp. 515–534, Dec. 2013.

[42] H. Hayashi, J. Taniuchi, N. Furuyashiki, S. Sugiyama, S. Hirano, N. Shigemoto, and T. Nonaka, "Efficient Recovery of Carbon Dioxide from Flue Gases of Coal-Fired Power Plants by Cyclic Fixed-Bed Operations over K2CO3-on-Carbon," *Industrial & Engineering Chemistry Research*, vol. 37, pp. 185–191, Jan. 1998.

[43] A. Okunev, V. Sharonov, Y. Aristov, and V. Parmon, "Sorption of Carbon Dioxide from Wet Gases by K2CO3-in-Porous Matrix: Influence of the Matrix Nature," *Reaction Kinetics and Catalysis Letters*, vol. 71, pp. 355–362, Nov. 2000.

[44] S. C. Lee, B. Y. Choi, T. J. Lee, C. K. Ryu, Y. S. Ahn, and J. C. Kim, "CO2 absorption and regeneration of alkali metal-based solid sorbents," *Catalysis Today*, vol. 111, pp. 385–390, Feb. 2006.

[45] S. Ahmed, A. Ramli, and S. Yusup, "CO2 adsorption study on primary, secondary and tertiary amine functionalized Si-MCM-41," *International Journal of Greenhouse Gas Control*, vol. 51, pp. 230–238, Aug. 2016.

[46] Sigma-Aldrich, "Mesoporous Silica and their Applications." Library Catalog: https://www.sigmaaldrich.com/technical-documents/articles/materials-science/renewable-alternative-energy/mesoporous-silica.html, viewed: 25.04.2020.

[47] A. Heydari-Gorji and A. Sayari, "CO2 capture on polyethylenimine-impregnated hydrophobic mesoporous silica: Experimental and kinetic modeling," *Chemical Engineering Journal*, vol. 173, pp. 72–79, Sept. 2011.

[48] S. Lagergren, "Zur theorie der sogenannten adsorption gelöster stoffe," *Kungliga Svenska Vetenskapsakademiens*, vol. 4, pp. 1–39, 1898.

[49] R. Serna-Guerrero and A. Sayari, "Modeling adsorption of CO2 on amine-functionalized mesoporous silica. 2: Kinetics and breakthrough curves," *Chemical Engineering Journal*, vol. 161, pp. 182–190, July 2010.

[50] A. Zhao, A. Samanta, P. Sarkar, and R. Gupta, "Carbon Dioxide Adsorption on Amine-Impregnated Mesoporous SBA-15 Sorbents: Experimental and Kinetics Study," *Industrial & Engineering Chemistry Research*, vol. 52, pp. 6480–6491, May 2013.

[51] L. Zhang, N. Zhan, Q. Jin, H. Liu, and J. Hu, "Impregnation of Polyethylen-imine in Mesoporous Multilamellar Silica Vesicles for CO2 Capture: A Kinetic Study," *Industrial & Engineering Chemistry Research*, vol. 55, pp. 5885–5891, May 2016.

[52] W. Stöber, A. Fink, and E. Bohn, "Controlled growth of monodisperse silica spheres in the micron size range," *Journal of Colloid and Interface Science*, vol. 26, pp. 62–69, Jan. 1968.

[53] S. Wang, "Synthesis of Low-Temperature Sorbent for CO2 Capture," master Thesis, Norwegian University of Science and Technology, Trondheim, Norway, 2019.

[54] K. Z. Gaca and J. Sefcik, "Mechanism and kinetics of nanostructure evolution during early stages of resorcinol–formaldehyde polymerisation," *Journal of Colloid and Interface Science*, vol. 406, pp. 51–59, Sept. 2013.

[55] V. M. Ortiz-Martínez, L. Gómez-Coma, A. Ortiz, and I. Ortiz, "Overview on the use of surfactants for the preparation of porous carbon materials by the sol-gel method: applications in energy systems," *Reviews in Chemical Engineering*, vol. 1, Mar. 2019.

[56] C. Lin and J. A. Ritter, "Effect of synthesis pH on the structure of carbon xerogels," *Carbon*, vol. 35, pp. 1271–1278, Jan. 1997.

[57] J. Wang, Q. Chen, X. Liu, W. Qiao, D. Long, and L. Ling, "Hard-templating synthesis of mesoporous carbon spheres with controlled particle size and mesoporous structure for enzyme immobilization," *Materials Chemistry and Physics*, vol. 129, pp. 1035–1041, Oct. 2011.

[58] J. Moeller-Siegert, J. Parmentier, K. Anselme, and C. Vix-Guterl, "Meso-porous hydroxyapatite by hard templating of silica and carbon foams for protein release," *Journal of Materials Science*, vol. 48, pp. 3722–3730, May 2013.

[59] I. Chorkendorff and J. W. Niemantsverdriet, *Concepts of Modern Catalysis and Kinetics.* DE: Wiley-VCH, John Wiley & Sons, Incorporated, 1. aufl. ed., 2003.

[60] X. Xu, C. Song, J. M. Andrésen, B. G. Miller, and A. W. Scaroni, "Preparation and characterization of novel CO2 "molecular basket" adsorbents based on polymer-modified mesoporous molecular sieve MCM-41," *Microporous and Mesoporous Materials*, vol. 62, pp. 29–45, Aug. 2003.

[61] J. Zhu, J. Yang, A. H. Lillebø, Y. Zhu, Y. Yu, A. Holmen, and D. Chen, "Compact reactor for Fischer–Tropsch synthesis based on hierarchically structured Co catalysts: Towards better stability," *Catalysis Today*, vol. 215, pp. 121–130, Oct. 2013.

[62] N. M. Deraz, "The comparative jurisprudence of catalysts preparation methods: I. Precipitation and impregnation methods.," *Journal of Industrial and Environmental Chemistry*, vol. 1, no. 2, 2017.

[63] K. P. d. Jong, ed., *Synthesis of Solid Catalysts*, vol. 1. John Wiley & Sons, Ltd, 1 ed., 2009.

[64] Sigma-Aldrich, "Polyethylenimine, Branched, Mw 600 (bPEI 600)." Library Catalog: https://www.polysciences.com/default/catalog-products/polyethylenimine-branched-bpei-600, viewed: 17.07.2020.

[65] G. Zhang, P. Zhao, L. Hao, and Y. Xu, "Amine-modified SBA-15(P): A promising adsorbent for CO2 capture," *Journal of CO2 Utilization*, vol. 24, pp. 22–33, Mar. 2018.

[66] C. F. Cogswell, H. Jiang, J. Ramberger, D. Accetta, R. J. Willey, and S. Choi, "Effect of Pore Structure on CO2 Adsorption Characteristics of Aminopolymer Impregnated MCM-36," *Langmuir*, vol. 31, pp. 4534–4541, Apr. 2015.

[67] C. H. Bartholomew, "Mechanisms of catalyst deactivation," *Applied Catalysis A: General*, vol. 212, pp. 17–60, Apr. 2001.

[68] W. Chen, C. Takai, H. R. Khosroshahi, M. Fuji, and T. Shirai, "Surfactant-free fabrication of SiO2-coated negatively charged polymer beads and monodisperse hollow SiO2 particles," *Colloids and Surfaces A: Physico-chemical and Engineering Aspects*, vol. 481, pp. 375–383, Sept. 2015.

[69] K. S. W. Sing, D. H. Everett, R. A. W. Haul, L. Moscou, R. A. Pierotti, J. Rouquerol, and T. Siemieniewska, "Reporting Physisorption Data for

Gas/Solid Systems with Special Reference to the Determination of Surface Area and Porosity," *International Union of Pure and Applied Chemistry*, vol. 57, no. 4, pp. 603–619, 1985.

[70] H. Knèozinger, H. Knözinger, J. Weitkamp, and G. Ertl, *Handbook of heterogeneous catalysis.* Place of publication not identified: VCH, 1997.

[71] A. W. Coats and J. P. Redfern, "Thermogravimetric analysis. A review," *Analyst*, vol. 88, pp. 906–924, Jan. 1963.

[72] TGA Q Series, "TGA Q Series Getting Started Guide." LibraryCatalog: https://www.usf.edu/research-innovation/rf/usf-connect/documents/tga-q500.pdf, viewed: 21.05.2020.

[73] K. J. MacKenzie, O. M. Dunens, and A. T. Harris, "Insights into carbon nanotube growth using an automated gravimetric apparatus," *Carbon*, vol. 59, pp. 344–365, Aug. 2013.

[74] K. Ge, Q. Yu, S. Chen, X. Shi, and J. Wang, "Modeling CO2 adsorption dynamics within solid amine sorbent based on the fundamental diffusion-reaction processes," *Chemical Engineering Journal*, vol. 364, pp. 328–339, May 2019.

[75] A. Abdollahi-Govar, A. D. Ebner, and J. A. Ritter, "New Kinetic Model That Describes the Reversible Adsorption and Desorption Behavior of CO2 in a Solid Amine Sorbent," *Energy & Fuels*, vol. 29, pp. 4492–4502, July 2015.

[76] Y. S. Ho and G. McKay, "Pseudo-second order model for sorption processes," *Process Biochemistry*, vol. 34, pp. 451–465, July 1999.

[77] E. C. N. Lopes, F. S. C. dos Anjos, E. F. S. Vieira, and A. R. Cestari, "An alternative Avrami equation to evaluate kinetic parameters of the interaction of Hg(II) with thin chitosan membranes," *Journal of Colloid and Interface Science*, vol. 263, pp. 542–547, July 2003.

[78] B. Ohs, M. Krödel, and M. Wessling, "Adsorption of carbon dioxide on solid amine-functionalized sorbents: A dual kinetic model," *Separation and Purification Technology*, vol. 204, pp. 13–20, Oct. 2018.

[79] E. Kreyszig, *Advanced Engineering Mathematics.* New York, United States: John Wiley & Sons Inc, 10 ed., 2011.

[80] "Least-Squares (Model Fitting) Algorithms - MATLAB

    & Simulink - MathWorks Nordic." Library Catalog: https://se.mathworks.com/help/optim/ug/least-squares-model-fitting-algorithms.html#f204, viewed: 25.05.2020.

[81] Hao Wen, Jing Ma, Meiju Zhang, and Guimei Ma, "The comparison research of nonlinear curve fitting in Matlab and LabVIEW," in *2012 IEEE Symposium on Electrical Electronics Engineering (EEESYM)*, pp. 74–77, June 2012.

[82] Y. K. Tovbin, "Molecular theory of adsorption in meso- and macropores and Kelvin equation," *Protection of Metals and Physical Chemistry of Surfaces*, vol. 46, pp. 197–201, Mar. 2010.

[83] X. Xu, C. Song, J. M. Andresen, B. G. Miller, and A. W. Scaroni, "Novel Polyethylenimine-Modified Mesoporous Molecular Sieve of MCM-41 Type as High-Capacity Adsorbent for CO2 Capture," *Energy & Fuels*, vol. 16, pp. 1463–1469, Nov. 2002.

[84] A. Heydari-Gorji, Y. Yang, and A. Sayari, "Effect of the Pore Length on CO2 Adsorption over Amine-Modified Mesoporous Silicas," *Energy & Fuels*, vol. 25, pp. 4206–4210, Sept. 2011.

[85] J. Zhao, F. Simeon, Y. Wang, G. Luo, and T. A. Hatton, "Polyethylenimine-impregnated siliceous mesocellular foam particles as high capacity CO2 adsorbents," *RSC Advances*, vol. 2, pp. 6509–6519, July 2012.

[86] J. L. Grinna, "A kinetic study of solid sorbents for low temperature carbon capture," specialization Project, Norwegian University of Science and Technology, Trondheim, Norway, Dec. 2019.

[87] X. Ma, X. Wang, and C. Song, ""Molecular Basket" Sorbents for Separation of CO2 and H2S from Various Gas Streams," *Journal of the American Chemical Society*, vol. 131, pp. 5777–5783, Apr. 2009.

[88] Y. Wang, T. Du, Z. Qiu, Y. Song, S. Che, and X. Fang, "CO2 adsorption on polyethylenimine-modified ZSM-5 zeolite synthesized from rice husk ash," *Materials Chemistry and Physics*, vol. 207, pp. 105–113, Mar. 2018.

Appendices

Appendix A

Calculation Formulas

A.1 Partial Pressure of Carbon Dioxide

The CO_2 partial pressure inside the quartz tube of the TGA was calculated by the following equation

$$p_{CO2} = \frac{F_{CO2} \cdot X_{CO2}}{F_{CO2} \cdot X_{CO2} + F_{N2} \cdot X_{N2}} \tag{A.1}$$

where F_{CO2} and F_{N2} are the flow rates of the CO_2 containing gas and the N_2 containing gas, respectively. X_{CO2} and X_{N2} are the factions of CO_2 and N_2 inside the gas cylinders.

A.2 Amine Loading

The following equation was used in order to take out the correct amount of PEI to give the wanted PEI loading of the sorbent

$$wt\%_{PEI} = \frac{m_{PEI}}{m_{PEI} + m_{support}} \tag{A.2}$$

where m_{PEI} and $m_{support}$ is the amount of PEI and support, respectively

A.3 Amine Efficiency

Amine efficiency of the sorbents were calculated as the moles of CO_2 per 2 moles of Nitrogen. An assumption that all amines were as effective as others were made in order to make the calculations less complex. Although it was mentioned in the theory section that tertiary amines may not be involved in dry conditions, this assumption gave an small overestimate of available active amine sites for CO_2 capture. Per 43.04 gram repeated PEI unit, there was one mole N, which gave a mass fraction of 0.325 nitrogen to PEI repeating monomer. Equation below shows how to calculate the amine efficiency of the sorbents

$$N_{eff} = \frac{q_e}{wt\%_{PEI} * X_N} * MW_N \tag{A.3}$$

where q_e is CO_2 adsorption capacity, $wt\%_{PEI}$ is the PEI loading, X_N is the fraction of nitrogen to PEI and MW_N is the molar weight of nitrogen. Below follows a calculation example of MSS-3/40PEI:

$$\begin{aligned} N_{eff} &= \frac{2.24 \quad [mmol_{CO2}/g]}{0.40 \quad [g_{PEI}/g] \cdot 0.325 \quad [g_N/g_{PEI}]} \cdot 14 \cdot 10^{-3} \quad [g_N/mmolN] \\ &= \underline{0.241} \quad [mmol_{CO2}/mmol_N] \end{aligned} \tag{A.4}$$

Since all experiment were done under dry conditions, it was assumed that one CO_2 molecule needed 2 N molecules to form carbamate. The amine efficiency then became:

$$N_{eff} = \frac{1}{2} \frac{[mmol_{CO2}]}{[mmol_N]} \cdot 0.241 = \underline{0.121} \quad [mmol_{CO2}]/2mmol_N] \tag{A.5}$$

A.4 Silica Coating

TESO, TMOMS and colloidal silica were used used as silica precursor in order to coat the sorbent with layers of protective silica. In order to find the correct amount of silica precursor for one layer coating, Equation A.6 were used:

$$m_s = \frac{S_{BET} \cdot MW_s}{S_N \cdot N_A} \tag{A.6}$$

where m_s is the calculated amount of silica precursor needed to coat the sorbent

with one layer, S_{BET} is the BET surface area of the sorbent, MW_s is the molar weight of the silica precursor, S_N is the surface area occupied by nitrogen molecule (0.162 nm^2) and N_A is Avogadro's number.

A.5 Kinetic Modelling Error

The error of the model fitting can be found by root mean square error ($RMSE$), which measure the differences between observed values (y_i) and predicted values ($\hat{y}_i$) by a model. $RMSE$ is given by equation A.7

$$RSME = \sqrt{\sum_{i=1}^{N} \frac{(\hat{y}_i - y_i)^2}{N}}, \tag{A.7}$$

where N is the total number of values. In addition, the average absolute percentage deviation (ADD) and coefficient of determination (R^2) was found in order to determine the sufficiency of the models. ADD was calculated by equation A.8

$$ADD = \sum_{i=1}^{N} \left| \frac{\hat{y}_i - y_i}{y_i} \right| \frac{100\%}{N} \tag{A.8}$$

The strength of the fitting between the relative movements of the experimental adsorption and modelled adsorption, was found by the correlation coefficient (R^2). This could be found by the `fitnlm` function in MATLAB. However, R^2 calculations had to be done additionally for the dual kinetic modelling. First it was necessary to calculate sum of squares error (SSE) and sum of squares total (SST):

$$SSE = \sum_{i=1}^{N} (y_i - \hat{y}_i)^2 \tag{A.9}$$

$$SST = \sum_{i=1}^{N} (y_i - \bar{y})^2 \tag{A.10}$$

where $\bar{y}$ is the average of observed values. R^2 could then be found by equation A.11.

$$R^2 = 1 - \frac{SSE}{SST} \tag{A.11}$$

R^2 was improved by an adjusted modification to R^2_{adj}. This adjustment takes into account the number of predicted values in the model:

$$R^2_{adj} = 1 - \frac{p-1}{p-b} \cdot (1 - R^2) \tag{A.12}$$

where p and b is the number of observed values and predicted parameters, respectively.

Appendix B

Experimental Data

B.1 Physical properties

Figure B.1 to B.14 shows nitrogen physisorption isotherms and pore size distributions for all mesoporous silica spheres support, PEI-impregnated sorbents and silica covered sorbents involved in this work, with some exceptions (sorbents made by previous master student)
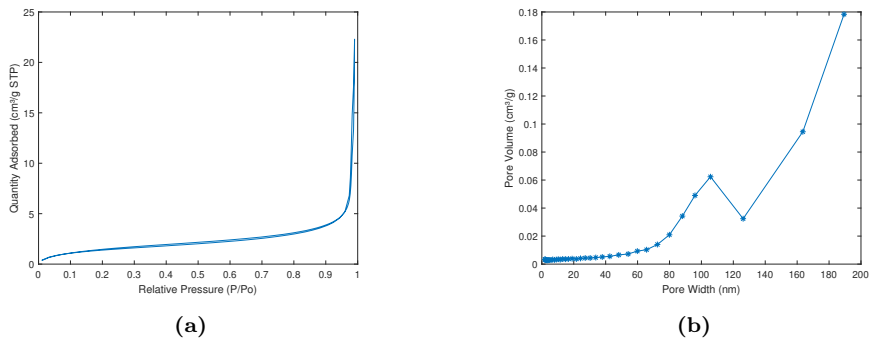

(a)

(b)
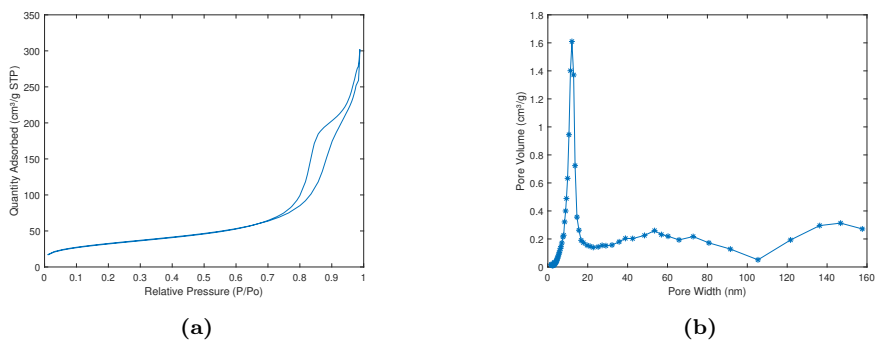
Figure B.1: Nitrogen physisorption isotherm (a) and pore size distribution (b) of MSS-1.
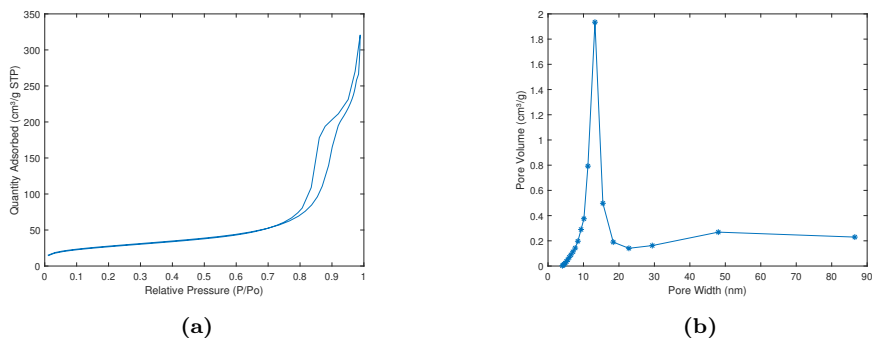
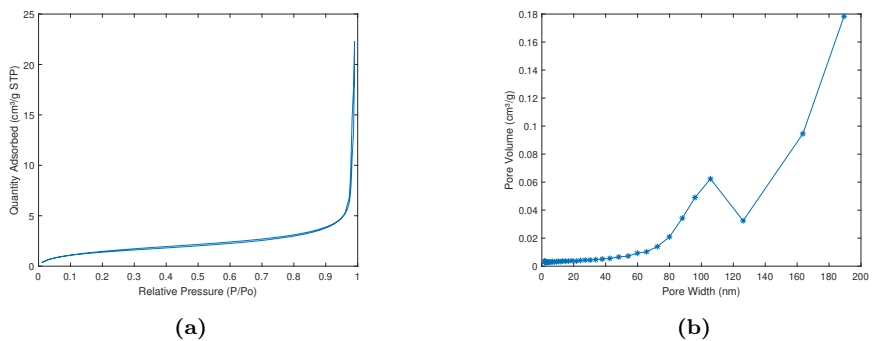**Figure B.2:** Nitrogen physisorption isotherm (a) and pore size distribution (b) of MSS-2.
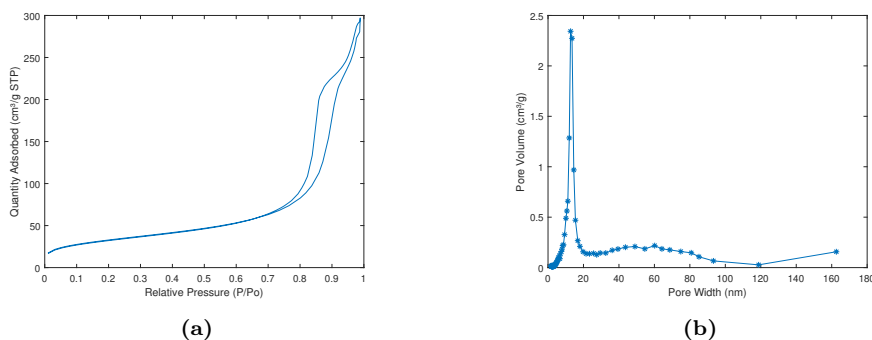
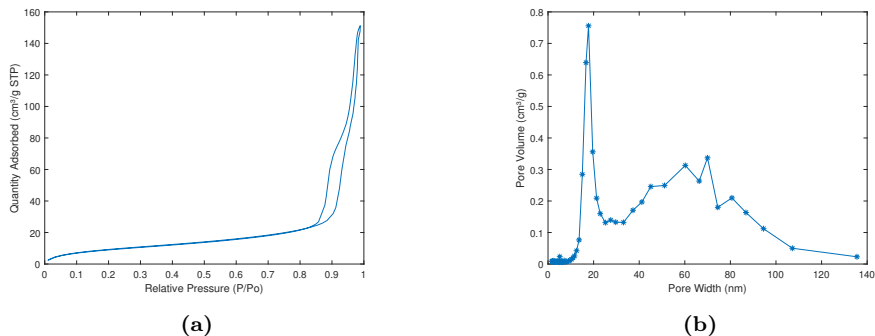**Figure B.3:** Nitrogen physisorption isotherm (a) and pore size distribution (b) of MSS-3.
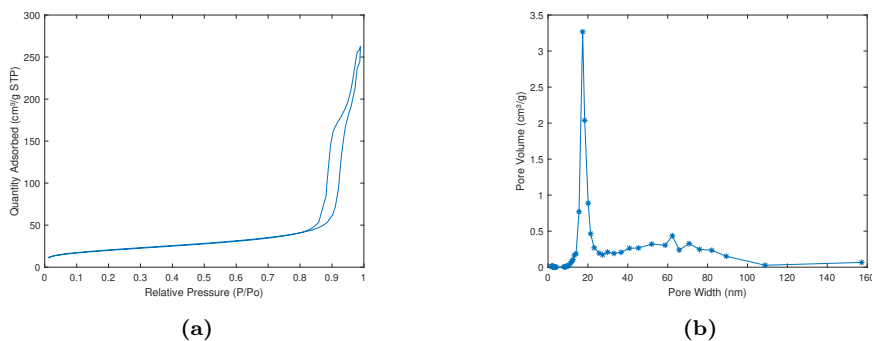
Figure B.4: Nitrogen physisorption isotherm (a) and pore size distribution (b) MSS-5.
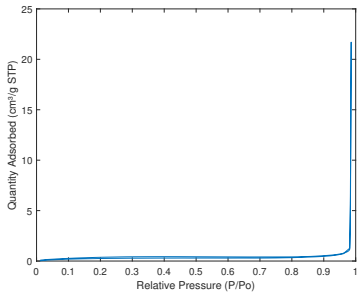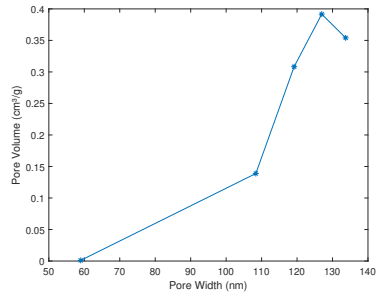
Figure B.5: Nitrogen physisorption isotherm (a) and pore size distribution (b) MSS-1/40PEI.
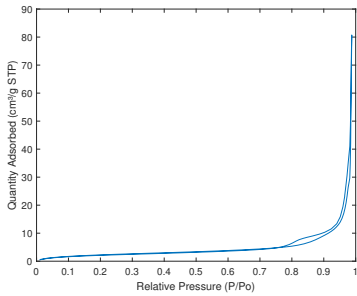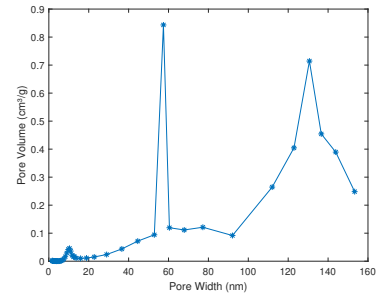
Figure B.6: Nitrogen physisorption isotherm (a) and pore size distribution (b) MSS-1/30PEI.
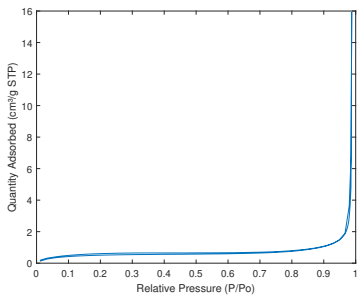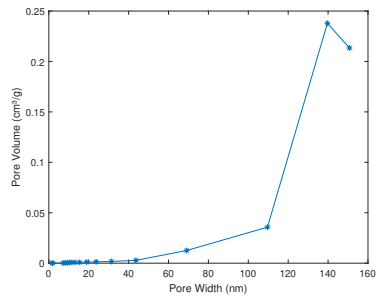
Figure B.7: Nitrogen physisorption isotherm (a) and pore size distribution (b) MSS-2/40PEI.
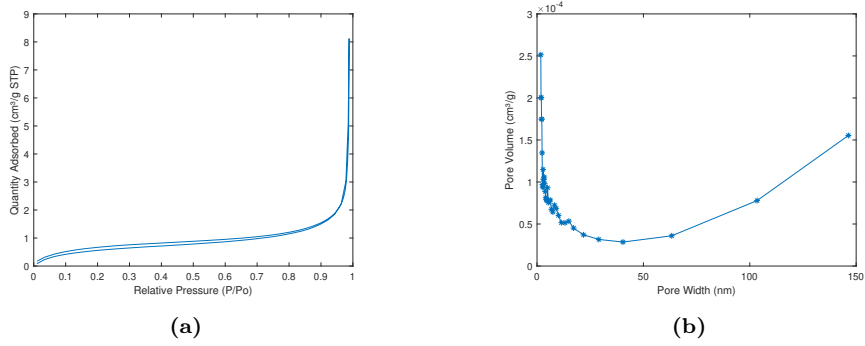
Figure B.8: Nitrogen physisorption isotherm (a) and pore size distribution (b) MSS-3/40PEI.
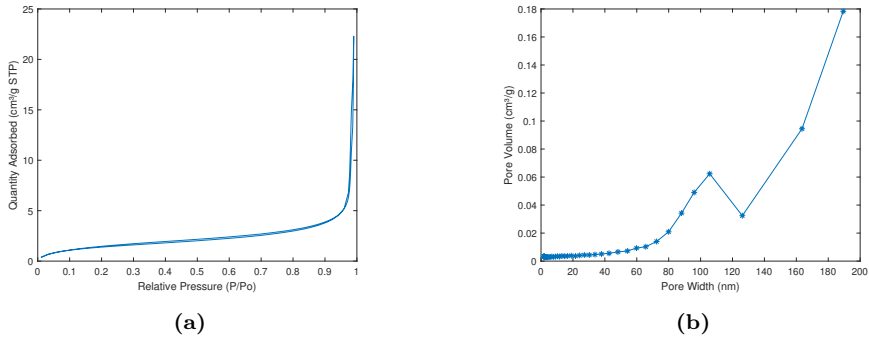
Figure B.9: Nitrogen physisorption isotherm (a) and pore size distribution (b) MSS-5/40PEI.
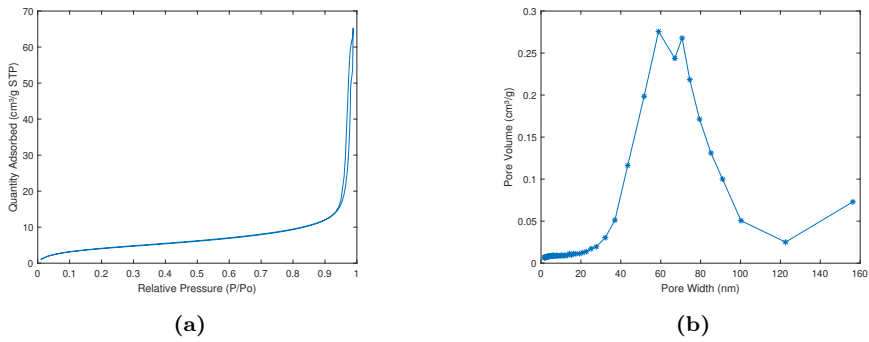
Figure B.10: Nitrogen physisorption isotherm (a) and pore size distribution (b) MSS-5/25PEI.
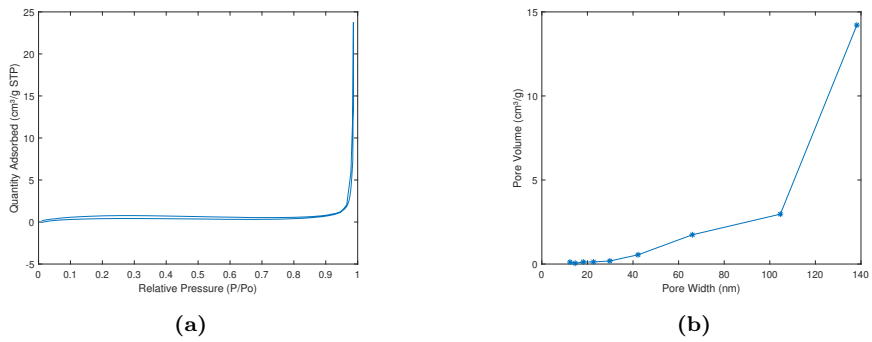
Figure B.11: Nitrogen physisorption isotherm (a) and pore size distribution (b) MSS-2/40PEI/1TEOS.

Figure B.12: Nitrogen physisorption isotherm (a) and pore size distribution (b) MSS-3/40PEI/2Col.

Figure B.13: Nitrogen physisorption isotherm (a) and pore size distribution (b) MSS-5/25PEI/2TMOMS.

Figure B.14: Nitrogen physisorption isotherm (a) and pore size distribution (b) MSS-5/40PEI/2TMOMS.

B.2 Thermogravimetric analysis

B.2.1 Dynamic adsorption/desorption profiles

FigureB.15 illustrate the dynamic adsorption and desorption behaviour in order to illustrate and compare the adsorption/desorption kinetics of all PEI-impregnated sorbents.
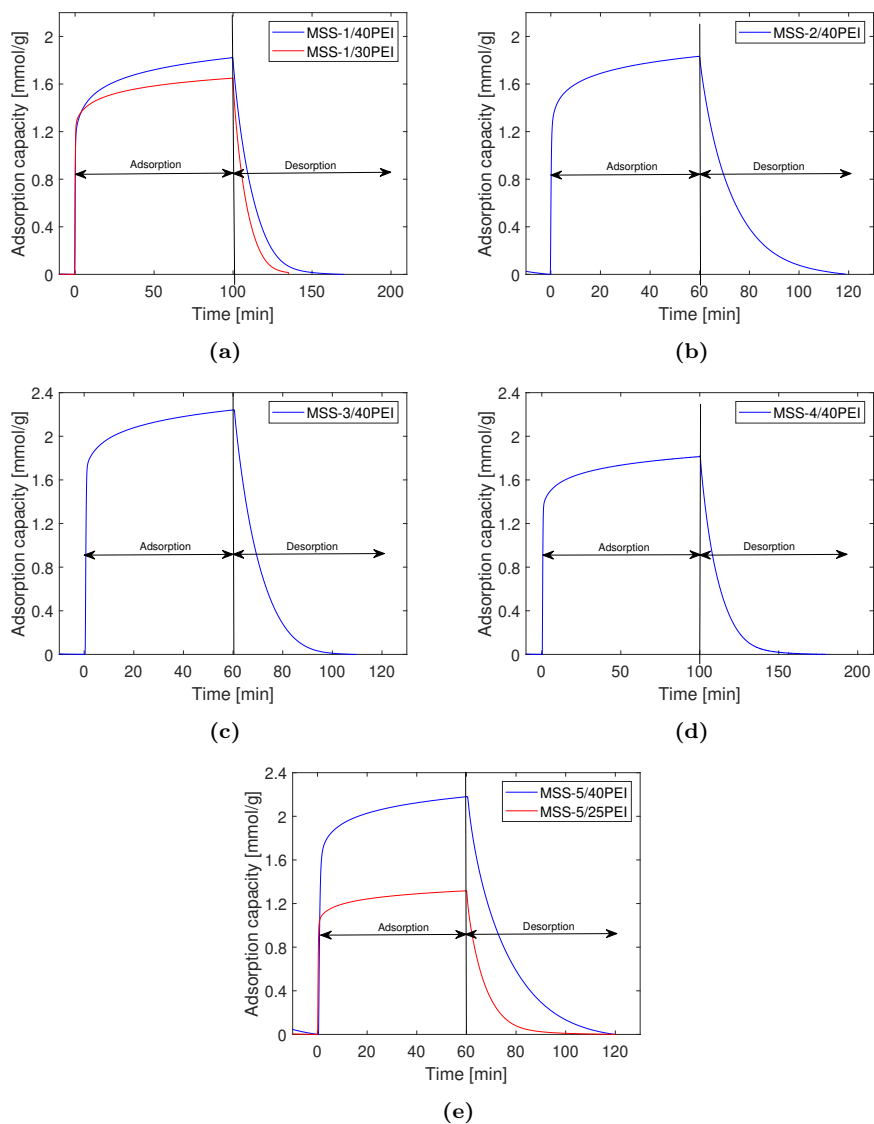
Figure B.15: Typical dynamic adsorption and desorption profiles for PEI impregnated (a) MSS-1, (b) MSS-2, (c) MSS-3, (d) MSS-4 and (e) MSS-5 at 75 ℃ in 5% CO_2 gas for adsorption and 100% N_2 gas for desorption.

B.2.2 Adsorption/Desorption Cycles

The figure B.16 to B.40 show the experimental adsorption and desertion cycles done on PEI impregnated MSS in order to describe the cyclic stability, in addition to, the capacity obtain at each cycle. Conditions are given in the figure text.
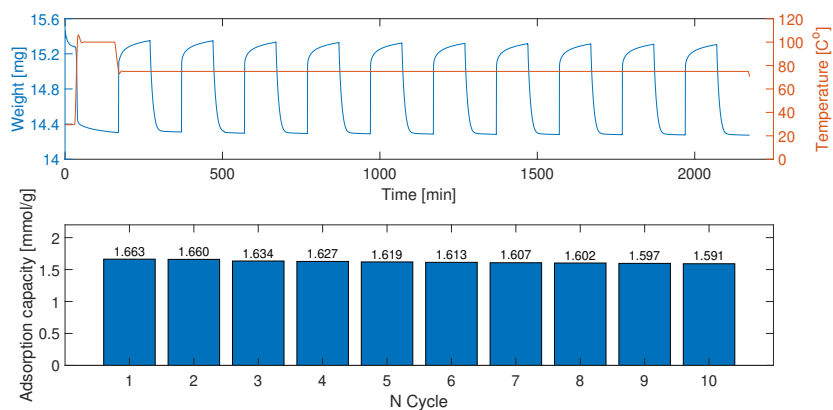
MSS-1 sorbent
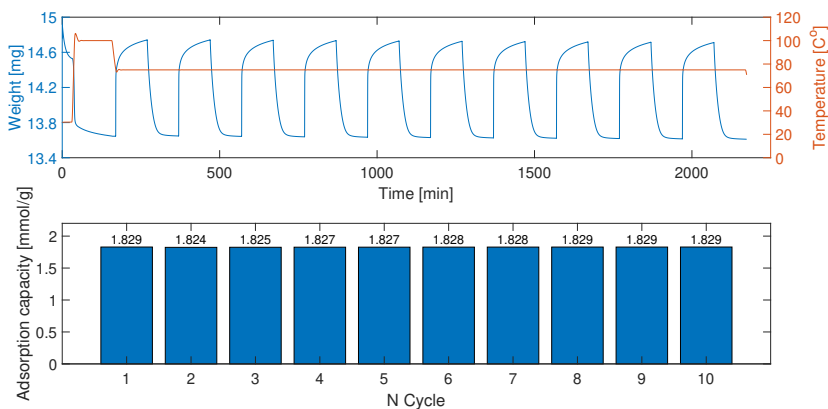
Figure B.16: 10 cycles CO_2 adsorption and desorption plot and cyclic CO_2 adsorption capacities of MSS-1 with 40 wt% PEI impregnation under following conditions: $T_{asd} = 75$ °C, $T_{des} = 75$ °C, $p_{CO_2,ads} = 0.05$ bar, $p_{CO_2,des} = 0$ bar.
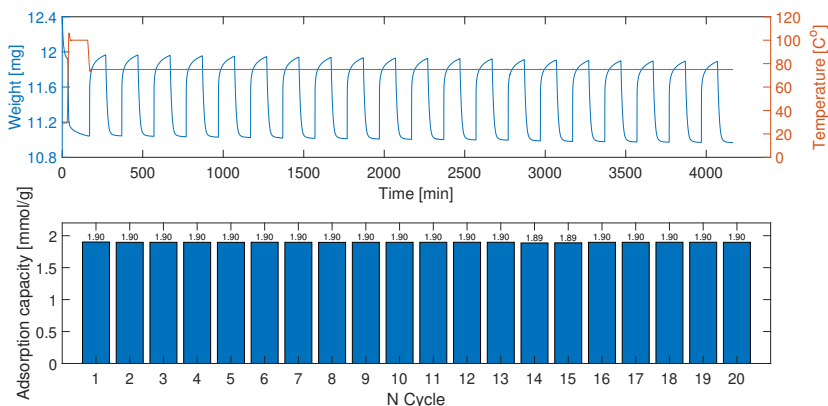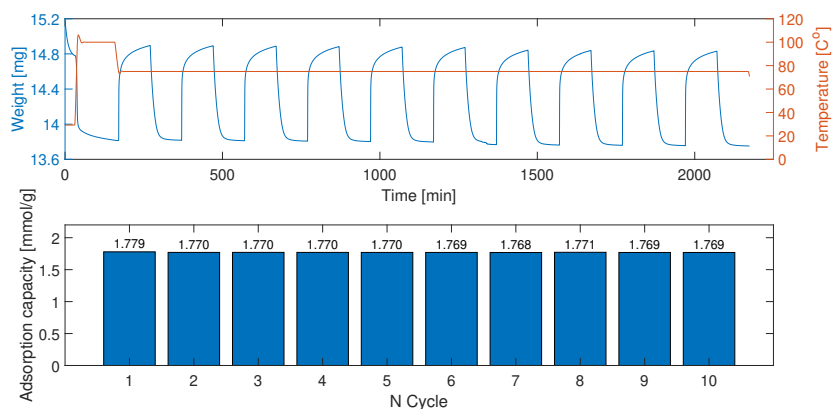

Figure B.17: 20 cycles CO_2 adsorption and desorption plot and cyclic CO_2 adsorption capacities of MSS-1 with 40 wt% PEI impregnation under following conditions: $T_{asd} = 75$ °C, $T_{des} = 75$ °C, $p_{CO_2,ads} = 0.05$ bar, $p_{CO_2,des} = 0$ bar.

Figure B.18: 10 cycles CO_2 adsorption and desorption plot and cyclic CO_2 adsorption capacities of MSS-1 with 30 wt% PEI impregnation under following conditions: $T_{asd} = 75$ °C, $T_{des} = 75$ °C, $p_{CO_2,ads} = 0.05$ bar, $p_{CO_2,des} = 0$ bar.
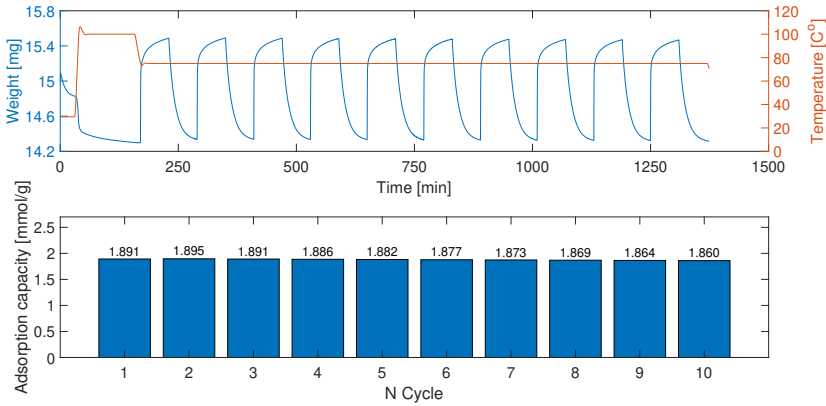

Figure B.19: 10 cycles CO_2 adsorption and desorption plot and cyclic CO_2 adsorption capacities of MSS-1 with 40 wt% PEI impregnation under following conditions: $T_{asd} = 75$ °C, $T_{des} = 75$ °C, $p_{CO_2,ads} = 0.02$ bar, $p_{CO_2,des} = 0$ bar.
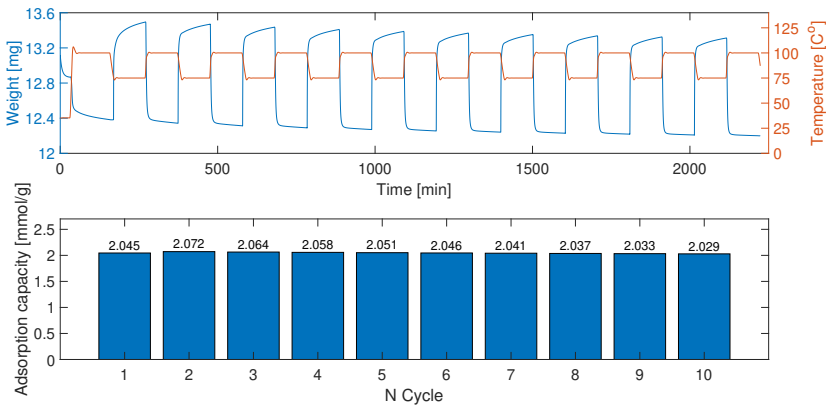
MSS-2 sorbent

Figure B.20: 10 cycles CO_2 adsorption and desorption plot and cyclic CO_2 adsorption capacities of MSS-2 with 40 wt% PEI impregnation under following conditions: $T_{asd} = 75$ ℃, $T_{des} = 75$ ℃, $p_{CO_2,ads} = 0.05$ bar, $p_{CO_2,des} = 0$ bar.

Figure B.21: 10 cycles CO_2 adsorption and desorption plot and cyclic CO_2 adsorption capacities of MSS-2 with 40 wt% PEI impregnation under following conditions: $T_{asd} = 75$ ℃, $T_{des} = 100$ ℃, $p_{CO_2,ads} = 0.05$ bar, $p_{CO_2,des} = 0$ bar.
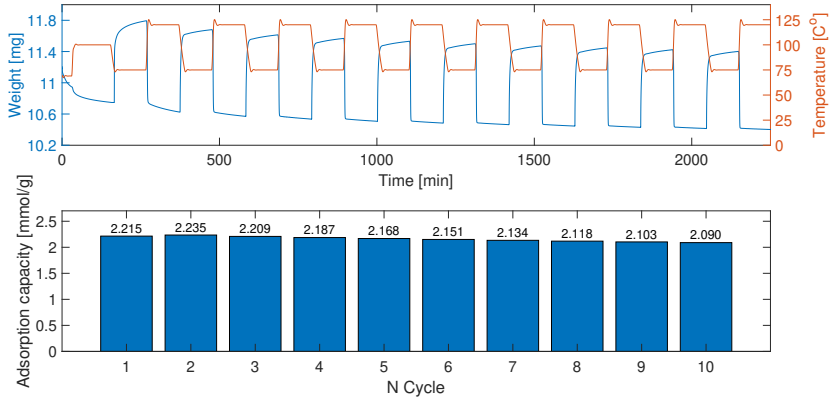
Figure B.22: 10 cycles CO_2 adsorption and desorption plot and cyclic CO_2 adsorption capacities of MSS-2 with 40 wt% PEI impregnation under following conditions: $T_{asd} = 75$ ℃, $T_{des} = 120$ ℃, $p_{CO_2,ads} = 0.05$ bar, $p_{CO_2,des} = 0$ bar.

MSS-2 w/silica coating

Figure B.23: 10 cycles CO_2 adsorption and desorption plot and cyclic CO_2 adsorption capacities of MSS-2 with 40 wt% PEI impregnation and coated with one layer TEOS under following conditions: $T_{asd} = 75$ ℃, $T_{des} = 75$ ℃, $p_{CO_2,ads} = 0.05$ bar, $p_{CO_2,des} = 0$ bar.
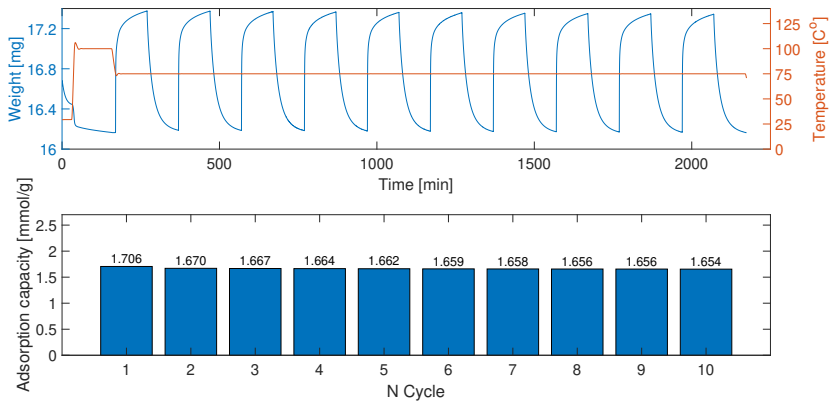
Figure B.24: 10 cycles CO_2 adsorption and desorption plot and cyclic CO_2 adsorption capacities of MSS-2 with 40 wt% PEI impregnation and coated with one layer TEOS under following conditions: $T_{asd} = 75$ °C, $T_{des} = 100$ °C, $p_{CO_2,ads} = 0.05$ bar, $p_{CO_2,des} = 0$ bar.
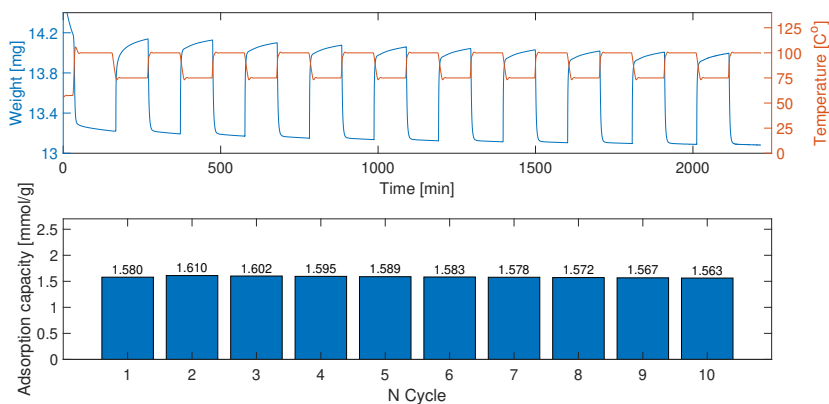

Figure B.25: 10 cycles CO_2 adsorption and desorption plot and cyclic CO_2 adsorption capacities of MSS-2 with 40 wt% PEI impregnation and coated with one layer TEOS under following conditions: $T_{asd} = 75$ °C, $T_{des} = 120$ °C, $p_{CO_2,ads} = 0.05$ bar, $p_{CO_2,des} = 0$ bar.

Figure B.26: 10 cycles CO_2 adsorption and desorption plot and cyclic CO_2 adsorption capacities of MSS-2 with 40 wt% PEI impregnation and coated with one layer TEOS under following conditions: $T_{asd} = 75$ ℃, $T_{des} = 120$ ℃, $p_{CO_2,ads} = 0.05$ bar, $p_{CO_2,des} = 0.70$ bar.
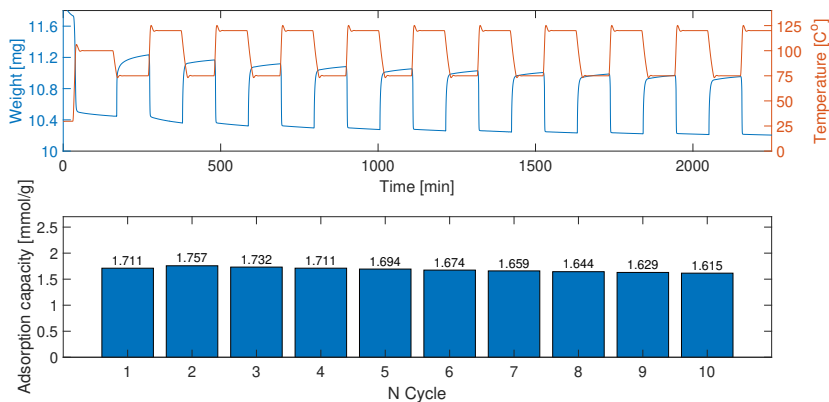
MSS-3 sorbent

Figure B.27: 10 cycles CO_2 adsorption and desorption plot and cyclic CO_2 adsorption capacities of MSS-3 with 40 wt% PEI impregnation under following conditions: $T_{asd} = 75$ ℃, $T_{des} = 75$ ℃, $p_{CO_2,ads} = 0.05$ bar, $p_{CO_2,des} = 0$ bar.

Figure B.28: 10 cycles CO_2 adsorption and desorption plot and cyclic CO_2 adsorption capacities of MSS-3 with 40 wt% PEI impregnation under following conditions: $T_{asd} = 75$ ℃, $T_{des} = 120$ ℃, $p_{CO_2,ads} = 0.05$ bar, $p_{CO_2,des} = 0$ bar.

MSS-3 w/silica coating

Figure B.29: 9 cycles CO_2 adsorption and desorption plot and cyclic CO_2 adsorption capacities of MSS-3 with 40 wt% PEI impregnation and coated with one layer TEOS under following conditions: $T_{asd} = 75$ ℃, $T_{des} = 120$ ℃, $p_{CO_2,ads} = 0.05$ bar, $p_{CO_2,des} = 0$ bar.
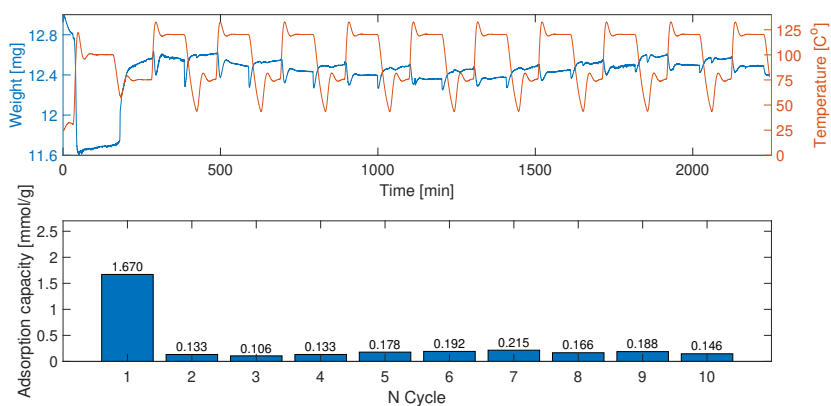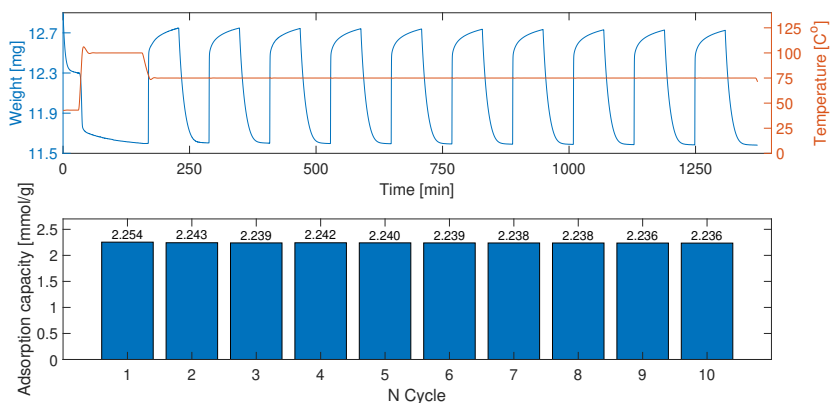
Figure B.30: 3 cycles CO_2 adsorption and desorption plot and cyclic CO_2 adsorption capacities of MSS-3 with 40 wt% PEI impregnation and coated with one layer colloidal silica under following conditions: $T_{asd} = 75$ °C, $T_{des} = 120$ °C, $p_{CO_2,ads} = 0.05$ bar, $p_{CO_2,des} = 0$ bar.
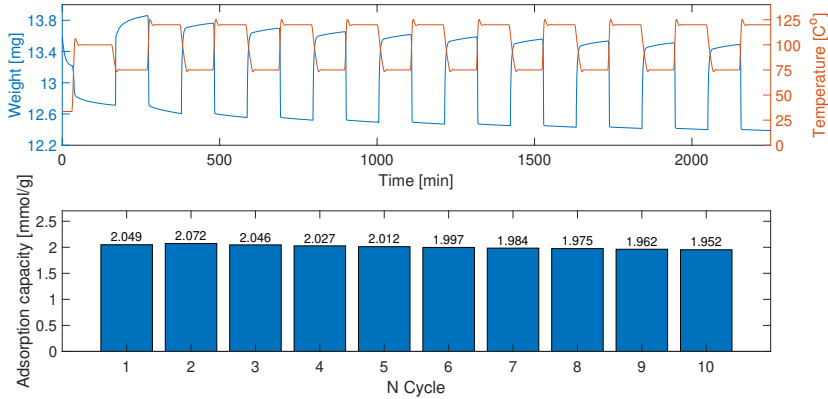

Figure B.31: 10 cycles CO_2 adsorption and desorption plot and cyclic CO_2 adsorption capacities of MSS-3 with 40 wt% PEI impregnation and coated with one layer colloidal silica (10 min mixing) under following conditions: $T_{asd} = 75$ °C, $T_{des} = 120$ °C, $p_{CO_2,ads} = 0.05$ bar, $p_{CO_2,des} = 0$ bar.
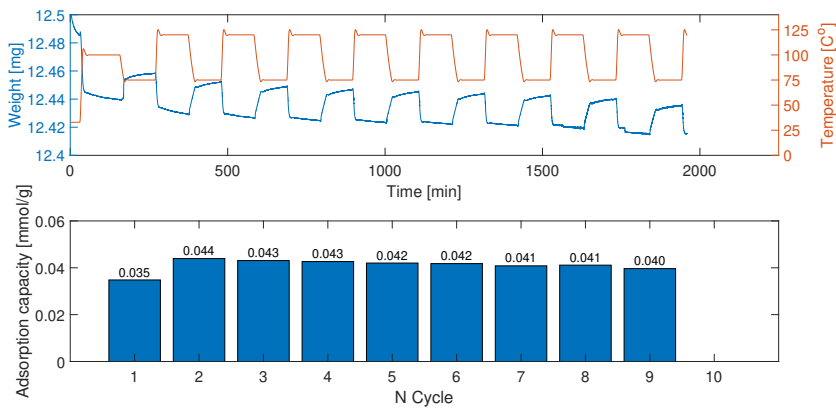
MSS-4 sorbent

Figure B.32: 10 cycles CO_2 adsorption and desorption plot and cyclic CO_2 adsorption capacities of MSS-4 with 40 wt% PEI impregnation under following conditions: $T_{asd} = 75$ °C, $T_{des} = 75$ °C, $p_{CO_2,ads} = 0.05$ bar, $p_{CO_2,des} = 0$ bar.

Figure B.33: 10 cycles CO_2 adsorption and desorption plot and cyclic CO_2 adsorption capacities of MSS-4 with 40 wt% PEI impregnation under following conditions: $T_{asd} = 75$ °C, $T_{des} = 120$ °C, $p_{CO_2,ads} = 0.05$ bar, $p_{CO_2,des} = 0$ bar.
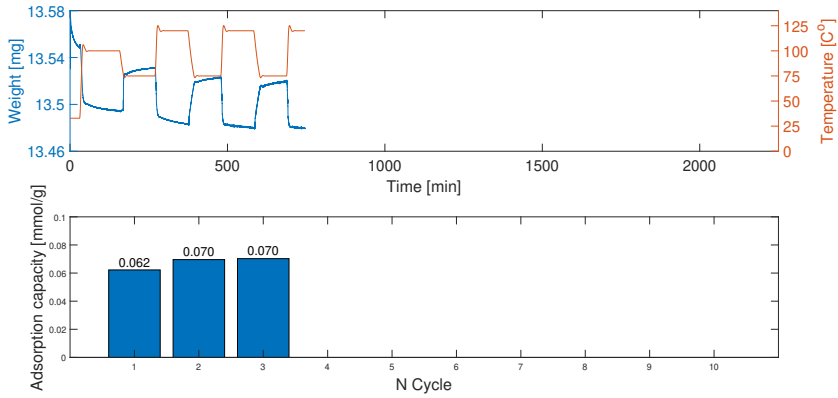
MSS-4 w/silica coating

Figure B.34: 10 cycles CO_2 adsorption and desorption plot and cyclic CO_2 adsorption capacities of MSS-3 with 40 wt% PEI impregnation and coated with one layer TEOS under following conditions: $T_{asd} = 75$ ℃, $T_{des} = 120$ ℃, $p_{CO_2,ads} = 0.05$ bar, $p_{CO_2,des} = 0$ bar.

MSS-5 sorbent
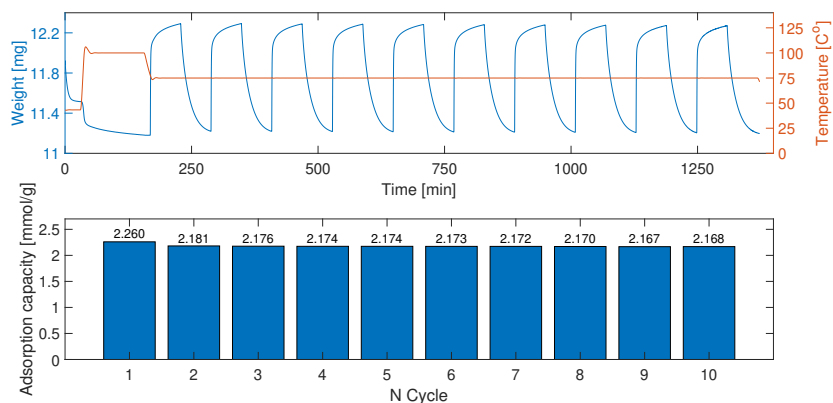
Figure B.35: 10 cycles CO_2 adsorption and desorption plot and cyclic CO_2 adsorption capacities of MSS-5 with 40 wt% PEI impregnation under following conditions: $T_{asd} = 75$ ℃, $T_{des} = 75$ ℃, $p_{CO_2,ads} = 0.05$ bar, $p_{CO_2,des} = 0$ bar.
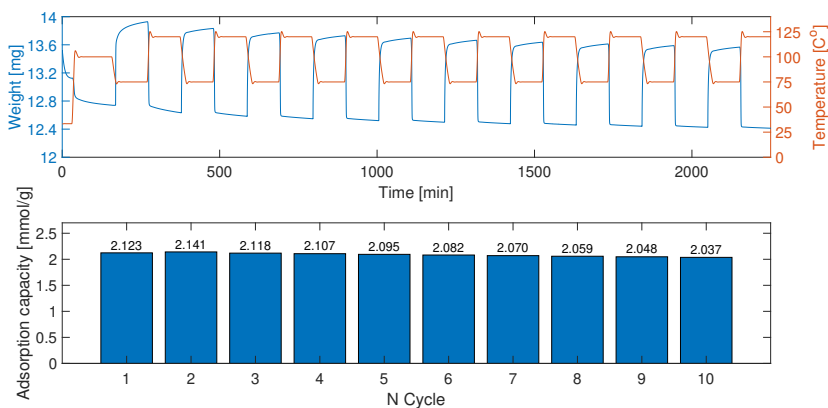
Figure B.36: 10 cycles CO_2 adsorption and desorption plot and cyclic CO_2 adsorption capacities of MSS-5 with 40 wt% PEI impregnation under following conditions: $T_{asd} = 75$ ℃, $T_{des} = 120$ ℃, $p_{CO_2,ads} = 0.05$ bar, $p_{CO_2,des} = 0$ bar.
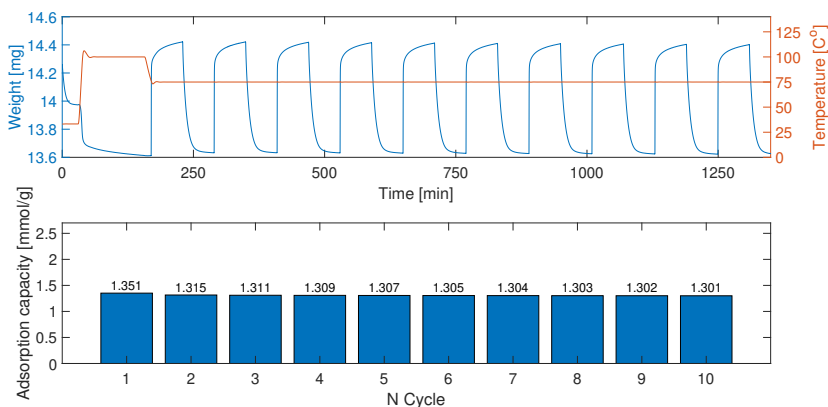
Figure B.37: 10 cycles CO_2 adsorption and desorption plot and cyclic CO_2 adsorption capacities of MSS-5 with 25 wt% PEI impregnation under following conditions: $T_{asd} = 75$ ℃, $T_{des} = 75$ ℃, $p_{CO_2,ads} = 0.05$ bar, $p_{CO_2,des} = 0$ bar.
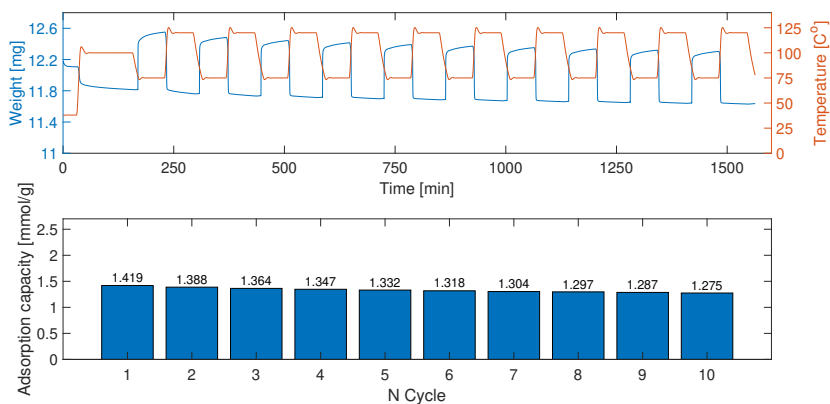
Figure B.38: 10 cycles CO_2 adsorption and desorption plot and cyclic CO_2 adsorption capacities of MSS-5 with 25 wt% PEI impregnation under following conditions: $T_{asd} = 75$ °C, $T_{des} = 120$ °C, $p_{CO_2,ads} = 0.05$ bar, $p_{CO_2,des} = 0$ bar.
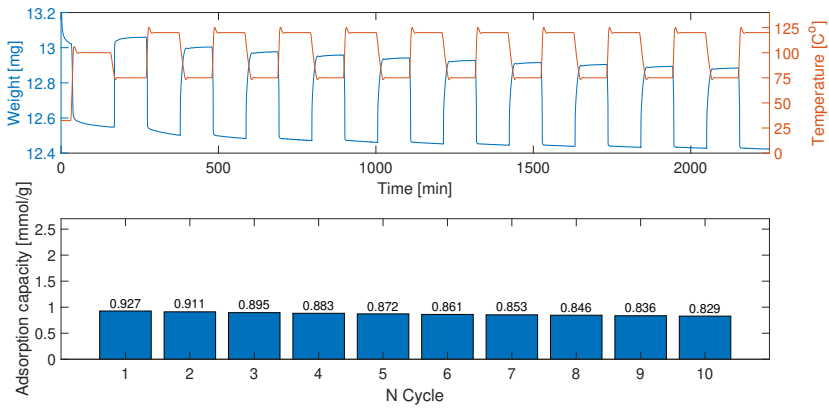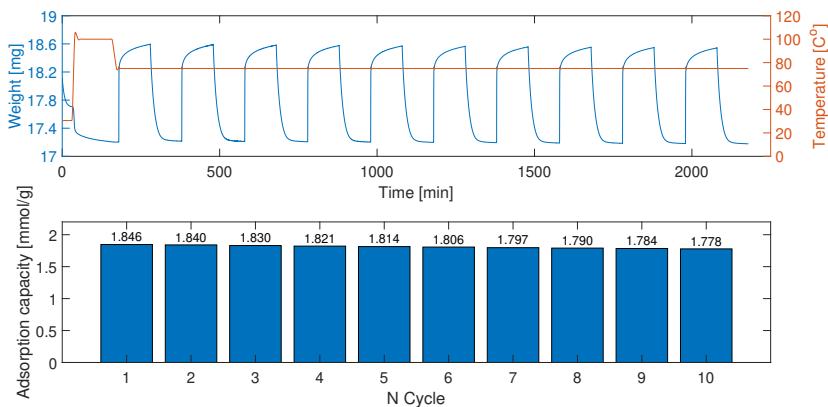
MSS-5 w/silica coating
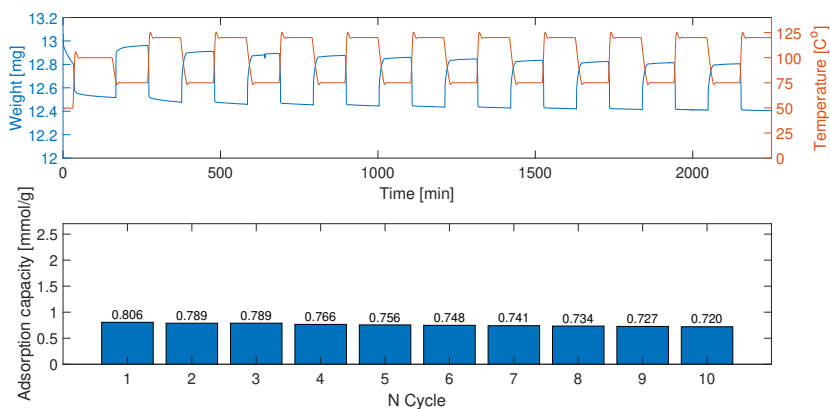
Figure B.39: 10 cycles CO_2 adsorption and desorption plot and cyclic CO_2 adsorption capacities of MSS-3 with 40 wt% PEI impregnation and coated with two layer TMOMS under following conditions: $T_{asd} = 75$ °C, $T_{des} = 120$ °C, $p_{CO_2,ads} = 0.05$ bar, $p_{CO_2,des} = 0$ bar.

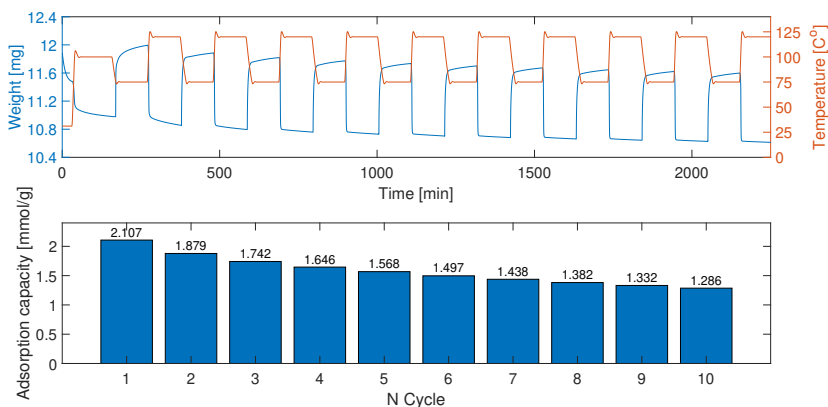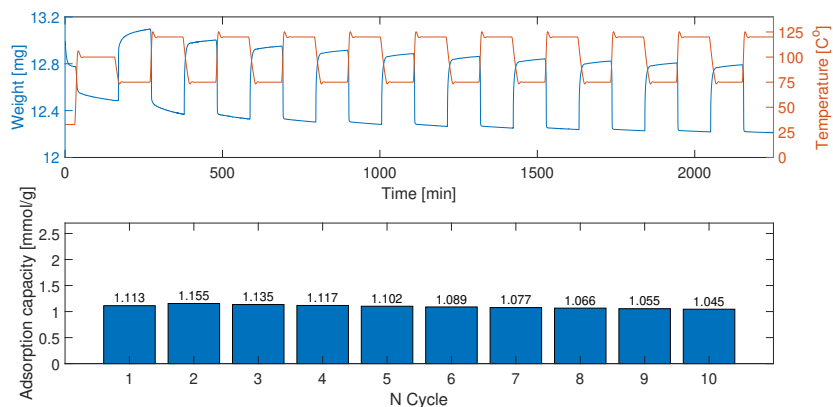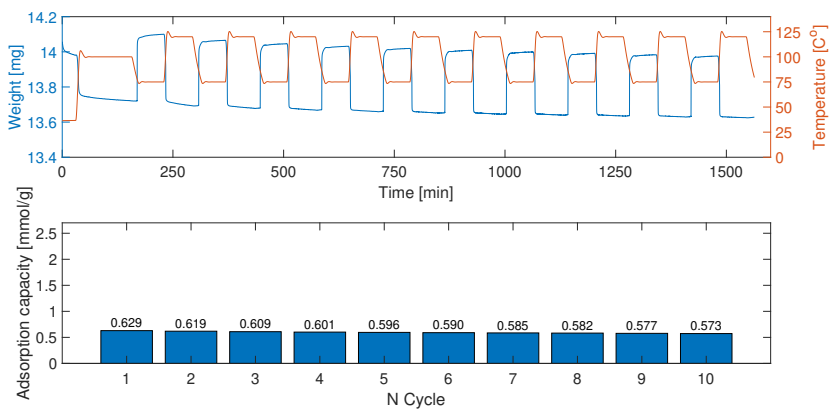**Figure B.40:** 10 cycles CO_2 adsorption and desorption plot and cyclic CO_2 adsorption capacities of MSS-3 with 25 wt% PEI impregnation and coated with two layer TMOMS under following conditions: $T_{asd} = 75$ ℃, $T_{des} = 120$ ℃, $p_{CO_2,ads} = 0.05$ bar, $p_{CO_2,des} = 0$ bar.

C | Appendix

Kinetics

C.1 Different Carbon Dioxide Partial Pressure

Figure C.1 and C.2 show the dynamic adsorption profiles of the first 3 seconds and the full length, respectively, of MSS-1/40PEI under different CO_2 partial pressures.
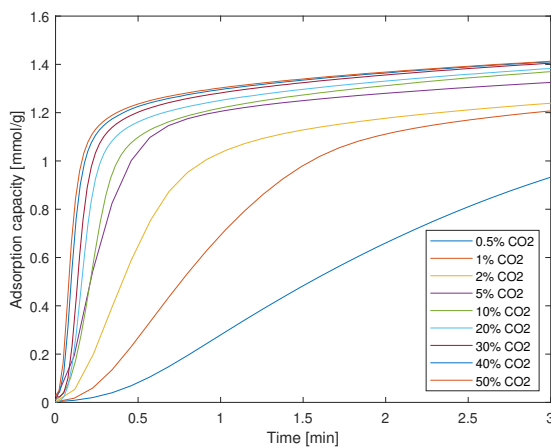
Figure C.1: Dynamic adsorption profiles of the first 3 seconds of MSS-1/40PEI under different CO_2 partial pressures at 75 ℃.
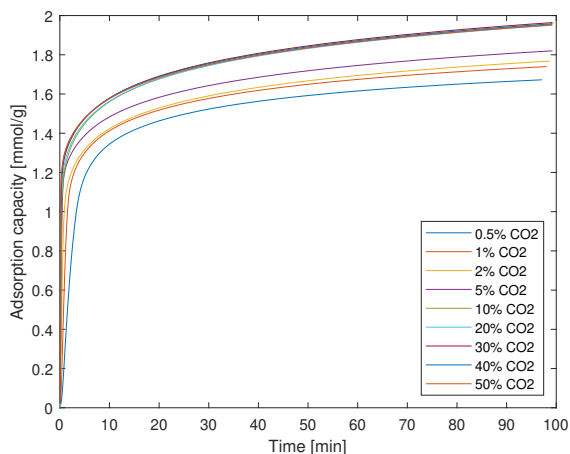
Figure C.2: Dynamic adsorption profiles of MSS-1/40PEI under different CO_2 partial pressures at 75 ℃.

C.2 Full Length Adsorption Kinetics

Figure C.3 and C.12 show the full length experimental CO_2 adsorption capacities and corresponding generated adsorption kinetic model profiles for all sorbents, and under different conditions.
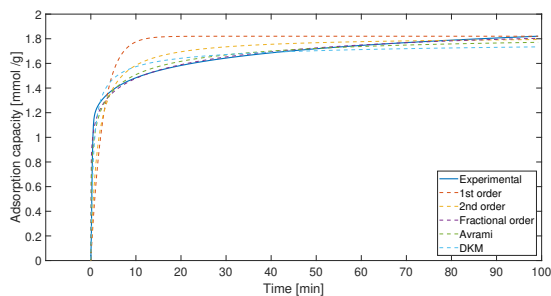
Figure C.3: Full length adsorption kinetic modelling of MSS-1/40PEI in 5% CO_2 at 75 ℃.
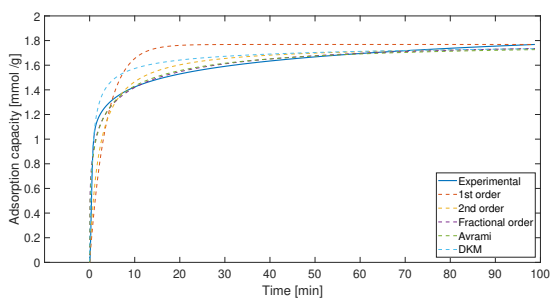
Figure C.4: Full length adsorption kinetic modelling of MSS-1/40PEI in 2% CO_2 at 75 ℃.
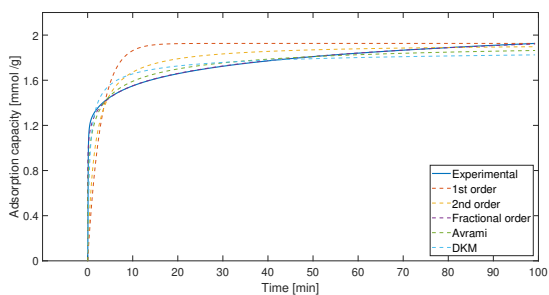
Figure C.5: Full length adsorption kinetic modelling of MSS-1/40PEI in 50% CO_2 at 75 ℃.
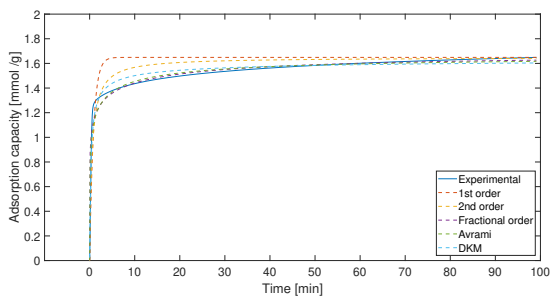
Figure C.6: Full length adsorption kinetic modelling of MSS-1/30PEI in 5% CO_2 at 75 ℃.
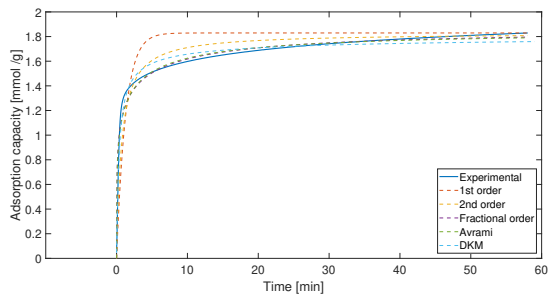
Figure C.7: Full length adsorption kinetic modelling of MSS-2/40PEI in 5% CO_2 at 75 ℃.
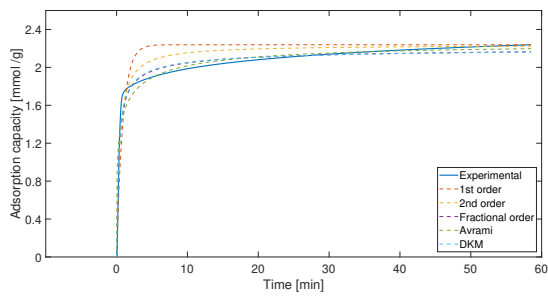
Figure C.8: Full length adsorption kinetic modelling of MSS-3/40PEI in 5% CO_2 at 75 ℃.
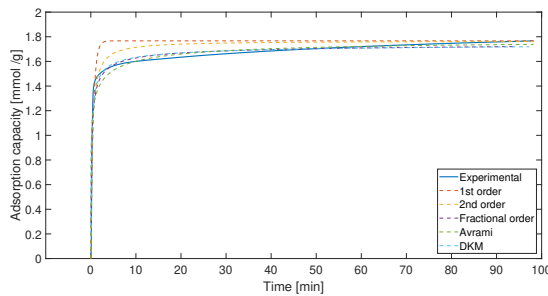
Figure C.9: Full length adsorption kinetic modelling of MSS-3/40PEI in 5% CO_2 at 50 ℃.
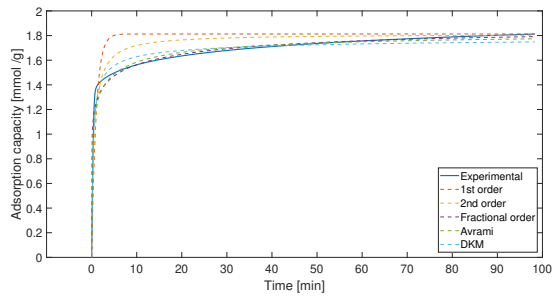
Figure C.10: Full length adsorption kinetic modelling of MSS-4/40PEI in 5% CO_2 at 75 ℃.
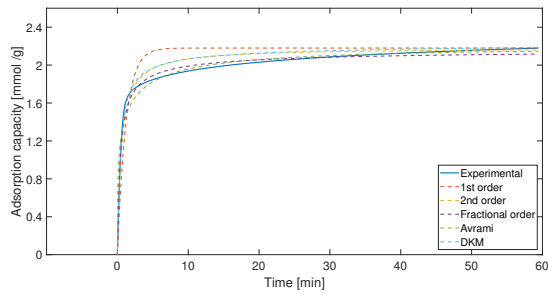
Figure C.11: Full length adsorption kinetic modelling of MSS-5/40PEI in 5% CO_2 at 75 ℃.
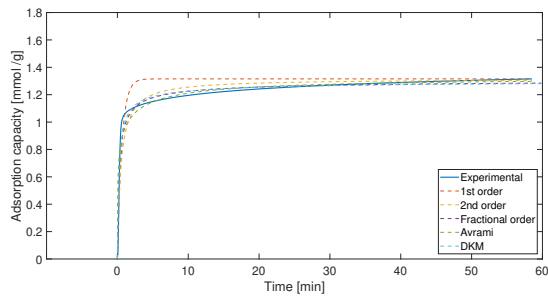
Figure C.12: Full length adsorption kinetic modelling of MSS-5/25PEI in 5% CO_2 at 75 ℃.

Appendix D

MATLAB code

D.1 Matlab code 1

The following MATLAB code is a pseudo code that explains how adsorption capacities, cyclic stability and adsorption kinetics were calculated. Code 1 includes calculation for kinetic parameters of pseudo-first-order model, pseudo-second-order model, Avrami kinetic model and fractional-order kinetic model.

```matlab
1   %% TKP4900 - Master's Thesis
2   % Author: Jorgen Lausund Grinna
3   % Date: July 2020
4   % Brief: Adsorption capacity, stability and kinetics
5   % This pseudo script was written at NTNU, spring 2020 as a part of the
6   % course TKP4900 - Chemical Process Technology, Master's Thesis.
7   % This pseudo scrip calculates adsorption capacity, stability and kinetics
8   % parameters for PEI impregnated mesoporous silica spheres.
9   % pseudo-first-order model, pseudo-second-order model, Avrami kinetic model
10  % and Fractional-order model are incuded in the script
11
12  %% Deleting memory
13  clear all; close all; clc;
14
15  %% Import of experimantal data
16  Time = xlsread('NameOfFile.xlsx','Sheet', 'm1:n1');
17  Temp = xlsread('NameOfFile.xlsx','Sheet', 'm2:n2');
18  Weight = xlsread('NameOfFile.xlsx','Sheet', 'm3:n3');
19
20  %% Declearing varibles
21  num_cyc = 10;                    counter = 0;
22  m_samp = ones(1,num_cyc)*500;    newTime = [];
23  CO2_ads = zeros(1,num_cyc);      CO2_MaxCap = [];
24  CO2_TimeCap = [];                CO2_stab = [];
25  CO2_TimeCap_2nd = [];            CO2_TimeCap_1st = [];
26  CO2_Kin_1st = [];                CO2_Kin_2nd = [];
27  CO2_TimeCap_frac = [];           CO2_TimeCap_Avrami = [];
28  AAD = [0 0 0 0];
29
30  %% Max. and min. weight of sample for each cycle
31  for i = 1:length(Time)
32
33      if Time(i) > 160 && Time(i) < 200      % 1st cycle
34          if Weight(i)<m_samp(1)
35              m_samp(1)=Weight(i);
36          end
37      end
```

```
38
39         if Time(i) > 260 && Time(i) < 280
40             if Weight(i)>CO2_ads(1)
41                 CO2_ads(1) = Weight(i);
42             end
43         end
44
45         if Time(i) > 360 && Time(i) < 400          % 2nd cycle
46             if Weight(i)<m_samp(2)
47                 m_samp(2)=Weight(i);
48             end
49         end
50
51         if Time(i) > 460 && Time(i) < 480
52             if Weight(i)>CO2_ads(2)
53                 CO2_ads(2) = Weight(i);
54             end
55         end
56
57         %:::::::::   3, 4, 5, 6, 7, 8 and 9th cycle    :::::::::
58
59         if Time(i) > 1960 && Time(i) < 2000          % 10th cycle
60             if Weight(i)<m_samp(10)
61                 m_samp(10)=Weight(i);
62             end
63         end
64
65         if Time(i) > 2060 && Time(i) < 2080
66             if Weight(i)>CO2_ads(10)
67                 CO2_ads(10) = Weight(i);
68             end
69         end
70     end
71
72     %% Adsorption capacity and cyclic stability calculation
73     for i = 1:num_cyc
74         CO2_MaxCap(i) = ((CO2_ads(i)-m_samp(i))*1000)/(44*m_samp(1));
75         if i > 1
76         CO2_stab(i-1) = CO2_MaxCap(i)/CO2_MaxCap(2);
77         end
78     end
79
80     %% Defining adsorption interval
81     for i = 1:length(Time)
82         if Time(i) > 369.65 && Time(i) < 373
83             if counter == 0
84                 intTime = Time(i);
85             end
86             counter = counter + 1;
87             newTime(counter) = (Time(i)-intTime);
88             CO2_TimeCap(counter) = ((Weight(i)-m_samp(2))*1000)/(44*m_samp(1));
89         end
90     end
91
92     %% Kinetic calculation (Least square nonlinear)
93     % Fractional order
94     x0 = [2 1 1]; %[n k m]
95     options = optimoptions(@lsqnonlin,'Algorithm','levenberg-marquardt');
96     fracFun = @(x1) max(CO2_TimeCap) - 1./(((x1(1)-1)*(x1(2)./x1(3)))*...
97         (newTime.^x1(3))+(1./(max(CO2_TimeCap).^(x1(1)-1)))).^(1./(x1(1)-1)))...
98         - CO2_TimeCap;
99     x1 = lsqnonlin(fracFun,x0,[],[],options);
100
101     % Avrami
102     x02 = [1 2]; %[k n]
103     options = optimoptions(@lsqnonlin,'Algorithm','levenberg-marquardt');
104     AvramiFun = @(x2) max(CO2_TimeCap)*(1-exp(-(x2(1)*newTime).^(x2(2))))...
105         - CO2_TimeCap;
106     x2 = lsqnonlin(AvramiFun,x02,[],[],options);
107
108     % First order
109     x03 = 2; %k
110     options = optimoptions(@lsqnonlin,'Algorithm','levenberg-marquardt');
111     PFOfun = @(x3) max(CO2_TimeCap)*(1-exp(-x3*newTime)) - CO2_TimeCap;
112     x3 = lsqnonlin(PFOfun,x03,[],[],options);
113
114     % Second order
115     x04 = 2; %k
116     options = optimoptions(@lsqnonlin,'Algorithm','levenberg-marquardt');
117     PSOfun = @(x4) (max(CO2_TimeCap)*newTime)./((1./(x4*max(CO2_TimeCap)))...
118         + newTime) - CO2_TimeCap;
119     x4 = lsqnonlin(PSOfun,x04,[],[],options);
120
121     %% Kinetic calculation (fit nonlinear model)
122     tbl = table(newTime', CO2_TimeCap');
123     AvramiFun2 = @(b,x5) max(CO2_TimeCap)*(1-exp(-(b(1)*x5(:,1)).^(b(2))));
```

```matlab
124    fracFun2 = @(b2,x6) max(CO2_TimeCap) - 1./((((b2(1)-1)*(b2(2)./b2(3)))...
125        *(x6(:,1).^b2(3))+(1./(max(CO2_TimeCap).^(b2(1)-1)))).^(1./(b2(1)-1)));
126    PFOfun2 = @(b3,x7) max(CO2_TimeCap).*(1-exp(-b3*x7(:,1)));
127    PSOfun2= @(b4,x8) (max(CO2_TimeCap)*x8(:,1))./((1./(b4*max(CO2_TimeCap)))...
128        +x8(:,1));
129
130    beta0 = [1 2]; beta1 = [2 1 1]; beta2 = 1; beta3 = 1;
131    Avrami_mdl = fitnlm(tbl,AvramiFun2,beta0)
132    fracFun_mdl = fitnlm(tbl,fracFun2,beta1)
133    PFOFun_mdl = fitnlm(tbl,PFOfun2,beta2)
134    PSOFun_mdl = fitnlm(tbl,PSOfun2,beta3)
135
136    %% Create vectors of modelled timedependent adsorion capacities
137    for i = 1:length(newTime)
138        CO2_TimeCap_2nd(i) = ( max(CO2_TimeCap)*newTime(i) )...
139            /( (1/(x3*max(CO2_TimeCap))) + newTime(i) );
140        CO2_TimeCap_1st(i) = ( max(CO2_TimeCap) )...
141            *( 1 - exp(-x3*newTime(i)) );
142        CO2_TimeCap_frac(i) = max(CO2_TimeCap) - 1./((((x1(1)-1)...
143            *(x1(2)/x1(3)))*(newTime(i).^x1(3))...
144            +(1/(max(CO2_TimeCap)^(x1(1)-1)))).^(1/(x1(1)-1)));
145        CO2_TimeCap_Avrami(i) = max(CO2_TimeCap)...
146            *(1-exp(-(x2(1)*newTime(i)).^(x2(2))));
147
148        AAD(1) = AAD(1) ...
149            + (abs(CO2_TimeCap(i)- CO2_TimeCap_1st(i)))/CO2_TimeCap(i);
150        AAD(2) = AAD(2) ...
151            + (abs(CO2_TimeCap(i)- CO2_TimeCap_2nd(i)))/CO2_TimeCap(i);
152        AAD(3) = AAD(3) ...
153            + (abs(CO2_TimeCap(i)- CO2_TimeCap_frac(i)))/CO2_TimeCap(i);
154        AAD(4) = AAD(4) ...
155            + (abs(CO2_TimeCap(i)- CO2_TimeCap_Avrami(i)))/CO2_TimeCap(i);
156    end
157
158    %% Average Absolute percentage Deviations
159    AAD = AAD/length(newTime)*100;
```

D.2 Matlab code 2

The following MATLAB code is a pseudo code that explains how adsorption capacities, cyclic stability and adsorption kinetics for dual kinetic model were calculated.

```matlab
1   %% TKP4900 - Master's Thesis
2   % Author: Jorgen Lausund Grinna
3   % Co-author: Jithin Gopakumar
4   % Date: July 2020
5   % Brief: Adsorption capacity, stability and kinetics
6   % This pseudo script was written at NTNU, spring 2020 as a part of the
7   % course TKP4900 - Chemical Process Technology, Master's Thesis.
8   % This pseudo scrip calculates adsorption capacity, stability and kinetic
9   % parameters for PEI impregnated mesoporous silica spheres.
10  % Dual kinetic model are incuded in the script
11
12  %% Deleting memory
13  clear all; close all; clc;clear all; close all; clc;
14
15  %% Import of experimantal data
16  Time = xlsread('NameOfFile.xlsx','Sheet', 'm1:n1');
17  Temp = xlsread('NameOfFile.xlsx','Sheet', 'm2:n2');
18  Weight = xlsread('NameOfFile.xlsx','Sheet', 'm3:n3');
19
20  %% Declearing varibles
21  global k CO2_TimeCap newTime y CO2_MaxCap
22  num_cyc = 10;
23  m_samp = ones(1,num_cyc)*500;
24  CO2_ads = [];            CO2_MaxCap = [];          CO2_TimeCap = [];
25  CO2_stab = [];           CO2_TimeCap_Avrami = [];     newTime = [];
26  counter = 0;   AAD = 0;   SSE = 0;   SST = 0;
27
28  %% Max. and min. weight of sample for each cycle
29  for i = 1:length(Time)
30
31      if Time(i) > 160 && Time(i) < 200        % 1st cycle
32          if Weight(i)<m_samp(1)
33              m_samp(1)=Weight(i);
34          end
35      end
36
37      if Time(i) > 260 && Time(i) < 280
38          if Weight(i)>CO2_ads(1)
39              CO2_ads(1) = Weight(i);
40          end
41      end
42
43      if Time(i) > 360 && Time(i) < 400        % 2nd cycle
44          if Weight(i)<m_samp(2)
45              m_samp(2)=Weight(i);
46          end
47      end
48
49      if Time(i) > 460 && Time(i) < 480
50          if Weight(i)>CO2_ads(2)
51              CO2_ads(2) = Weight(i);
52          end
53      end
54
55      %::::::::::  3, 4, 5, 6, 7, 8 and 9th cycle    :::::::::
56
57      if Time(i) > 1960 && Time(i) < 2000        % 10th cycle
58          if Weight(i)<m_samp(10)
59              m_samp(10)=Weight(i);
60          end
61      end
62
63      if Time(i) > 2060 && Time(i) < 2080
64          if Weight(i)>CO2_ads(10)
65              CO2_ads(10) = Weight(i);
66          end
67      end
68  end
69
70  %% Adsorption capacity and cyclic stability calculation
71  for i = 1:num_cyc
72      CO2_MaxCap(i) = ((CO2_ads(i)-m_samp(i))*1000)/(44*m_samp(1));
73      CO2_stab(i) = CO2_MaxCap(i)/CO2_MaxCap(1);
74  end
75
76  %% Defining adsorption interval
77  for i = 1:length(Time)
```

```
78          if Time(i) > 369.65 && Time(i) < 373
79              if counter == 0
80                  intTime = Time(i);
81              end
82              counter = counter + 1;
83              newTime(counter) = Time(i)-intTime;
84              CO2_TimeCap(counter) = ((Weight(i)-m_samp(2))*1000)/(44*m_samp(1));
85
86          end
87      end
88
89      %% Kinetic calculation (Least square nonlinear)
90      k_result = [2 3 4]; %k b n
91      opts = optimoptions(@lsqnonlin,'Algorithm','levenberg-marquardt');
92      k_result=lsqnonlin(@ode,k_result,[],[],opts)
93
94      %% Error calculation
95      for i = 1:length(newTime)
96              AAD = AAD + (abs(CO2_TimeCap(i)- y(i)))/CO2_TimeCap(i);
97              SSE = SSE + (CO2_TimeCap(i)- y(i))^2;
98              SST = SST + (CO2_TimeCap(i)- mean(CO2_TimeCap))^2;
99      end
100     le = immse(CO2_TimeCap',y)
101     V1 = CO2_TimeCap';
102     RMSE = sqrt(mean((V1-y).^2));
103     AAD = AAD/length(newTime)*100;
104     R = 1-SSE/SST;
105     R_adj = 1-((length(CO2_TimeCap)-1)...
106         /(length(CO2_TimeCap)-length(k_result)))*(1-R);
107
108     %% ODE solver
109     function le=ode(k1)
110     global k CO2_TimeCap newTime y
111     k = k1;
112     q = CO2_TimeCap(1);
113     opts = odeset('NonNegative',1);
114     [t,y]=ode45(@dualFun,newTime',q,opts);
115     le = immse(CO2_TimeCap',y);
116     end
117
118     %% ODE function
119     function dq_dt=dualFun(t,q)
120     global k CO2_TimeCap
121     qmax = CO2_TimeCap(end);
122     dq_dt = k(1)*(1+k(2)*q)*(qmax - q).^(k(3));
123     end
```

Appendix E

Risk Assessment

The following pages contain the risk assessment related to the laboratory work done by the author of the master thesis. The risk assessment defines all risk and danger related to chemicals used and the activity done in the lab.

ID	35772		Status	Date
Risk Area	Risikovurdering: Helse, miljø og sikkerhet (HMS)		Created	24.01.2020
Created by	Jørgen Lausund Grinna		Assessment started	24.01.2020
Responsible	Jørgen Lausund Grinna		Measures decided	
			Closed	

Risk Assessment:

CAT, Master student, 2020, Jørgen Lausund Grinna

Valid from-to date:

1/29/2020 - 12/31/2020

Location:

IKP

Goal / purpose

This risk assessment contains risk assess to Master student Jørgen Lausund Grinnas work on preparation of solid materials, catalyst characterization for low temperature carbon dioxide adsorption/desorption and all the activities he will perform in the labs of the Catalysis group.

Background

Preparation of product, catalyst caracterization and kinetic study

Product synthesis 1:
1. Preparation of Mesoporus Silica Spheres:
  - Chemicals: Parafin oil, Span80, Formaldehyde, Resorcinol, Colloidal silicon nanoparticles, Acetone
  - Instrument: Laboratory Stirrer, Hot plate, oil bath, Furnace
  - Methods: Polymer sphere synthesis/Hard template, calcination
2. PEI Impregnation
  - Chemicals: Polyethylenimine (PEI), methanol
  - Instruments: Laboratory Stirrer, Furnace
  - Methods: Wet impregnation
3. TEOS Coating
  - Chemicals: Tetraethylorthosilicate (TEOS)
  - Instruments: Laboratory Stirrer, Furnace
  - Methods: Wet impregnation
4. Methyltrimethoxysilane Coating
  - Chemicals: Methyltrimethoxysilane
  - Instruments: Laboratory Stirrer, Furnace
  - Methods: Incipient wetness impregnation

Product synthesis 2:
1. Preparation of Mesoporus Silica Spheres:
  - Chemicals: Ethanol, Ammonia, Formaldehyde, Resorcinol, Colloidal silicon nanoparticles
  - Instrument: Centrifuge, Vacuum dryer, Ultrasonic equipment
  - Methods: Ultaronication, Calcination
2. PEI Impregnation
  - Chemicals: Polyethylenimine (PEI), Methanol
  - Instruments: Laboratory Stirrer, Furnace
  - Methods: Wet impregnation

Product synthesis 3:
1. Preparation of Mesoporus Silica Spheres:
  - Chemicals: Fumed silica, silica solution
  - Instruments: Spray dryer, calcination Furnace
  - Method: Spary drying
2. Impregnation
  - Chemicals: Polyethylenimine (PEI), methanol, Piperazine
  - Instruments: Laboratory Stirrer, Furnace
  - Methods: Wet impregnation

Catalyst characterization:
 1. Nitrogen Physisorption (BET)
  - Instrument: Micromeritics TriStar 3000 Surface Area and Porosity Analyser, VACPREP 061
 2. Scanning Electorn Microscope (SEM)
 3. Thermogravimetric Analyser (TGA, Lineseis)

Kinetic study:
  - Fluidized bed reactor
  - Will use micro-balance set-up (K5-448)

Description and limitations

The preparation of Mesoporus Silica Spheres involves toxic, flammable and physical damage chemicals:

- Formaldehyde
Hazard statement(s):
H226 Flammable liquid and vapour.
H301 + H311 + H331 Toxic if swallowed, in contact with skin or if inhaled.
H314 Causes severe skin burns and eye damage.
H317 May cause an allergic skin reaction.
H335 May cause respiratory irritation.
H341 Suspected of causing genetic defects.
H350 May cause cancer.
H370 Causes damage to organs.

Precautionary statements:
P210 Keep away from heat, hot surfaces, sparks, open flames and other ignition sources. No smoking.
P260 Do not breathe dust/ fume/ gas/ mist/ vapours/ spray.
P280 Wear protective gloves/ protective clothing/ eye protection/ face protection.

P370 + P378 In case of fire: Use dry sand, dry chemical or alcohol-resistant foam to extinguish.

- Resorcinol
Hazard statements:
H302 Harmful if swallowed.
H315 Causes skin irritation.
H318 Causes serious eye damage.
H400 Very toxic to aquatic life.

Precautionary statements:
P280 Wear eye protection/ face protection.

- Methanol
Hazard statements
H225 Highly flammable liquid and vapour.
H301 + H311 + H331 Toxic if swallowed, in contact with skin or if inhaled.
H370 Causes damage to organs.

Precautionary statements
P210 Keep away from heat, hot surfaces, sparks, open flames and other ignition sources. No smoking.
P280 Wear protective gloves/ protective clothing.

- Ethanol
Hazard statements
H225 Highly flammable liquid and vapour.
H319 Causes serious eye irritation.

Precautionary statements
P210 Keep away from heat, hot surfaces, sparks, open flames and other ignition sources. No smoking.

- Acetone
Hazard statements
H225 Highly flammable liquid and vapour.
H319 Causes serious eye irritation.
H336 May cause drowsiness or dizziness.

Precautionary statements
P210 Keep away from heat, hot surfaces, sparks, open flames and other ignition sources. No smoking.
P261 Avoid breathing vapours.

- PEI
Hazard statements
H302 Harmful if swallowed.
H318 Causes serious eye damage.
H411 Toxic to aquatic life with long lasting effects.

Precautionary statements
P273 Avoid release to the environment.
P280 Wear eye protection/ face protection.

- Piperazine
Hazard statement
H314 Causes severe skin burns and eye damage.
H317 May cause an allergic skin reaction.
H334 May cause allergy or asthma symptoms or breathing difficulties if inhaled.
H361fd Suspected of damaging fertility. Suspected of damaging the unborn child.

Precautionary statements
P201 Obtain special instructions before use.
P261 Avoid breathing dust/ fume/ gas/ mist/ vapours/ spray.
P280 Wear protective gloves/ protective clothing/ eye protection/ face protection.

- TEOS
Hazard statements
H226 Flammable liquid and vapour.
H319 Causes serious eye irritation.
H332 Harmful if inhaled.
H335 May cause respiratory irritation.

Precautionary statements
P210 Keep away from heat, hot surfaces, sparks, open flames and other ignition sources. No smoking.
P261 Avoid breathing dust/ fume/ gas/ mist/ vapours/ spray.
P280 Wear eye protection/ face protection.

Methyltrimethoxysilane:
Hazard statements
H225 Highly flammable liquid and vapour
Precautionary statements:
P210 Keep away from heat/sparks/open flames/hot surfaces. - No smoking.
P262 Do not get in eyes, on skin, or on clothing.
P403 + P235 Store in a well-ventilated place. Keep cool.

Paraffin oil, colloidal silica nanoparticles and Span80 are not considered as hazardous materials.

The distribution of all chemicals during the hard template method will be done in atmospheric pressure and the temperature up to 100 degrees Celsius. It is still recommended to use the chemicals carefully in a ventilated place and with personal protective equipment such as gloves, labcoat, face mask/goggles, respiratory mask with chemical corresponding filters. This is because some of the chemicals are extremely toxic and flammable. The waste disposal should be realized in a very careful manner (marked containers).

Catalyst characterization:

Nitrogen Physisorption:
- Instrument training
- Special gloves, pants, boots for handeling liquid nitrogen.

TGA:
- Instrument training
- Low temperature (75-120 Celsius degrees);
- Not toxic, but high pressure gases in cylinder: CO_2, O_2, N_2
- Steam
- low pressures (0.05 bar)

Calcination/Furnace :
- High temperatures (550, 650, 750 degrees Celsius)
- Protection: wearing goggles, heat-protecting gloves

Kinetic study:

Fluidized bed reactor:
- Low temperature (75-120 Celsius degrees)
- Low pressure (0.05 bar)

Microbalance reactor:
- Compressed gas
- Hot zone of furnace

April-Mai 2020 - preventive measures towards Covid-situation:
1) Switch off procedure for my set-up:
- TGA Q500 (K5-441)
Press stop-button and make sure the experiment stopped. Open furnace, remove the sample from the sample-pan and those it the red container. Close the furnace and reduce the balance flow in "Notes window"
- TGA Lienses (K5-420)
Press stop button and make sure the experiment stopped. Open furnace, remove the sample from the crucible and those it the red container. Close the furnace.
- BET Tristar3000 (K5-425)
Under degas: Open the valve, remove the sample from sample tube and clean the sample tube. Place the sample tube in furnace for drying
While analyzing: Stop the experiment, remove sample tube(s) from the machine and remove the sample from sample tube. Clean the sample tube and place the sample tube in furnace for drying.
- Synthesis of Silica Spheres (K5-321)
This method is time-consuming (ca. 3 days) However, if a shut down appears the synthesis will stop and the chemicals/solutions/sorbent will be those in correct containers. Equipment used will be washed.
Under calcination: Turn off high temperature furnace and open the furnace-door. When cooled down, those sample in the red container.

2) Risk related to shortage of personnel in the labs:
Formaldehyde is used for synthesis of silica spheres. Fume hood, gas mask and working alone-alarm will be used.
Lab-activities on K5-441, K5-420 and K5-425, does not include high risk. However, gas-cylinders with high pressure may cause high risk if they are not correctly handled. Try to avoid any adjustment of the gas cylinder-valves.

3) Safety measures related to spread of covid19 infection:
- Avoid touching the face.
- Use own lab-coat and googles.
- Disinfection before and after with ethanol on all surfaces you are in contact with (door knob – card reader with code panel – keyboard – mouse – screen – desk).
- Keep 2m distance from colleagues.
- Use nitrile gloves when touching shared lab set-ups and equipment.
- Wash hands as often as possible.

Prerequesites, assumptions and simplifications
The SDS of the chemicals involved in the project are presented in Attachments.
New SDS will be uploaded if using new chemicals

Attachments
Acetone.pdf
PEI.pdf
Colloidal silica.pdf
Span_80.pdf
TEOS.pdf
Methanol.pdf
Fumed silica.pdf
Formaldehyde_solution.pdf
Resorcinol.pdf
Paraffin_oil.pdf
ethanol.PDF
ammonia.PDF
CO2.pdf
O2.pdf
apparatus card_Microbalance.pdf
Piperazine.pdf
APPARATURKORT-Eng.pdf
Trimethoxymethylsilane.pdf

References
[Ingen registreringer]

Summary, result and final evaluation

The summary presents an overview of hazards and incidents, in addtition to risk result for each consequence area.

Hazard:	**Preparation of product**

Incident:	**Spill of Formaldehyde on skin when measuring volume of the solution for product preparation**

Consequence area:	Helse	Risk before measures:	🟡	Risiko after measures:	⚪

Incident:	**Spill of Formaldehyde and inhale vapor when measuring volume of the solution for product preparation**

Consequence area:	Helse	Risk before measures:	🔴	Risiko after measures:	⚪

Incident:	**Spill of Resorciol on skin when measuring volume of the solution for product preparation**

Consequence area:	Helse	Risk before measures:	🟡	Risiko after measures:	⚪

Incident:	**Spill of Resorcinol and swollow when measuring volume of the solution for product preparation**

Consequence area:	Helse	Risk before measures:	🟡	Risiko after measures:	⚪

Incident:	**Spill of Paraffin Oil on skin or inhale parafin oil when heating up**

Consequence area:	Helse	Risk before measures:	🟢	Risiko after measures:	⚪

Incident:	**Spill of Colloidal Silica on skin**

Consequence area:	Helse	Risk before measures:	🟢	Risiko after measures:	⚪

Incident:	**Inhale Acetone in the washing step of Mesoporus Silica Spheres**

Consequence area:	Helse	Risk before measures:	🟢	Risiko after measures:	⚪

Hazard:	Preparation of product				

Incident: Spill of Methanol on skin when impreganting with PEI

| Consequence area: | Helse | | Risk before measures: | 🟡 | Risiko after measures: | ⚪ |

Incident: Inhale vapor of Methanol when heating up the PEI-Methanol solution

| Consequence area: | Helse | | Risk before measures: | 🟡 | Risiko after measures: | ⚪ |

Incident: Inhale TEOS while coating the Mesoporus Silica sphares

| Consequence area: | Helse | | Risk before measures: | 🟡 | Risiko after measures: | ⚪ |

Incident: Spill of TEOS on skin while coating the Mesoporus Silica sphares

| Consequence area: | Helse | | Risk before measures: | 🟢 | Risiko after measures: | ⚪ |

Incident: Spill of Span_80 on skin or inhale when heating up in the synthesis procedure

| Consequence area: | Helse | | Risk before measures: | 🟢 | Risiko after measures: | ⚪ |

Incident: Spill of Ammonia on skin when measuring volume of the solution for product preparation

| Consequence area: | Helse | | Risk before measures: | 🟡 | Risiko after measures: | ⚪ |

Incident: Inhale Ammonia when measuring volume of the solution for product preparation

| Consequence area: | Helse | | Risk before measures: | 🟡 | Risiko after measures: | ⚪ |

Incident: Spill of ethanol on skin when measuring volume of the solution for product preparation

| Consequence area: | Helse | | Risk before measures: | 🟢 | Risiko after measures: | ⚪ |

Norges teknisk-naturvitenskapelige universitet (NTNU)
Unntatt offentlighet jf. Offentlighetsloven § 14

Print date: 01.07.2020

Printed by: Estelle Marie M. Vanhaecke

Page: 7/39

Hazard:	**Preparation of product**			
Incident:	**Spill of fumed Silica on skin**			
Consequence area:	Helse	Risk before measures:	🟢 Risiko after measures:	⚪
Incident:	**Spillage of Piperazine on skin during impregantion**			
Consequence area:	Helse	Risk before measures:	🟡 Risiko after measures:	⚪
Incident:	**Inhale Trimethoxymethylsilane while coating the Mesoporus Silica sphares**			
Consequence area:	Helse	Risk before measures:	🟢 Risiko after measures:	⚪
Incident:	**Spill of Trimethoxymethylsilane on skin while coating the Mesoporus Silica sphares**			
Consequence area:	Helse	Risk before measures:	🟢 Risiko after measures:	⚪

Hazard:	**Spill of chemicals in drain**			
Incident:	**Spillage of Resorcinol**			
Consequence area:	Ytre miljø	Risk before measures:	🟡 Risiko after measures:	⚪
Incident:	**Spillage of Aceton**			
Consequence area:	Ytre miljø	Risk before measures:	🟢 Risiko after measures:	⚪
Incident:	**Spillage of PEI**			
Consequence area:	Ytre miljø	Risk before measures:	🟡 Risiko after measures:	⚪

Norges teknisk-naturvitenskapelige universitet (NTNU)
Unntatt offentlighet jf. Offentlighetsloven § 14

Print date:
01.07.2020

Printed by:
Estelle Marie M. Vanhaecke

Page:
8/39

Hazard:	Spill of chemicals in drain				
Incident:	**Spillage of Ammonia**				
Consequence area:	Ytre miljø	Risk before measures:		Risiko after measures:	
Incident:	**Spillage of Piperazine**				
Consequence area:	Helse	Risk before measures:		Risiko after measures:	
	Ytre miljø	Risk before measures:		Risiko after measures:	

Hazard:	Handling instruments				
Incident:	**Skin burn on hot plate when preparing Mesoporous Silica sphares**				
Consequence area:	Helse	Risk before measures:		Risiko after measures:	
Incident:	**Skin burn when operating with Calcination Furnace**				
Consequence area:	Helse	Risk before measures:		Risiko after measures:	
Incident:	**Frostbite when hanling Liquid Nitrogen during Nitrogen Physisortion**				
Consequence area:	Helse	Risk before measures:		Risiko after measures:	
Incident:	**Loud noise for ears while using ultrasonication on the solution**				
Consequence area:	Helse	Risk before measures:		Risiko after measures:	
Incident:	**Leakages of pressurized CO2, N2 when operating with Microbalance reactor**				
Consequence area:	Helse	Risk before measures:		Risiko after measures:	

Hazard:	**Handling instruments**			
Incident:	**Skin burn when operating with Microbalance reactor**			
Consequence area:	Helse	Risk before measures:	🟢 Risiko after measures:	⚪

Hazard:	**Handling pressurized gas**			
Incident:	**Leakages of pressurized CO2, N2, O2, Argon**			
Consequence area:	Helse	Risk before measures:	🟢 Risiko after measures:	⚪

Hazard:	**Working in the lab under covid-situation**			
Incident:	**Contact with surfaces**			
Consequence area:	Helse	Risk before measures:	🟡 Risiko after measures:	⚪
Incident:	**Faint/Pass out during experiment**			
Consequence area:	Helse	Risk before measures:	🟡 Risiko after measures:	⚪
Incident:	**Spread of Covid-19**			
Consequence area:	Helse	Risk before measures:	🟢 Risiko after measures:	⚪

Final evaluation

Norges teknisk-naturvitenskapelige universitet (NTNU)
Unntatt offentlighet jf. Offentlighetsloven § 14

Print date:
01.07.2020

Printed by:
Estelle Marie M. Vanhaecke

Page:
10/39

Organizational units and people involved

A risk assessment may apply to one or more organizational units, and involve several people. These are lsited below.

Organizational units which this risk assessment applies to

- Institutt for kjemisk prosessteknologi

Participants

De Chen

Kumar Ranjan Rout

Readers

Anne Hoff

Estelle Marie M. Vanhaecke

Karin Wiggen Dragsten

May Grete Sætran

Others involved/stakeholders

[Ingen registreringer]

The following accept criteria have been decided for the risk area Risikovurdering: Helse, miljø og sikkerhet (HMS):

Helse   **Materielle verdier**   **Omdømme**   **Ytre miljø**

Overview of existing relevant measures which have been taken into account

The table below presents existing measures which have been take into account when assessing the likelihood and consequence of relevant incidents.

Hazard	Incident	Measures taken into account
Preparation of product	Spill of Formaldehyde on skin when measuring volume of the solution for product preparation	Goggles
	Spill of Formaldehyde on skin when measuring volume of the solution for product preparation	Labcoat
	Spill of Formaldehyde on skin when measuring volume of the solution for product preparation	Chemical protecting gloves
	Spill of Formaldehyde on skin when measuring volume of the solution for product preparation	SDS
	Spill of Formaldehyde and inhale vapor when measuring volume of the solution for product preparation	Goggles
	Spill of Formaldehyde and inhale vapor when measuring volume of the solution for product preparation	Labcoat
	Spill of Formaldehyde and inhale vapor when measuring volume of the solution for product preparation	Chemical protecting gloves
	Spill of Formaldehyde and inhale vapor when measuring volume of the solution for product preparation	SDS
	Spill of Formaldehyde and inhale vapor when measuring volume of the solution for product preparation	Fume hood
	Spill of Resorciol on skin when measuring volume of the solution for product preparation	Goggles
	Spill of Resorciol on skin when measuring volume of the solution for product preparation	Labcoat
	Spill of Resorciol on skin when measuring volume of the solution for product preparation	Chemical protecting gloves
	Spill of Resorciol on skin when measuring volume of the solution for product preparation	SDS
	Spill of Resorcinol and swollow when measuring volume of the solution for product preparation	SDS
	Spill of Resorcinol and swollow when measuring volume of the solution for product preparation	Fume hood
	Spill of Paraffin Oil on skin or inhale parafin oil when heating up	Goggles
	Spill of Paraffin Oil on skin or inhale parafin oil when heating up	Labcoat
	Spill of Paraffin Oil on skin or inhale parafin oil when heating up	Chemical protecting gloves

Preparation of product	Spill of Paraffin Oil on skin or inhale parafin oil when heating up	SDS
	Spill of Paraffin Oil on skin or inhale parafin oil when heating up	Fume hood
	Spill of Colloidal Silica on skin	Goggles
	Spill of Colloidal Silica on skin	Labcoat
	Spill of Colloidal Silica on skin	Chemical protecting gloves
	Spill of Colloidal Silica on skin	SDS
	Spill of Colloidal Silica on skin	Dust mask
	Inhale Acetone in the washing step of Mesoporus Silica Spheres	Goggles
	Inhale Acetone in the washing step of Mesoporus Silica Spheres	Labcoat
	Inhale Acetone in the washing step of Mesoporus Silica Spheres	Chemical protecting gloves
	Inhale Acetone in the washing step of Mesoporus Silica Spheres	SDS
	Inhale Acetone in the washing step of Mesoporus Silica Spheres	Fume hood
	Spill of Methanol on skin when impreganting with PEI	Goggles
	Spill of Methanol on skin when impreganting with PEI	Labcoat
	Spill of Methanol on skin when impreganting with PEI	Chemical protecting gloves
	Spill of Methanol on skin when impreganting with PEI	SDS
	Inhale vapor of Methanol when heating up the PEI-Methanol solution	SDS
	Inhale vapor of Methanol when heating up the PEI-Methanol solution	Fume hood
	Inhale TEOS while coating the Mesoporus Silica sphares	SDS
	Inhale TEOS while coating the Mesoporus Silica sphares	Fume hood
	Inhale TEOS while coating the Mesoporus Silica sphares	Dust mask
	Spill of TEOS on skin while coating the Mesoporus Silica sphares	Goggles
	Spill of TEOS on skin while coating the Mesoporus Silica sphares	Labcoat
	Spill of TEOS on skin while coating the Mesoporus Silica sphares	Chemical protecting gloves
	Spill of TEOS on skin while coating the Mesoporus Silica sphares	SDS
	Spill of Span_80 on skin or inhale when heating up in the synthesis procedure	Goggles
	Spill of Span_80 on skin or inhale when heating up in the synthesis procedure	Labcoat
	Spill of Span_80 on skin or inhale when heating up in the synthesis procedure	Chemical protecting gloves
	Spill of Span_80 on skin or inhale when heating up in the synthesis procedure	SDS

Preparation of product	Spill of Span_80 on skin or inhale when heating up in the synthesis procedure	Fume hood
	Spill of Span_80 on skin or inhale when heating up in the synthesis procedure	Dust mask
	Spill of Ammonia on skin when measuring volume of the solution for product preparation	Goggles
	Spill of Ammonia on skin when measuring volume of the solution for product preparation	Labcoat
	Spill of Ammonia on skin when measuring volume of the solution for product preparation	Chemical protecting gloves
	Spill of Ammonia on skin when measuring volume of the solution for product preparation	SDS
	Inhale Ammonia when measuring volume of the solution for product preparation	SDS
	Inhale Ammonia when measuring volume of the solution for product preparation	Fume hood
	Spill of ethanol on skin when measuring volume of the solution for product preparation	Goggles
	Spill of ethanol on skin when measuring volume of the solution for product preparation	Labcoat
	Spill of ethanol on skin when measuring volume of the solution for product preparation	Chemical protecting gloves
	Spill of ethanol on skin when measuring volume of the solution for product preparation	SDS
	Spill of fumed Silica on skin	Goggles
	Spill of fumed Silica on skin	Labcoat
	Spill of fumed Silica on skin	Chemical protecting gloves
	Spill of fumed Silica on skin	SDS
	Spillage of Piperazine on skin during impregantion	Goggles
	Spillage of Piperazine on skin during impregantion	Labcoat
	Inhale Trimethoxymethylsilane while coating the Mesoporus Silica sphares	Fume hood
	Inhale Trimethoxymethylsilane while coating the Mesoporus Silica sphares	Ventilated cabinets
	Spill of Trimethoxymethylsilane on skin while coating the Mesoporus Silica sphares	Labcoat
	Spill of Trimethoxymethylsilane on skin while coating the Mesoporus Silica sphares	Chemical protecting gloves
	Spill of Trimethoxymethylsilane on skin while coating the Mesoporus Silica sphares	Fume hood
Spill of chemicals in drain	Spillage of Resorcinol	Waste disposal containers
	Spillage of Aceton	Waste disposal containers
	Spillage of PEI	Waste disposal containers
	Spillage of Ammonia	

Spill of chemicals in drain	Spillage of Piperazine	Goggles
	Spillage of Piperazine	Labcoat
	Spillage of Piperazine	SDS
Handling instruments	Skin burn on hot plate when preparing Mesoporous Silica sphares	Heat protecting gloves
	Skin burn when operating with Calcination Furnace	Heat protecting gloves
	Skin burn when operating with Calcination Furnace	Instrument training
	Frostbite when hanling Liquid Nitrogen during Nitrogen Physisortion	Gloves for cold materials
	Loud noise for ears while using ultrasonication on the solution	Instrument training
	Leakages of pressurized CO2, N2 when operating with Microbalance reactor	Goggles
	Leakages of pressurized CO2, N2 when operating with Microbalance reactor	Labcoat
	Skin burn when operating with Microbalance reactor	Goggles
	Skin burn when operating with Microbalance reactor	Labcoat
	Skin burn when operating with Microbalance reactor	Heat protecting gloves
Handling pressurized gas	Leakages of pressurized CO2, N2, O2, Argon	Goggles
Working in the lab under covid-situation	Contact with surfaces	Goggles
	Contact with surfaces	Labcoat
	Faint/Pass out during experiment	Goggles
	Faint/Pass out during experiment	Labcoat
	Faint/Pass out during experiment	Fume hood
	Faint/Pass out during experiment	Dust mask
	Spread of Covid-19	Goggles
	Spread of Covid-19	Labcoat
	Spread of Covid-19	Dust mask

Existing relevant measures with descriptions:

Goggles
[Ingen registreringer]

Labcoat
[Ingen registreringer]

Chemical protecting gloves
[Ingen registreringer]

SDS
[Ingen registreringer]

Norges teknisk-naturvitenskapelige universitet (NTNU)
Unntatt offentlighet jf. Offentlighetsloven § 14

Print date: 01.07.2020

Printed by: Estelle Marie M. Vanhaecke

Page: 15/39

Fume hood
[Ingen registreringer]

Dust mask
[Ingen registreringer]

Waste disposal containers
[Ingen registreringer]

Heat protecting gloves
[Ingen registreringer]

Instrument training
[Ingen registreringer]

Gloves for cold materials
[Ingen registreringer]

Ventilated cabinets
[Ingen registreringer]

Gas detection
[Ingen registreringer]

Risk analysis with evaluation of likelihood and consequence

This part of the report presents detailed documentation of hazards, incidents and causes which have been evaluated. A summary of hazards and associated incidents is listed at the beginning.

The following hazards and incidents has been evaluated in this risk assessment:

- **Preparation of product**
    - Spill of Formaldehyde on skin when measuring volume of the solution for product preparation
    - Spill of Formaldehyde and inhale vapor when measuring volume of the solution for product preparation
    - Spill of Resorciol on skin when measuring volume of the solution for product preparation
    - Spill of Resorcinol and swollow when measuring volume of the solution for product preparation
    - Spill of Paraffin Oil on skin or inhale parafin oil when heating up
    - Spill of Colloidal Silica on skin
    - Inhale Acetone in the washing step of Mesoporus Silica Spheres
    - Spill of Methanol on skin when impreganting with PEI
    - Inhale vapor of Methanol when heating up the PEI-Methanol solution
    - Inhale TEOS while coating the Mesoporus Silica sphares
    - Spill of TEOS on skin while coating the Mesoporus Silica sphares
    - Spill of Span_80 on skin or inhale when heating up in the synthesis procedure
    - Spill of Ammonia on skin when measuring volume of the solution for product preparation
    - Inhale Ammonia when measuring volume of the solution for product preparation
    - Spill of ethanol on skin when measuring volume of the solution for product preparation
    - Spill of fumed Silica on skin
    - Spillage of Piperazine on skin during impregantion
    - Inhale Trimethoxymethylsilane while coating the Mesoporus Silica sphares
    - Spill of Trimethoxymethylsilane on skin while coating the Mesoporus Silica sphares
- **Spill of chemicals in drain**
    - Spillage of Resorcinol
    - Spillage of Aceton
    - Spillage of PEI
    - Spillage of Ammonia
    - Spillage of Piperazine
- **Handling instruments**
    - Skin burn on hot plate when preparing Mesoporous Silica sphares
    - Skin burn when operating with Calcination Furnace
    - Frostbite when hanling Liquid Nitrogen during Nitrogen Physisortion
    - Loud noise for ears while using ultrasonication on the solution
    - Leakages of pressurized CO2, N2 when operating with Microbalance reactor
    - Skin burn when operating with Microbalance reactor
- **Handling pressurized gas**
    - Leakages of pressurized CO2, N2, O2, Argon
- **Working in the lab under covid-situation**
    - Contact with surfaces

- Faint/Pass out during experiment
- Spread of Covid-19

Detailed view of hazards and incidents:

Hazard: Preparation of product

Incident: Spill of Formaldehyde on skin when measuring volume of the solution for product preparation

Likelihood of the incident (common to all consequence areas):   **Less likely (2)**

Kommentar:

Use of gloves and labcoat

P210 Keep away from heat, hot surfaces, sparks, open flames and other ignition sources. No smoking.
P260 Do not breathe dust/ fume/ gas/ mist/ vapours/ spray.
P280 Wear protective gloves/ protective clothing/ eye protection/ face protection.

Consequence area: Helse   *Risk:*

Assessed consequence: **Large (3)**

Comment: Formaledehyde:

H350 Kan forårsake kreft.
H341 Mistenkes å kunne gi genetiske skader.
H301+H311+H331 Giftig ved svelging, hudkontakt eller inhalering
H370 Forårsaker organskader.
H314 Gir alvorlige etseskader på hud og øyne.
H335 Kan forårsake irritasjon av luftveiene.
H317 Kan utløse en allergisk hudreaksjon.

Incident: Spill of Formaldehyde and inhale vapor when measuring volume of the solution for product preparation

- -

Likelihood of the incident (common to all consequence areas):   **Less likely (2)**

> *Kommentar:*
>
> Use of gloves, labcoat and fume hood
>
> P210 Keep away from heat, hot surfaces, sparks, open flames and other ignition sources. No smoking.
> P260 Do not breathe dust/ fume/ gas/ mist/ vapours/ spray.
> P280 Wear protective gloves/ protective clothing/ eye protection/ face protection.

Consequence area: Helse   *Risk:*

> *Assessed consequence:* **Catastrophical (5)**
>
> *Comment:* Formaldehyde:
>
> H226 Flammable liquid and vapour.
> H301 + H311 + H331 Toxic if swallowed, in contact with skin or if inhaled.
> H314 Causes severe skin burns and eye damage.
> H317 May cause an allergic skin reaction.
> H335 May cause respiratory irritation.
> H341 Suspected of causing genetic defects.
> H350 May cause cancer.
> H370 Causes damage to organs (Eyes).

Incident: Spill of Resorciol on skin when measuring volume of the solution for product preparation

- -

Likelihood of the incident (common to all consequence areas):   **Less likely (2)**

> *Kommentar:*
>
> Use of gloves and labcoat
>
> Precautionary statement(s)
> P280 Wear eye protection/ face protection.

Consequence area: Helse   *Risk:*

> *Assessed consequence:* **Large (3)**
>
> *Comment:* Hazard statement(s)
> H302 Harmful if swallowed.
> H315 Causes skin irritation.
> H318 Causes serious eye damage.
> H400 Very toxic to aquatic life.

Incident: Spill of Resorcinol and swollow when measuring volume of the solution for product preparation
- -

Likelihood of the incident (common to all consequence areas):   **Less likely (2)**

   Kommentar:

   Use of fume hood

   Precautionary statement(s)
   P280 Wear eye protection/ face protection.

Consequence area: Helse   *Risk:*

   Assessed consequence: **Large (3)**

       Comment: Hazard statement(s)
                   H302 Harmful if swallowed.
                   H315 Causes skin irritation.
                   H318 Causes serious eye damage.
                   H400 Very toxic to aquatic life.

Incident: Spill of Paraffin Oil on skin or inhale parafin oil when heating up
- -

Likelihood of the incident (common to all consequence areas):   **Less likely (2)**

   Kommentar:

   Use of glove, labcoat, fume hood

Consequence area: Helse   *Risk:*

   Assessed consequence: **Small (1)**

       Comment: Not a hazardous substance or mixture according to Regulation (EC) No.
                   1272/2008.

Incident: Spill of Colloidal Silica on skin

- -

Likelihood of the incident (common to all consequence areas): **Less likely (2)**

    Kommentar:

    Use of gloves, labcoat and dust mask

Consequence area: Helse   *Risk:*

    Assessed consequence: **Small (1)**

           Comment: Not a hazardous substance or mixture according to Regulation (EC) No. 1272/2008.
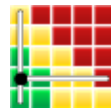
Incident: Inhale Acetone in the washing step of Mesoporus Silica Spheres

- -

Likelihood of the incident (common to all consequence areas): **Less likely (2)**

    Kommentar:

    Use of fume hood

    Precautionary statement(s)
    P210 Keep away from heat, hot surfaces, sparks, open flames and other ignition sources. No smoking.
    P261 Avoid breathing vapours.

Consequence area: Helse   *Risk:*

    Assessed consequence: **Medium (2)**

           Comment: Hazard statement(s)
                      H319 Causes serious eye irritation.
                      H336 May cause drowsiness or dizziness.

Incident: Spill of Methanol on skin when impreganting with PEI

- -

Likelihood of the incident (common to all consequence areas):   **Less likely (2)**

Kommentar:

Use of gloves, labcoat

Precautionary statement(s)
P210 Keep away from heat, hot surfaces, sparks, open flames and other ignition sources. No smoking.
P280 Wear protective gloves/ protective clothing.

Consequence area: Helse   *Risk:*

Assessed consequence: **Large (3)**

Comment: Hazard statement(s)
H301 + H311 + H331 Toxic if swallowed, in contact with skin or if inhaled.

Incident: Inhale vapor of Methanol when heating up the PEI-Methanol solution

- -

Likelihood of the incident (common to all consequence areas):   **Less likely (2)**

Kommentar:

Use of fume hood

P210 Keep away from heat, hot surfaces, sparks, open flames and other
ignition sources. No smoking.
P280 Wear protective gloves/ protective clothing.

Consequence area: Helse   *Risk:*

Assessed consequence: **Very large (4)**

Comment: Hazard statement(s)
H225 Highly flammable liquid and vapour.
H301 + H311 + H331 Toxic if swallowed, in contact with skin or if inhaled.
H370 Causes damage to organs.

Incident: Inhale TEOS while coating the Mesoporus Silica sphares
- -

Likelihood of the incident (common to all consequence areas): **Less likely (2)**

    Kommentar:

    Use of fume hood, filter mask

    Precautionary statement(s)
    P261 Avoid breathing dust/ fume/ gas/ mist/ vapours/ spray.

Consequence area: Helse *Risk:*

    Assessed consequence: **Large (3)**

        Comment: Hazard statement(s)
                H319 Causes serious eye irritation.
                H332 Harmful if inhaled.
                H335 May cause respiratory irritation.

Incident: Spill of TEOS on skin while coating the Mesoporus Silica sphares
- -

Likelihood of the incident (common to all consequence areas): **Less likely (2)**

    Kommentar:

    Use of gloves, labcoat

    Precautionary statement(s)
    P280 Wear eye protection/ face protection.

Consequence area: Helse *Risk:*

    Assessed consequence: **Medium (2)**

        Comment: [Ingen registreringer]

	Print date:	**Printed by:**		**Page:**
Norges teknisk-naturvitenskapelige universitet (NTNU)				
Unntatt offentlighet jf. Offentlighetsloven § 14	01.07.2020	Estelle Marie M. Vanhaecke		24/39

Incident: Spill of Span_80 on skin or inhale when heating up in the synthesis procedure

- -

Likelihood of the incident (common to all consequence areas):   **Less likely (2)**

        Kommentar:

        Use of gloves, labcoat, fume hood/dust mask

Consequence area: Helse   *Risk:*

    Assessed consequence: **Small (1)**

       Comment: Not a hazardous substance or mixture according to Regulation (EC) No 1272/2008
This substance is not classified as dangerous according to Directive 67/548/EEC.

Incident: Spill of Ammonia on skin when measuring volume of the solution for product preparation

- -

Likelihood of the incident (common to all consequence areas):   **Less likely (2)**

        Kommentar:

        Use of gloves, labcoat

        Precautionary statements
P280 Wear protective gloves/ protective clothing/ eye protection/ face protection.

Consequence area: Helse   *Risk:*

    Assessed consequence: **Very large (4)**

       Comment: Hazard statements
H314 Causes severe skin burns and eye damage.

Incident: Inhale Ammonia when measuring volume of the solution for product preparation

- -

Likelihood of the incident (common to all consequence areas): **Less likely (2)**

    Kommentar:

    Use of fume hood

    Precautionary statements
    P273 Avoid release to the environment.

Consequence area: Helse   *Risk:*

    Assessed consequence: **Large (3)**

        Comment: Hazard statements
                    H335 May cause respiratory irritation.

Incident: Spill of ethanol on skin when measuring volume of the solution for product preparation

- -

Likelihood of the incident (common to all consequence areas): **Less likely (2)**

    Kommentar:

    Use of gloves, fume hood

    Precautionary statements
    P210 Keep away from heat, hot surfaces, sparks, open flames and other ignition sources. Nosmoking.
    P240 Ground/bond container and receiving equipment.

Consequence area: Helse   *Risk:*

    Assessed consequence: **Small (1)**

        Comment: Hazard statements
                    H319 Causes serious eye irritation.

Incident: Spill of fumed Silica on skin

- -

Likelihood of the incident (common to all consequence areas):   **Less likely (2)**

      Kommentar:

Use of gloves, labcoat

Consequence area: Helse   *Risk:*

    Assessed consequence: **Small (1)**

            Comment: Not a hazardous substance or mixture according to Regulation (EC) No. 1272/2008.
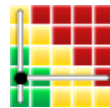
Incident: Spillage of Piperazine on skin during impregantion

- -

Likelihood of the incident (common to all consequence areas):   **Unlikely (1)**

      Kommentar:

Use of gloves, labcoat

Precautory statements:
P201 Obtain special instructions before use.
P261 Avoid breathing dust/ fume/ gas/ mist/ vapours/ spray.
P280 Wear protective gloves/ protective clothing/ eye protection/ face protection.

Consequence area: Helse   *Risk:*

    Assessed consequence: **Very large (4)**

            Comment: Hazard statements
H314 Causes severe skin burns and eye damage.
H317 May cause an allergic skin reaction.
H334 May cause allergy or asthma symptoms or breathing difficulties if inhaled.
H361fd Suspected of damaging fertility. Suspected of damaging the unborn child.

Incident: Inhale Trimethoxymethylsilane while coating the Mesoporus Silica sphares

- -

Likelihood of the incident (common to all consequence areas): **Unlikely (1)**

> *Kommentar:*
> Working in fume hood

Consequence area: Helse　　　　　　　　　　　　　　　　　　　　*Risk:*

> *Assessed consequence:* **Medium (2)**

> > *Comment:* P262 Do not get in eyes, on skin, or on clothing.
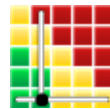
Incident: Spill of Trimethoxymethylsilane on skin while coating the Mesoporus Silica sphares

- -

Likelihood of the incident (common to all consequence areas): **Less likely (2)**

> *Kommentar:*
> Use labcoat, gloves, googles

Consequence area: Helse　　　　　　　　　　　　　　　　　　　　*Risk:*

> *Assessed consequence:* **Medium (2)**

> > *Comment:* Hazard statements
> > H225 Highly flammable liquid and vapour
> >
> > Precautionary statements
> > P210 Keep away from heat/sparks/open flames/hot surfaces. - No smoking.
> > P262 Do not get in eyes, on skin, or on clothing.
> > P403 + P235 Store in a well-ventilated place. Keep cool.
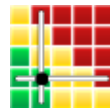
Hazard: Spill of chemicals in drain

Incident: Spillage of Resorcinol

Likelihood of the incident (common to all consequence areas):   **Unlikely (1)**

  Kommentar:
  Use of special containers

Consequence area: Ytre miljø

Assessed consequence: **Large (3)**

  Comment: Hazard statement(s)
  H400 Very toxic to aquatic life.

Risk:

Incident: Spillage of Aceton

Likelihood of the incident (common to all consequence areas):   **Unlikely (1)**

  Kommentar:
  Use of special container for organic solvent

Consequence area: Ytre miljø

Assessed consequence: **Medium (2)**

  Comment: Prevent further leakage or spillage if safe to do so. Do not let product enter drains.

Risk:

Incident: Spillage of PEI

- -

Likelihood of the incident (common to all consequence areas):   **Unlikely (1)**

       Kommentar:

       Use of special waste containers for such a material

Consequence area: Ytre miljø   *Risk:*

    Assessed consequence: **Very large (4)**

        Comment: Hazard statement(s)
               H411 Toxic to aquatic life with long lasting effects.
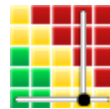
Incident: Spillage of Ammonia

- -

Likelihood of the incident (common to all consequence areas):   **Unlikely (1)**

       Kommentar:

       Use of special waste containers

Consequence area: Ytre miljø   *Risk:*

    Assessed consequence: **Very large (4)**

        Comment: Hazard statements
               H290 May be corrosive to metals.
               H400 Very toxic to aquatic life.
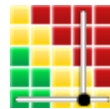
Incident: Spillage of Piperazine

- -

Likelihood of the incident (common to all consequence areas):   **Unlikely (1)**

        Kommentar:

        Use of special waste containers for such a material

Consequence area: Helse   *Risk:*

    Assessed consequence: **Very large (4)**

        Comment: H314 Causes severe skin burns and eye damage.
                H317 May cause an allergic skin reaction.
                H334 May cause allergy or asthma symptoms or breathing difficulties if
                inhaled.
                H361fd Suspected of damaging fertility. Suspected of damaging the unborn
                child.

Consequence area: Ytre miljø   *Risk:*

    Assessed consequence: **Small (1)**

        Comment: This substance/mixture contains no components considered to be either
                persistent,
                bioaccumulative and toxic (PBT), or very persistent and very
                bioaccumulative (vPvB) at
                levels of 0.1% or higher

Hazard: Handling instruments

Incident: Skin burn on hot plate when preparing Mesoporous Silica sphares
- -

Likelihood of the incident (common to all consequence areas): **Unlikely (1)**

    Kommentar:

    Use of heat protecting gloves and/or crucible tongs

Consequence area: Helse

    Assessed consequence: **Medium (2)**

        Comment: Burns are characterized by severe skin damage that causes the affected skin cells to die

Risk:

Incident: Skin burn when operating with Calcination Furnace
- -

Likelihood of the incident (common to all consequence areas): **Unlikely (1)**

    Kommentar:

    Use of heat protective gloves and instrument training .
    Screen showing the temperature

Consequence area: Helse

    Assessed consequence: **Medium (2)**

        Comment: Temperature should be read on the screen and/or use heat protecting gloves resistant to a limited temperature value so skin burn damage can be avoid

Risk:

Incident: Frostbite when hanling Liquid Nitrogen during Nitrogen Physisortion

- -

Likelihood of the incident (common to all consequence areas):   **Unlikely (1)**

> *Kommentar:*
> Use of gloves for cold materials, boots, apron and long pants

Consequence area: Helse   *Risk:*

> *Assessed consequence:* **Large (3)**
>
> > *Comment:* If liquid nitrogen has direct contact with the skin, it will burn.

Incident: Loud noise for ears while using ultrasonication on the solution

- -

Likelihood of the incident (common to all consequence areas):   **Unlikely (1)**

> *Kommentar:*
> Use of hearing protection

Consequence area: Helse   *Risk:*

> *Assessed consequence:* **Large (3)**
>
> > *Comment:* Damage to/or hearing loss

Incident: Leakages of pressurized CO2, N2 when operating with Microbalance reactor

- -

Likelihood of the incident (common to all consequence areas):   **Unlikely (1)**

> *Kommentar:*
>
> Training for handlig valve and gas-cylinder

Consequence area: Helse   *Risk:*

> *Assessed consequence:* **Medium (2)**
>
> > *Comment:* A person can suffer a suffoction is the gas leak is large

Incident: Skin burn when operating with Microbalance reactor

- -
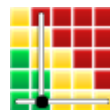
Likelihood of the incident (common to all consequence areas):   **Unlikely (1)**

> *Kommentar:*
>
> Use of heat protective gloves and instrument training .

Consequence area: Helse   *Risk:*

> *Assessed consequence:* **Medium (2)**
>
> > *Comment:* Temperature should be read on the screen and/or use heat protecting gloves resistant to a limited temperature value so skin burn damage can be avoid

Hazard: Handling pressurized gas

Incident: Leakages of pressurized CO2, N2, O2, Argon
- -

Likelihood of the incident (common to all consequence areas):   **Unlikely (1)**

  Kommentar:
 Training for handlig valve and gas-cylinder

Consequence area: Helse   *Risk:*

  Assessed consequence: **Medium (2)**

        Comment: A person can suffer a suffoction is the gas leak is large

Hazard: Working in the lab under covid-situation

Incident: Contact with surfaces

- -

Likelihood of the incident (common to all consequence areas):   **Unlikely (1)**

Kommentar:

Use of lab-coat and googles. Disinfection before and after with ethanol on all surfaces I am in contact with

Consequence area: Helse   *Risk:*

Assessed consequence: **Large (3)**

Comment: Covid-19 may be spread

Incident: Faint/Pass out during experiment

- -

Likelihood of the incident (common to all consequence areas):   **Unlikely (1)**

Kommentar:

Use of fume hood, gas mask and work alone alarm. Make sure I feel healthy before going to lab

Consequence area: Helse   *Risk:*

Assessed consequence: **Large (3)**

Comment: Spill of chemicals, breathing problems.

Norges teknisk-naturvitenskapelige universitet (NTNU)   **Print date:**   **Printed by:**   **Page:**

Unntatt offentlighet jf. Offentlighetsloven § 14   01.07.2020   Estelle Marie M. Vanhaecke   36/39

Incident: Spread of Covid-19

- -

Likelihood of the incident (common to all consequence areas): **Less likely (2)**

      Kommentar:

      Stay home if feeling sick. Use gloves, lab-coat and googles when using common equipment. Don't touch face.
Wash hands often.

Consequence area: Helse   *Risk:*

    Assessed consequence: **Medium (2)**

           Comment: Spread of virus that cause fever, cough, and shortness of breath and in
worst case result in death.

Norges teknisk-naturvitenskapelige universitet (NTNU)

Unntatt offentlighet jf. Offentlighetsloven § 14

Print date:

01.07.2020

Printed by:

Estelle Marie M. Vanhaecke

Page:

37/39

Overview of risk mitiating measures which have been decided:

Below is an overview of risk mitigating measures, which are intended to contribute towards minimizing the likelihood and/or consequence of incidents:

Overview of risk mitigating measures which have been decided, with description:

Detailed view of assessed risk for each hazard/incident before and after mitigating measures

Jørgen Lausund Grinna

Master's Thesis

NTNU
Norwegian University of
Science and Technology